SALT CONTROL ON SEDIMENTARY PROCESESS IN

EARLY PLEISTOCENE: SHIP SHOAL SOUTH ADDITION

BLOCKS 349-358, GULF OF MEXICO

A Thesis

by

MUNJI SYARIF

Submitted to the Office of Graduate Studies of
Texas A&M University
in partial fulfillment of the requirements for the degree of

MASTER OF SCIENCE

December 2002

Major Subject: Geophysics

SALT CONTROL ON SEDIMENTARY PROCESESS IN

EARLY PLEISTOCENE: SHIP SHOAL SOUTH ADDITION

BLOCKS 349-358, GULF OF MEXICO

A Thesis

by

MUNJI SYARIF

Submitted to Texas A&M University
in partial fulfillment of the requirements
for the degree of

MASTER OF SCIENCE

Approved as to style and content by:

Joel S. Watkins	Richard L. Gibson
(Chair of Committee)	(Member)
Walter B. Ayers	Duane A. McVay
(Member)	(Member)

Andrew Hajash
(Head of Department)

December 2002

Major Subject: Geophysics

ABSTRACT

Salt Control on Sedimentary Processes in Early Pleistocene: Ship Shoal South Addition

Blocks 349-358, Gulf of Mexico. (December 2002)

Munji Syarif, B.S., Bandung Institute of Technology (ITB)

Chair of Advisory Committee: Dr. Joel S. Watkins

The interpretation of 3D seismic data from Ship Shoal South Addition Blocks 349-358, Gulf of Mexico shows a complex interaction between salt, faults, and sedimentary strata.

Reconstruction of the geometry of early Pliestocene (about 3.65 Ma) through recent salt and associated sediments reveals the evolution of a supralobal basin in the study area. The basin depocenter shifted from the northeastern part to the center of the study area through time. A small, bulb-shaped, salt-stock structure occurs in the northwest, and a salt sheet structure is present in the southeastern part of the study area. Those structures are part of a pennant-shaped structure bounded by counter regional faults trending northeastward.

Salt movements created instability and triggered extensive faulting of the overlying strata. Three-dimensional reconstruction suggests that salt blocked the sediment during the early Pleistocene. The sediment was diverted around the salt high on both east and west sides of the salt body to the southwest and southeast.

Stratigraphic interpretation of the interval between 1.35 Ma and 1.95 Ma led to the identification of a highstand systems tract (HST), a transgressive systems tract

(TST), and two lowstand systems tracts (LST). The strata are developed normally in the depocenter area, whereas the strata at the basin margin were deformed by salt movement and faulting.

Each systems tract is uniquely associated with a certain seismic facies. Three seismic facies were identified associated with LST, TST, and HST. Additionally, seismic sections reveal channel geometries in the LST. Seismic attribute analysis elucidates facies distribution in the systems tracts.

Because of its ability to move, to divert sediment, to create instability, and to block sediment transport pathways, salt exercises the main control on the sedimentary processes in the study area.

DEDICATION

This thesis is dedicated to my parents, my brothers and my sisters, for their faith, enthusiasm and enduring support.

vi

ACKNOWLEDGEMENTS

I thank God Almighty, the most merciful the most gracious, for guiding me throughout my study and every aspect of my life: Alhamdulellah.

I thank Dr. Joel S. Watkins, for serving as my committee chair, for providing the data I needed in my research, and for his time and advice during my research and study. I thank Dr. Walter B. Ayers, my committee member, for his time, suggestions and discussions. I also thank the other committee members, Dr. Richard L. Gibson and Dr. Duane A. McVay, for their time, support and advice. I thank Dr. Jerry Jensen for his valuable time during my thesis defense presentation.

I thank BHP Petroleum for their 3D seismic data set. Thanks to Seismic Micro-Technology, Inc. (SMT) for the Kingdom software. I thank also the Integrated Reservoir Investigations Group (IRIG) project at TAMU for providing well-log data.

I thank Rasheed Jaradat, my office mate, for sharing the office and the discussions during my stay in the office. I thank also other graduate students, Rahadian Adhyaksawan, Sadun Arzuman, Fitrix Putro, Yanyan Triyana, Maria Meirita, Javier Perez, Mursal, and many other students although I cannot mention all of them in such short acknowledgements. Thanks also to James "Bo" Slone, Susilo Utomo and Darla-Jean Weatherford for the manuscript correction.

My TAMU experience would have been impossible without financial assistance from Pertamina Consortium Study Abroad Program and Repsol-YPF Jakarta (now under CNOOC management), and P.T. Indodaya Eratama for some paperwork support.

TABLE OF CONTENTS

LIST OF FIGURES

CHAPTER I

INTRODUCTION

Before the discovery of Mahogany field in 1993, workers focused their attention on suprasalt hydrocarbon exploration, but after the discovery of this subsalt field (Mahogany field), subsalt exploration became more interesting for hydrocarbon exploration in this area.

Hydrocarbon play is not limited to subsalt play because the problem of hydrocarbon migration remains unsolved. Migration is not the only problem; suprasalt production in the area remains an indication that the suprasalt strata are also interesting for the research and exploration.

Objectives

The objective of the study is to describe salt control on sedimentary processes as part of salt/sediment interaction. This study also addresses salt evolution and the sequence stratigraphic framework for the early Pleistocene (1.35 Ma to 1.95 Ma) period.

Location

The study area, which covers approximately 55 km^2 (21 square miles), is located in the central offshore Louisiana shelf margin in Ship Shoal South Addition Blocks 349, 350, 358, and 359, adjacent to Ewing Bank.

This thesis follows the style and format of the Bulletin of the American Association of Petroleum Geologists.

The study area, known as Mahogany field (SS-349, SS-359), is the first commercial subsalt discovery in the northern Gulf of Mexico. The discovery well was drilled by Phillips, Anadarko, and Amoco in 1993 (Camp, 2000, Rowan et al., 2001).

Since March 2000, the Mahogany field had produced 11.4 million bbl oil and 22.3 bcf gas from nine wells; two wells are suprasalt (Rowan et al., 2001).

The Mahogany salt body has maximum dimensions of 29 km in the north-south direction and 14 km in the east-west direction (Rowan et al., 2001). The coordinates of the study area are 28.0268°N to 28.0823°N and 90.9922°W to 91.0877°W.

Data Base

The primary data source is a BHP 3D seismic data set acquired in 1998 and recorded using a 4-ms sampling rate. The data consist of 550 crosslines and 350 inlines with a 3000-ms vertical time length. The distance is 16.7 m (55 ft) between crosslines and 16.7 m (55 ft) between inlines.

Paleotops data are available in eight locations. Wireline logs from five wells are available and they include sonic, density, and electric logs. Two of the wells are located inside the study area, whereas three are outside the study area and hence were used as pseudo wireline logs data (Figure 1). The data were loaded on the Kingdom Suite software package for interpretation.
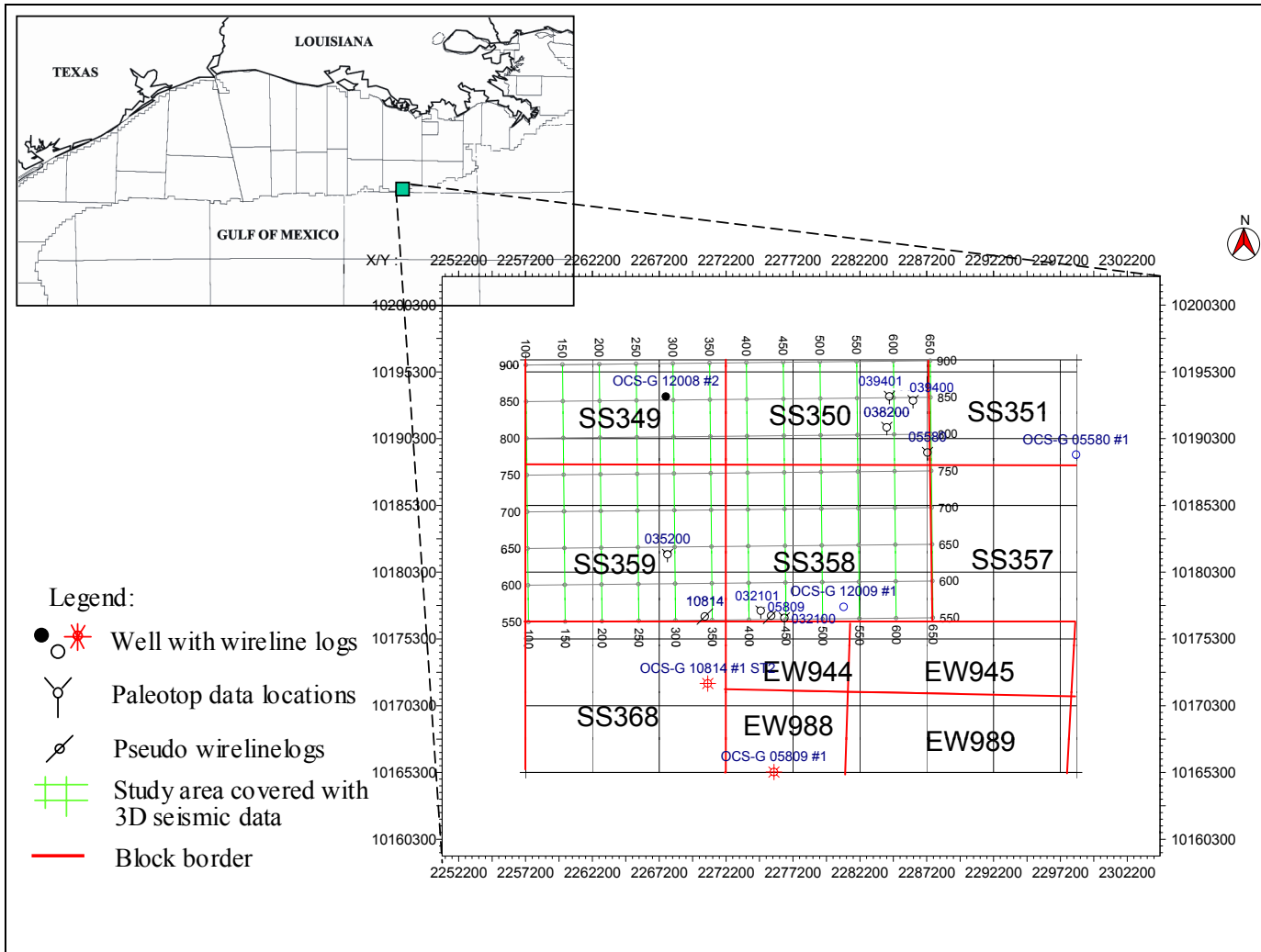
Figure 1. Location of the study area with 3D seismic survey and location of well data.

Methods and Procedure

The methods and procedures used in this study are as follows:

1. Horizon and fault interpretation.

   Interpreted five horizons representing maximum flooding surface (mfs) or condensed section and two other horizons representing the top and the bottom of the salt. Horizons are tied to well-log data with synthetic seismic generated from sonic and density logs and tied to paleotops data and a biostratigraphic chart. Fault interpretation was performed to identify structural setting and salt occurrence.

2. Paleosurface reconstruction of top salt using the isochron method as an approach to progressive flattening methods in 3D reconstruction.

3. Time-depth conversion

   Converted generated time maps to depth sections.

4. Stratigraphic interpretation.

   Choose time period from 1.35 Ma to 1.95 Ma that hypotheses suggested would have the most significant role in designing the structural and stratigraphic framework.

   Generated isopach maps and determined systems tract using phantom horizons and volume seismic-amplitude attribute maps.

5. Combined all interpretative work.

Significance of the Study

Although the northern Gulf of Mexico basin is one of the most extensively studied and explored sedimentary basins in the world, there is no general consensus among geoscientists with respect to many problems or issues. Many publications refer to areas adjacent to the study area, but only a few specifically address the Ship Shoal South Addition Blocks 349-358. The migration pathway is unknown, and only two wells in the area are producing oil or gas suprasalt (Rowan et al., 2001).

The important questions that need to be addressed in this study that will lead to a better understanding of the area include:

1) What are the changing characteristics of the depocenter of the mini basin since the late Pliocene?

2) Which factor is most important to deposition in the early Pleistocene period: sedimentation rate, sea level change or salt movement?

3) What and how and where did the facies and systems tracts develop for this 1.35-Ma to 1.95-Ma period?

CHAPTER II

BACKGROUND AND PREVIOUS STUDIES

Regional Geology

The Gulf of Mexico is a small ocean basin that formed as a consequence of rifting and attendant crustal stretching and thinning during the Late Triassic-Early Jurassic as the North American plate separated from the African and South American plates, followed by Early Cretaceous seafloor spreading (Salvador, 1987, Zhang, 1994, McBride et al., 1998, etc.).

The evolution of Gulf of Mexico basin includes several stages (Figure 2): 1) a Late Triassic to Middle Jurassic rift stage and formation of a transitional crust, culminating with the widespread deposition of evaporites (Louann Salt); 2) a brief Late Jurassic period of oceanic crust formation in the deep central Gulf of Mexico; 3) a Late Jurassic through Early Cretaceous period of cooling and subsidence of the crust and buildup of extensive carbonate platforms surrounding the deep basin; 4) formation of a widespread Middle Cretaceous unconformity (Buffler et al., 1985, Zhang, 1994).

Numerous regional unconformities and depositional hiatuses subdivide the Mesozoic and Cenozoic (McBride et al., 1998). Mesozoic synrift and postrift strata consist of non marine siliciclastics overlain by evaporites, marine carbonates and shales. Cenozoic strata record a history of thick, prograding, siliciclastic wedges, located primarily along the basin's northwestern and northern margins, and major episodes of allochthonous salt extrusion and evacuation (McBride et al., 1998). Mesozoic subsidence
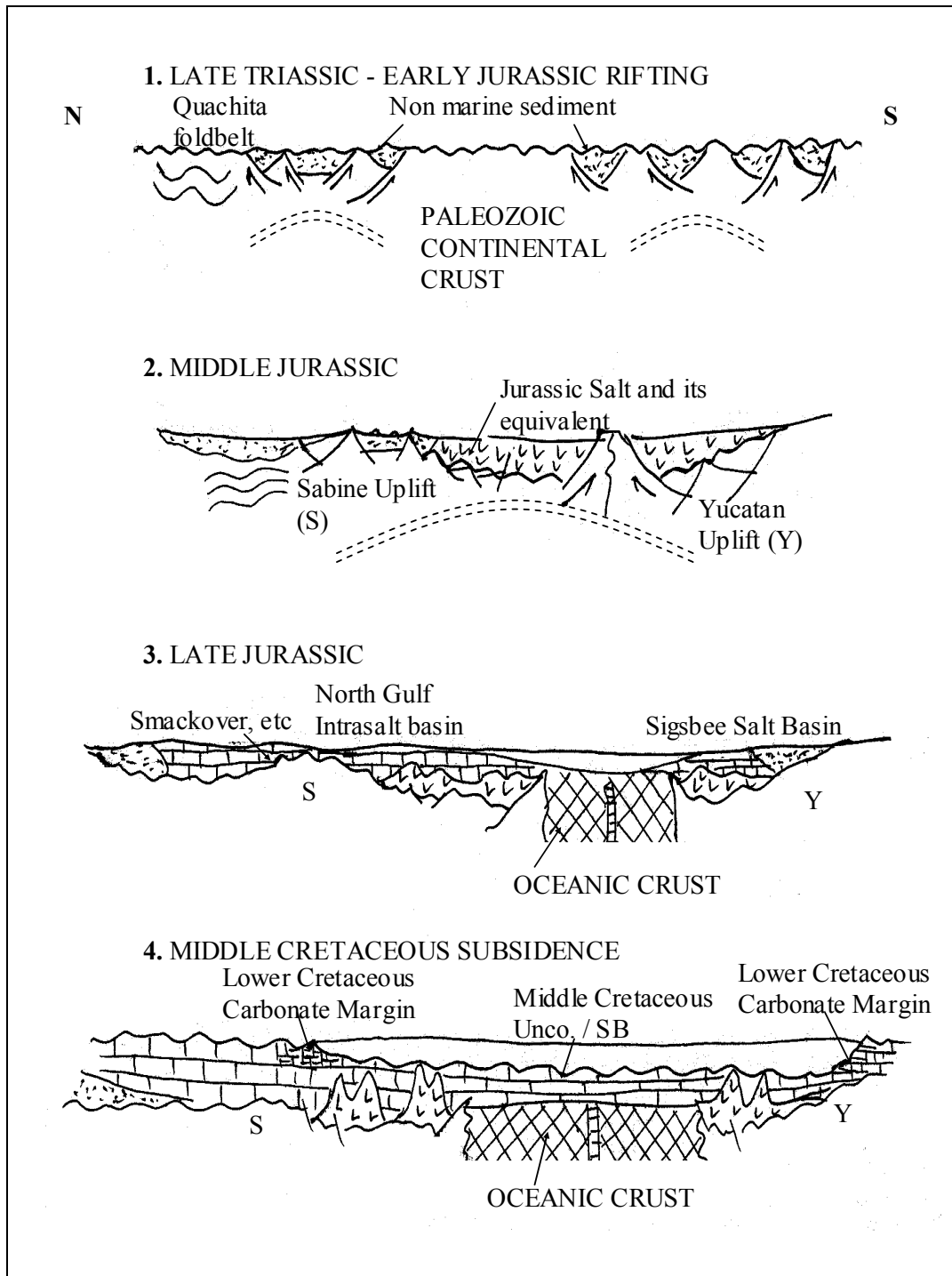
Figure 2. Schematic diagram illustrating the early evolution of the Gulf of Mexico basin. Modified from Buffler and Sawyer (1985).

was greatest within the central portion of the basin due to thermal effects; Cenozoic subsidence was greatest along the northern margin of the basin due to sedimentary loading beneath regional depocenters (McBride et al., 1998).

Growth faults play an important role in providing sediment accommodation space, in development of intrasalt basins, and in migration and trapping of hydrocarbons (Zhang and Watkins, 1994). There are at least three end-member types of structural complexes in the northern Gulf of Mexico (Figure 3). These are shale-based detachment systems (gravitational sliding), salt-withdrawal minibasins (shelf-loaded or slope-loaded), and salt-based detachment systems (roho systems or combinations of gravitational and salt withdrawal) (Karlo et al., 2000).

Growth faulting is ubiquitous on the continental shelf. These faults trend parallel to the coastline. The displacement is mainly down-to-basin, but locally it may be down-to-coast (counter regional).

Salt Tectonics

Salt deformation is one of the most important phenomena in the Gulf of Mexico. Zhang (1994) describes six salt structures in his study of central offshore Louisiana. They are salt pillows, salt rollers, salt ridges, salt pods, salt sheets and salt stocks. Most present-day salt structures in Gulf of Mexico are allochthonous salt. The salt is extensive and often escapes to shallow depth.

Salt tectonics and sequence stratigraphy have also been described (Zhang, 1994). Diegel et al. (1995) proposed a structural chronology and tectono-stratigraphic
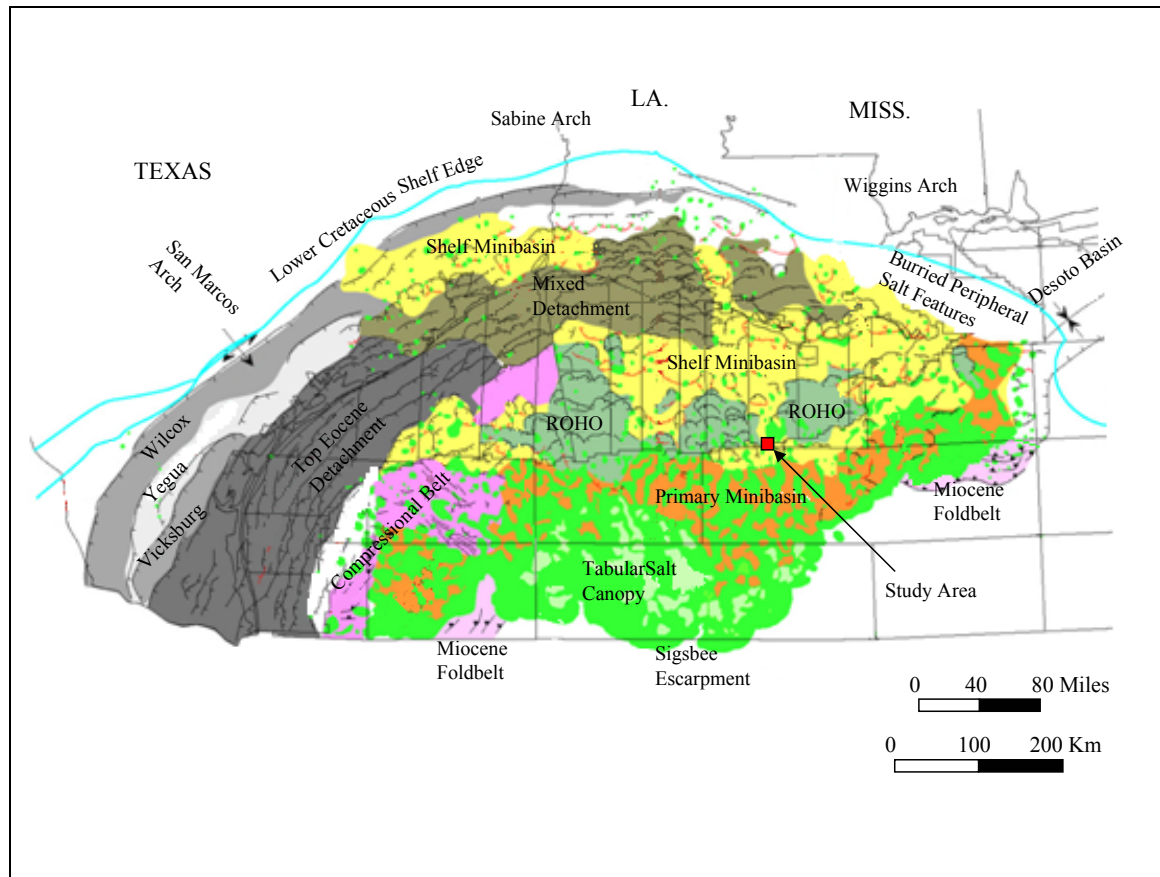
Figure 3. Main structural provinces in the Gulf of Mexico basin. The study area is in complex structural provinces. Buried peripheral salt features are buried beneath Upper Tertiary shelf sediments and structures; detachment provinces are the shale-based withdrawal basin (gravitational sliding); the shelf minibasin is a shelf-loaded salt withdrawal basin; the primary mini basin is a slope-loaded salt withdrawal basin; ROHO is salt-based detachment, a combination of gravitational and salt withdrawal; tabular-canopy salt is thick tablets of salt. Modified from Karlo et al. (2000).

framework for the Cenozoic era, which is controlled by progradation of sediment over deforming, largely allochthonous salt structures derived from an underlying autochthonous Jurassic salt. Rowan et al. (1999) explained salt-related fault families and fault welds in the northern Gulf of Mexico using classifications based on three-dimensional geometry of the faults or welds, deformed strata and associated salt.

Karlo et al. (2000) classified syndepositional systems and tectonic provinces of the northern Gulf of Mexico. These syndepositional systems are large-scale structural complexes formed in response to syndepositional loading of an unstable substrate comprising a number of different, -- yet genetically related -- components that occur in an orderly repetitive pattern within the systems. The tectonic provinces are described as detachment province, shelf mini-basin province, and roho province (Karlo et al., 2000).

Rowan et al. (2001) characterized the emplacement and evolution of the Mahogany salt body by 3D restoration. They suggest that the Mahogany salt body did not influence the trap style of the subsalt Mahogany field or hydrocarbon migration into the pay sands, but it affected sediment transport pathways.

The history of the Mahogany salt body has been explained in six stages from Miocene to recent (Figure 4) (Rowan et al., 2001).

1. "Stepped counter regional stage" (Pre-7.50 Ma)

This stage is quite speculative, suggesting that the Mahogany salt sheet was allochthonous and was sourced directly from the Jurassic Louann salt through its own deep feeders to the northeast of the study area. At this stage there was a northwest-trending salt-ridge extrusion in the lower bathyal water depth from a salt sheet located to

the northeast that may have blocked the sediment pathway (Figure 4a) (Rowan et al., 2001).

2. "Salt-stock expansion stage" (7.50-4.30 Ma)

Although it is a counterregional salt system, the Mahogany salt radially expanded to form bulb-shaped salt stock rather than extrude asymmetrically. Accommodation for a thick wedge of growth strata in the hanging wall of the counterregional fault system was created by salt evacuation from the deep sheet into the expanding stock in the lower to middle bathyal depths that formed small protobasins presumably containing a highly condensed section (Figure 4b). A bathymetric barrier was also formed by the expanding stock, and sediment transport was blocked so turbidites flowed around both west and east sides of the body (Rowan et al., 2001).

3. "Salt-tongue extrusion stage" (4.30-3.65 Ma)

The maximum length (about 30 km) of Mahogany salt body was attained at this time and locally amalgamated with the "NE" salt body. The process blocked the sediment fairway on the east side of the Mahogany salt body (Figure 4c). The tongue extrusion continues basinward but then the basinward tongue was rafted along suprasalt protobasins by sediment overburden. The evacuation and weld processes along the protobasin translation happened quickly (Rowan et al., 2001).

4. "Burial/quiescent stage" (3.65-1.95 Ma)

Sedimentation was reduced at this time and the salt body became relative quiescent. Although the Mahogany salt body still contained large amounts of salt, withdrawal and diapirism did not continue but effectively ceased because of the timing
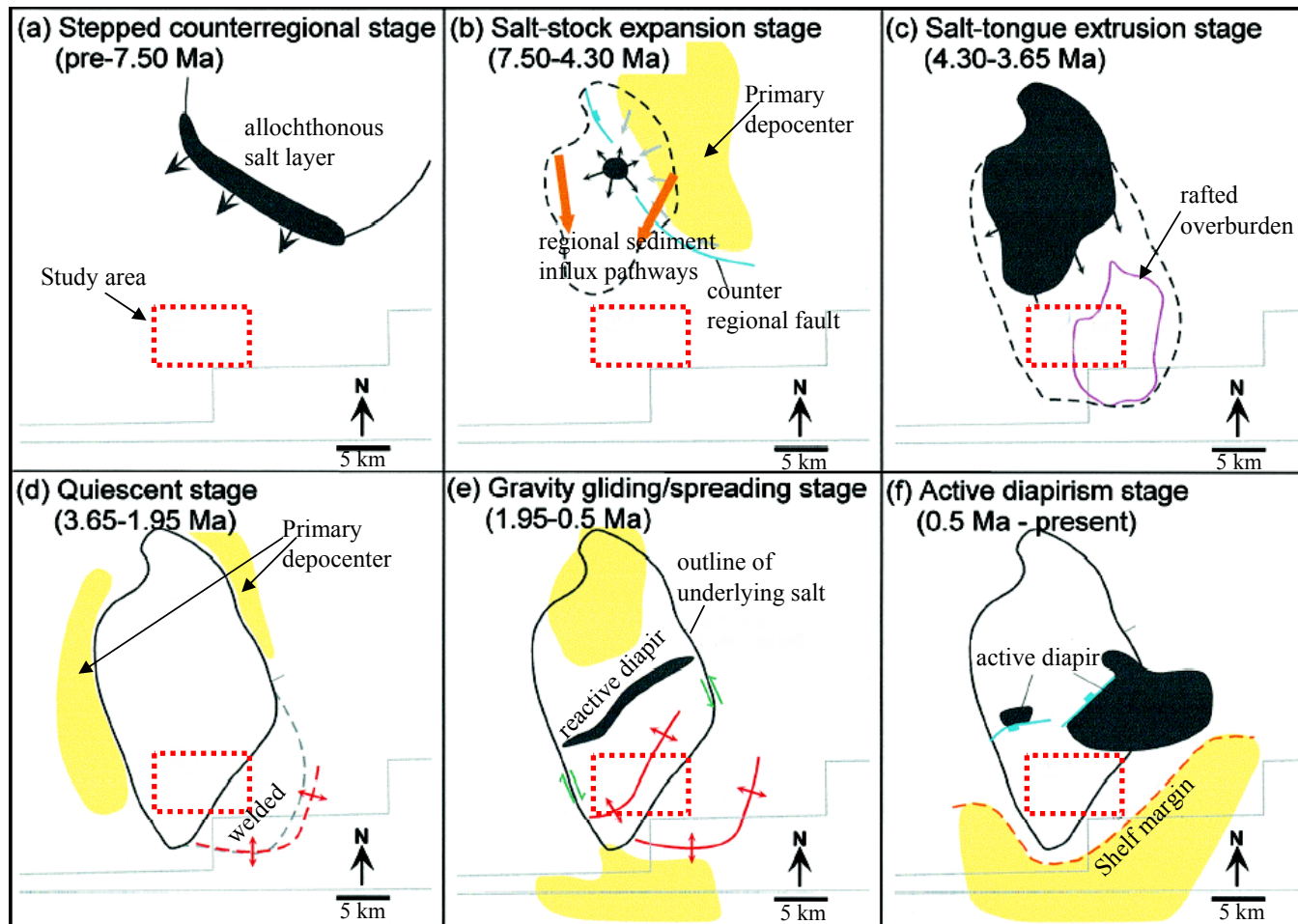
Figure 4. Schematic diagram showing Mahogany salt evolution, after Rowan et al. (2001). (a) Allochthonous salt layer sourced from northeast. (b) Salt expanding radially. (c,d) Salt extrusion rafted overburden and primary depocenter shifted to west and east sides. (e) Strike-slip fault and contractional fold (red line) occurred at 1.95 Ma, and depocenter shifted to the north and south. (f) Salt now in active diapirism stage and just next to the shelf margin.

of initial evacuation relative to regional sedimentation (Figure 4d). Gravity failure, which was the trigger for initial loading and evacuation salt, was immediately followed by more than 1 m.y. of relatively slow sedimentation. The Mahogany salt body was gradually buried during this time (Rowan et al., 2001).

5. "Gravity gliding/spreading stage" (1.95-~0.5 Ma)

This stage represents the time when the Mahogany salt body was in middle to upper bathyal water depths. A reactive diapir was formed by basinward translation of the overburden (Figure 4e). The diapir marked the main point of breakaway between stock and tongue parts of the Mahogany salt body, where material on the basinward side moved relative to the northwest. The translation happened because the overburden could slide more easily on the subhorizontal salt tongue than up the updip southern margin of the stock (Rowan et al., 2001). A contractional fold was formed at the edge of the rafted overburden trending northeast-southwest along the strike-slip deformation zone. The depocenter gradually migrated to the center of the bulb-shaped part.

6. "Active diapirism stage" (~0.5 Ma-Present)

Shelf margin sediments had prograded past the Mahogany salt body to its present location just south of the salt body at this time (Figure 4f). Basinward translation of the overburden ceased, but minor subsidence still existed over the stock. Two reactivated, normal faults accommodated differential subsidence/uplift, without any net extension on the overburden. This process still continues today.

As part of the counterregional system, the "CR" salt body just southwest of Mahogany is a salt tongue, whereas salt-stock canopy was formed in the Mahogany and

the "NE" salt bodies, which have individual components that expanded radially before merging (Figure 5). Therefore, the greater Mahogany area contains both salt tongues and bulb-shaped salt stock in close proximity to one another (Figure 5) (Rowan et al., 2001).

A salt stock is defined as a plug-like salt diapir piercing the overburden with or without a bulb (Zhang, 1994), subcircular, and often with radial faulting resulting from slow upwarping of overlying strata by deep-seated salt. A salt stock is diapiric and discordant, cutting overlying strata; salt pillows are concordant with adjacent sediments. The terms *salt stocks*, *salt plugs*, and *salt domes* are synonymous (Edgell, 1996).

The term *salt sheet* refers to allochthonous tabular salt bodies whose width is several times greater than thickness (Zhang, 1994). Salt sheet are horizontally emplaced and generally have clear features at top and bottom.

Simmons (1992) classified intrasalt basins into three categories based on the position of the basin fill with respect to the structural style of neighboring salt (Figure 6): 1) Interdomal basins generally occur on the present-day inner and middle shelf area between salt domes, stocks, ridges, and pillows. The basin is bounded by counter regional growth faults (Zhang, 1994).

2) Interlobal basins occur between salt sheets or tongues or between allochthonous salt lobes in the middle and outer shelf area. This is similar to the type "C" basin of Lee (1990); the sediment onlaps onto the adjacent salt along the basin margins or occur as horizontal or conformable strata (Lee, G.H., 1990).

3) A supralobal basin is characterized by counter-regional growth faulting or down to the basin growth, faulting along both sides above the allochthonous salt.
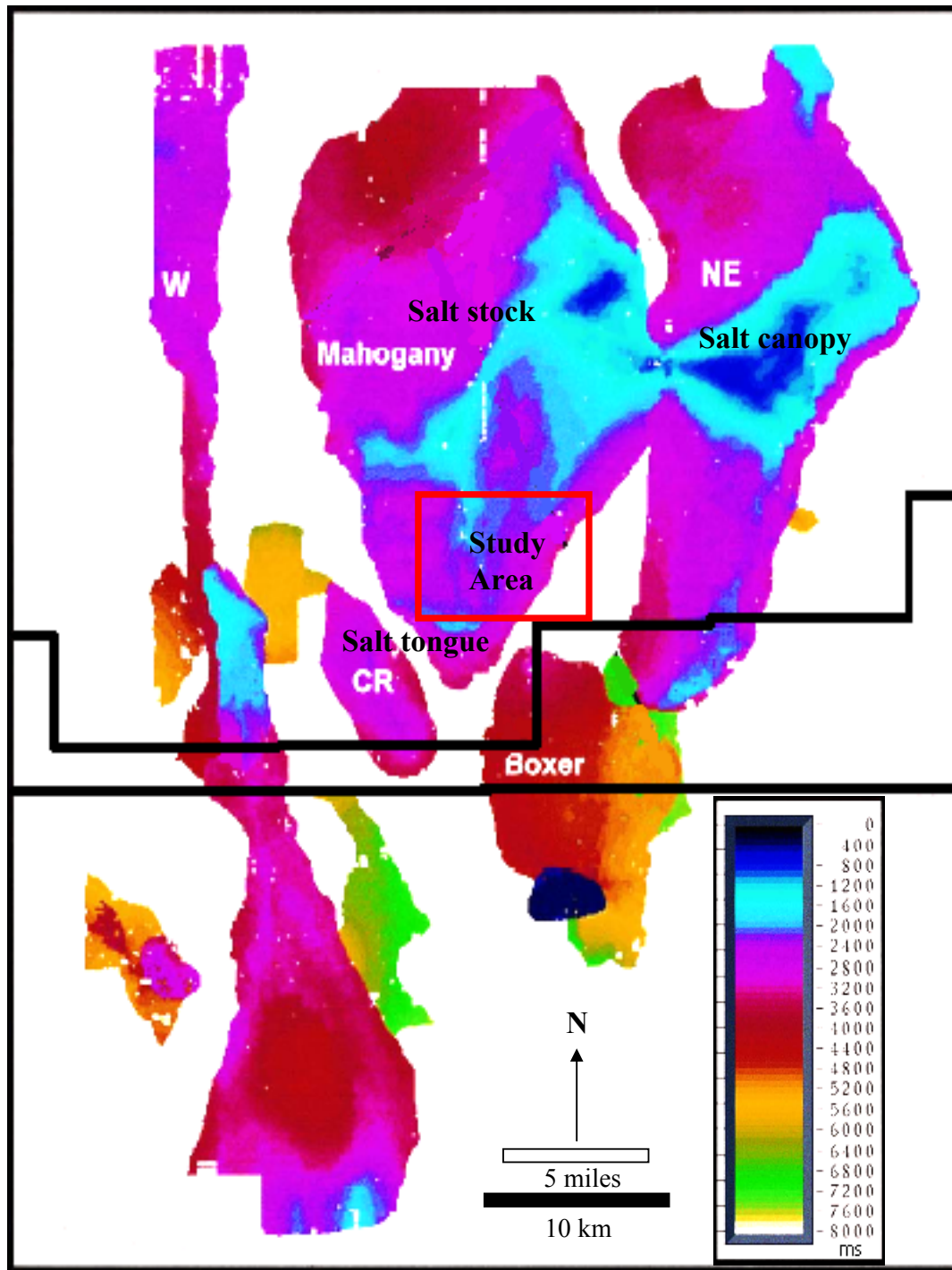
Figure 5. Salt-structure distribution in the greater Mahogany area. Modified after Rowan et al. (2001). The Mahogany salt body is salt stock. The "NE" salt body is salt canopy. They are surrounded by salt tongue on the flank ("CR" and Boxer salt body).

Interdomal Basin	Interlobal Basin	Supralobal Basin
Bounded by down-to-basin faults	Usually no faults along basin margin	Bounded by down-to-basin faults
Bounded by counter-regional faults	No salt under basin	Bounded by counter-regional faults
Salt evacuated	Located mostly at outer shelf, slope or deep water	Salt layer continuous
Located mostly at shelf or shelf edge		Located mostly at outer shelf, slope or deep water

Figure 6. Intrasalt basin classification. Modified after Zhang (1994) and Simmons (1992).

Sequence Stratigraphy

The Mississippi River has dominated sediment supply to the northern Gulf of Mexico for at least the past 15 million years. At least 16 major sea-level cycles and their associated sequences have been identified for the Pliocene-Pleistocene, and have been tied to paleo data (Figure 7). Amplitude, rate and frequency of sea-level changes are likely to affect patterns of slope deposition by contributing to the balance and timing of accommodation space, particularly in shelfal environments (Pulham, 1993).

Plio-Pleistocene strata in offshore Louisiana were deposited along an unstable progradational continental margin. Systems tracts differ greatly from those described for stable progradational continental margins (Figure 8) (Pacht et al., 1990).

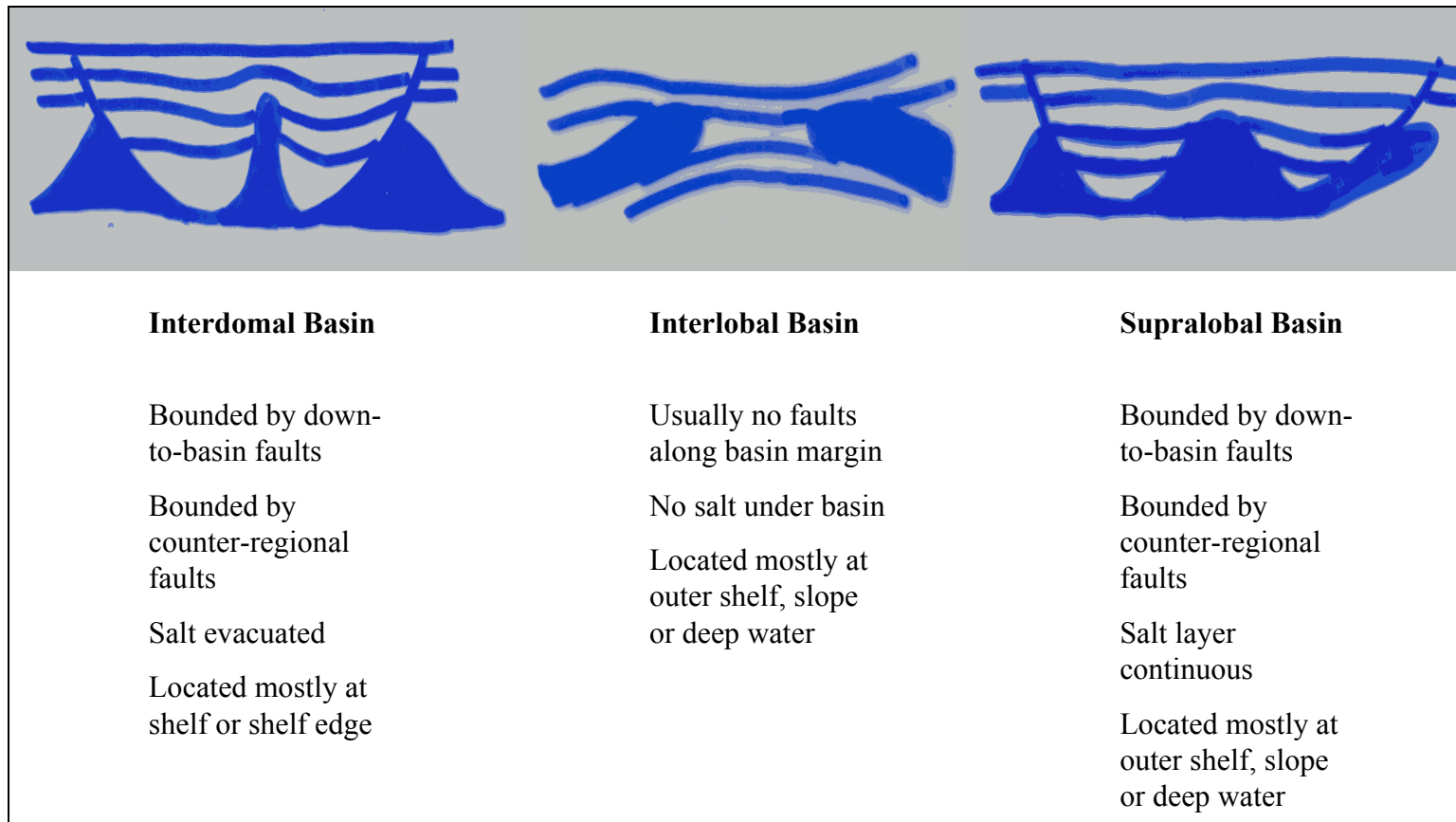Depositional sequences in Plio-Pleistocene strata offshore Louisiana are characterized by abundant peaks of planktonic microfossils at the top of the transgressive systems tract and lowstand slope fan (Pacht et al., 1990).

Many geoscientists have addressed many aspects of the Gulf of Mexico, specifically in the continental shelf margin offshore Louisiana. A classic paper from Stuart et al. (1977) documented seismic facies and sedimentology of terrigenous (from continental shelf to continental slope) Pleistocene deposits in northwest and central Gulf of Mexico.

Pacht et al. (1990) studied depositional facies and systems tracts from seismic reflection. Armentrout (1996) studied sequence stratigraphy during the late Pliocene – early Pleistocene of Ship Shoal 351 to Ewing Bank 988 (adjacent to the east from the
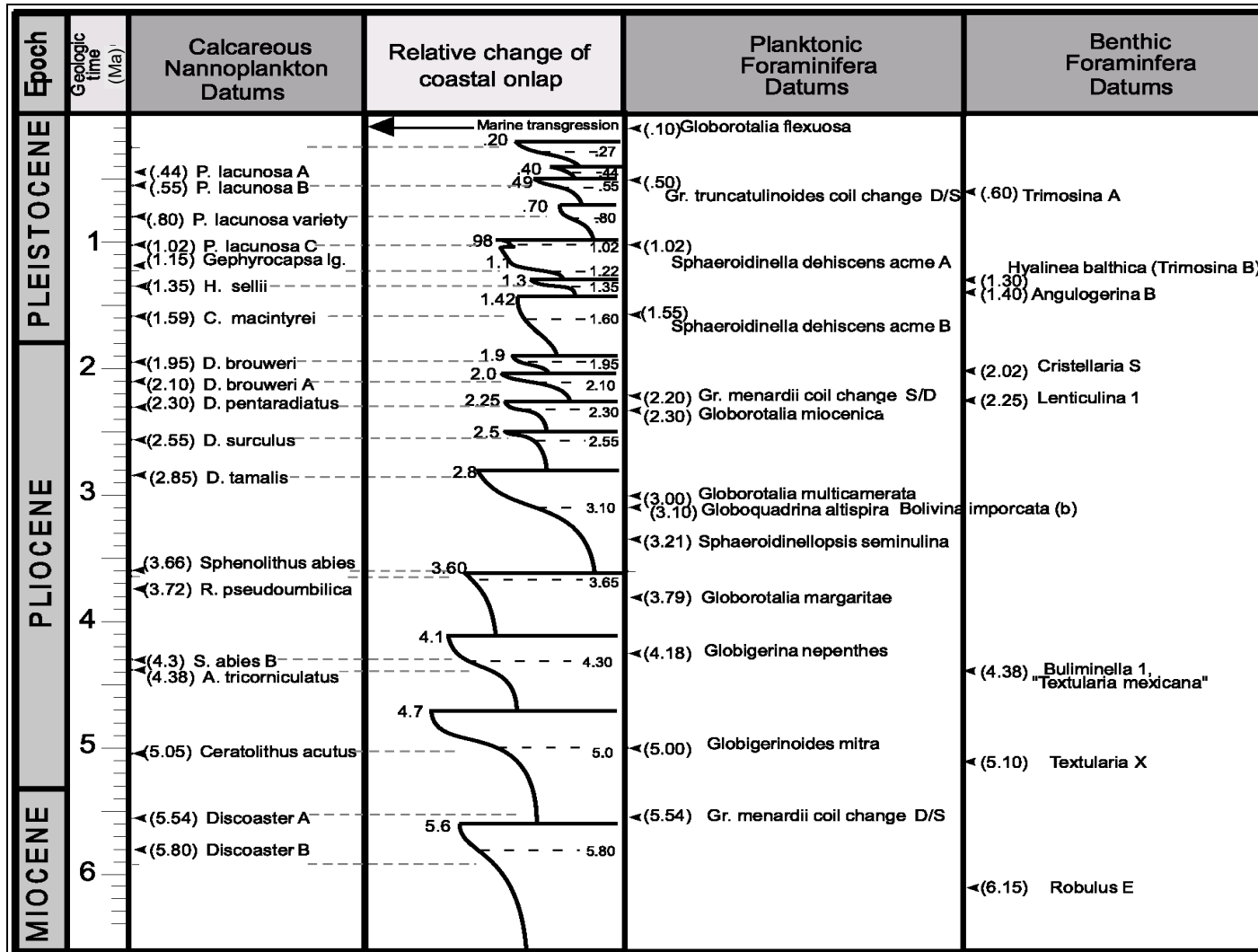
Figure 7. Sixteen major sea-level cycles during Pliocene-Pleistocene and their associated paleo data. After Crews et al. (2000). The salt reconstruction in this study begins from 3.65 Ma. The stratigraphic interpretation is in the 1.95 Ma to1.35 Ma interval.
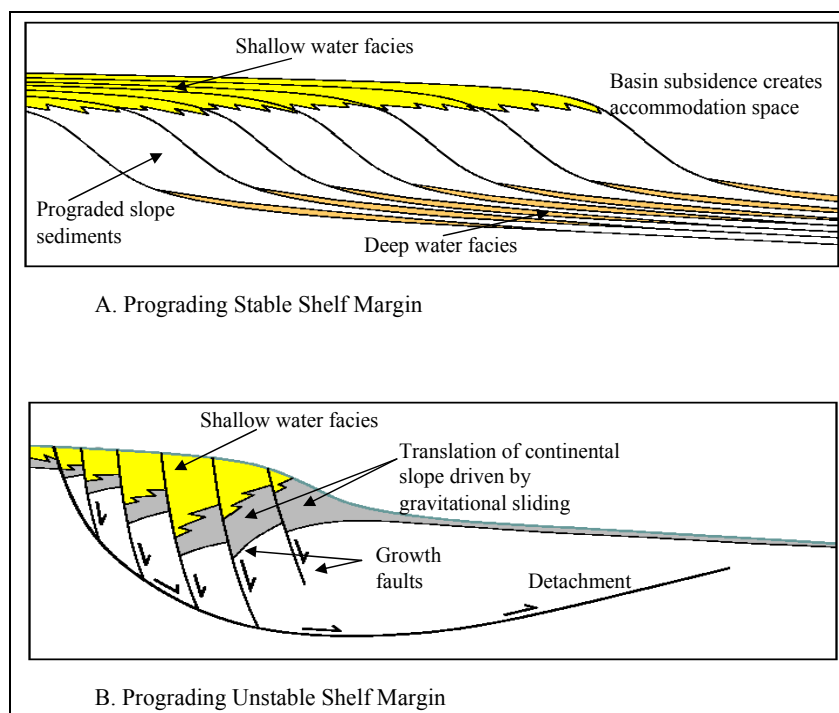
Figure 8. The difference between stable and unstable shelf margins. Offhore Louisiana was deposited along an unstable margin during Plio-Pleistocene. Modified from Edwards (2000).

study area) using high-resolution biostratigraphy analysis and interpreted depositional systems as channel lobe systems.

Many researchers (Zhang et al., 1993; Zhang, 1994; Acosta and Weimer, 1994; Martinez and Weimer, 1994; Budhijanto and Weimer, 1995; Navarro and Weimer, 1995; Weimer et al., 1998) have also analyzed the sequence stratigraphy of Pliocene-Pleistocene sediment of the north and central Gulf of Mexico. They generally conclude that most of the sequences consist primarily of channel levee systems and overbank deposits (slope-fan facies) (Figure 9).

Later publications documented an integrated approach to condensed-section identification of the Pliocene-Pleistocene using wireline logs, biostratigraphy data, mud-logs and seismic data (Crews et al., 2000).

Figure 9. Slope-fan facies depositional model in offshore Louisiana, north-central Gulf of Mexico. Adapted from Pacht et al. (1990).

Camp (2000) developed a geologic model and reservoir description in the area for deeper sections and described proximal levee, distal levee, basal levee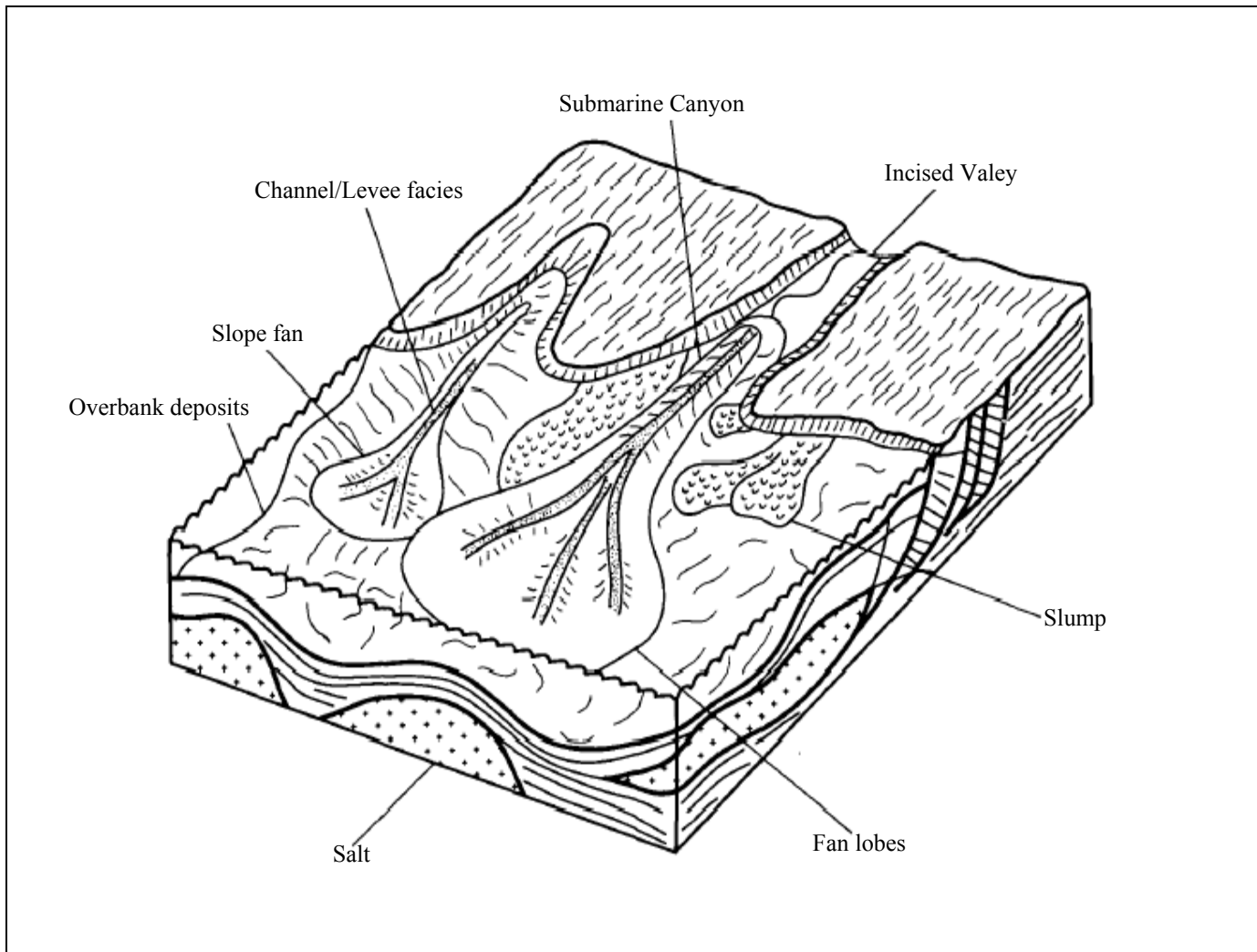, and channel-fill facies. The oil pay occurs primarily within the upper member of the submarine channel-levee deposit (Camp, 2000).

Systems Tracts Identification

A systems tract is a package of depositional units in three dimensions, characterized by the nature of its boundary and internal geometry. The term *systems tract* was first defined by Brown and Fisher (1977) as a "seismic-stratigraphic unit," and contemporaneous depositional systems as a three-dimensional assemblage of lithofacies, genetically linked by active (modern) or inferred (ancient) processes and environments.

Systems tract identification from seismic is different from well-log interpretation in terms of resolution and coverage area. Well-log data provide high-resolution data but small (local) coverage, while seismic data provide lower resolution but wider coverage.

Eustasy, subsidence, sediment supply and climate are the main factors affecting the development of systems tracts (Posamentier, et al. 1988). Each segment of the eustatic curve is associated with each systems tract. Curves of relative sea-level changes can be associated with systems tracts because a curve of relative sea-level changes is a function of eustatic changes and subsidence.

Sequence stratigraphic interpretations using well-log data are known as high-resolution sequence stratigraphy. Analysis of stacking patterns of prograding (forestepping) vs. retrograding (backstepping) log-motif funnels can define transgressive

vs. regressive depositional trends and candidate systems tracts and sequences (Figure 10) (Armentrout, 1999).

A lowstand fan consists of a basin-floor fan and a slope fan, recognized as a fan unit bounded by a condensed marine interval, where the fan package could be demonstrated to correlate with a basin-margin sequence (Emery and Myers, 1996). The basin-floor fan is dominated by sand and may be deposited at the mouth of a canyon. The gamma ray log response of this type of fan usually has an amalgamated or blocky shape (Figure 11a). The slope fan is usually made up of turbidite-leeved channel and overbank deposits overlying the basin-floor fan and is downlapped by the overlying lowstand wedge (Van Wagoner et al., 1990). The channel/overbank deposits in this systems tract is characterized by fining-upward sediments with sharp bases as a gamma ray log response (Figure 11b). "A lowstand prograding wedge is recognized as a prograding basin margin unit succeeding a sequence boundary, and bounded above by a maximum progradation surface" (Emery and Myers, 1996). The lowstand wedge is composed of one or more progradational parasequences with the gamma ray log characterized by a coarsening-upward signature (Figure 11c).

The transgressive systems tract is characterized as a group of retrogradational (backstepping) parasequences with prograding parasequences, fining and thinning upward and bounded below by transgressive surface and above by maximum flooding surface or the downlap surface (Figure 11d) (Van Wagoner et al., 1990; Vail and Wornardt, 1991; Emery and Myers, 1996).

Biofacies	Stacking Pattern	Cycle Shape	Log Profile	System Tract	
middle neritic / inner neritic	Back stepping Thickening Upward	Funnels		TST	back stepping wedge
condensed interval (ci)	Fore stepping Thinning Upward	Blocky / Funnels		TS/SB — ivf / SB? HST	fore stepping wedge
				mfs — cs	
inner neritic	Back stepping Thickening Upward	Funnels		TST	back stepping wedge
middle neritic	Fore stepping Thinning Upward	Funnels		TS / LST	pro-grading complex
outer neritic / ci	Crescentic	Spiky / Blocky / Spiky		LST	slope front thick
upper bathyal / ci	Crescentic	Spiky		LST	slope front thick
ci	Sharp based	Blocky		LST	basin floor thick
bathyal		Spiky		SB / HST	cs

Figure 10. Stacking pattern of lithology-log response associated with each systems tracts. Modified after Armentrout (1999).
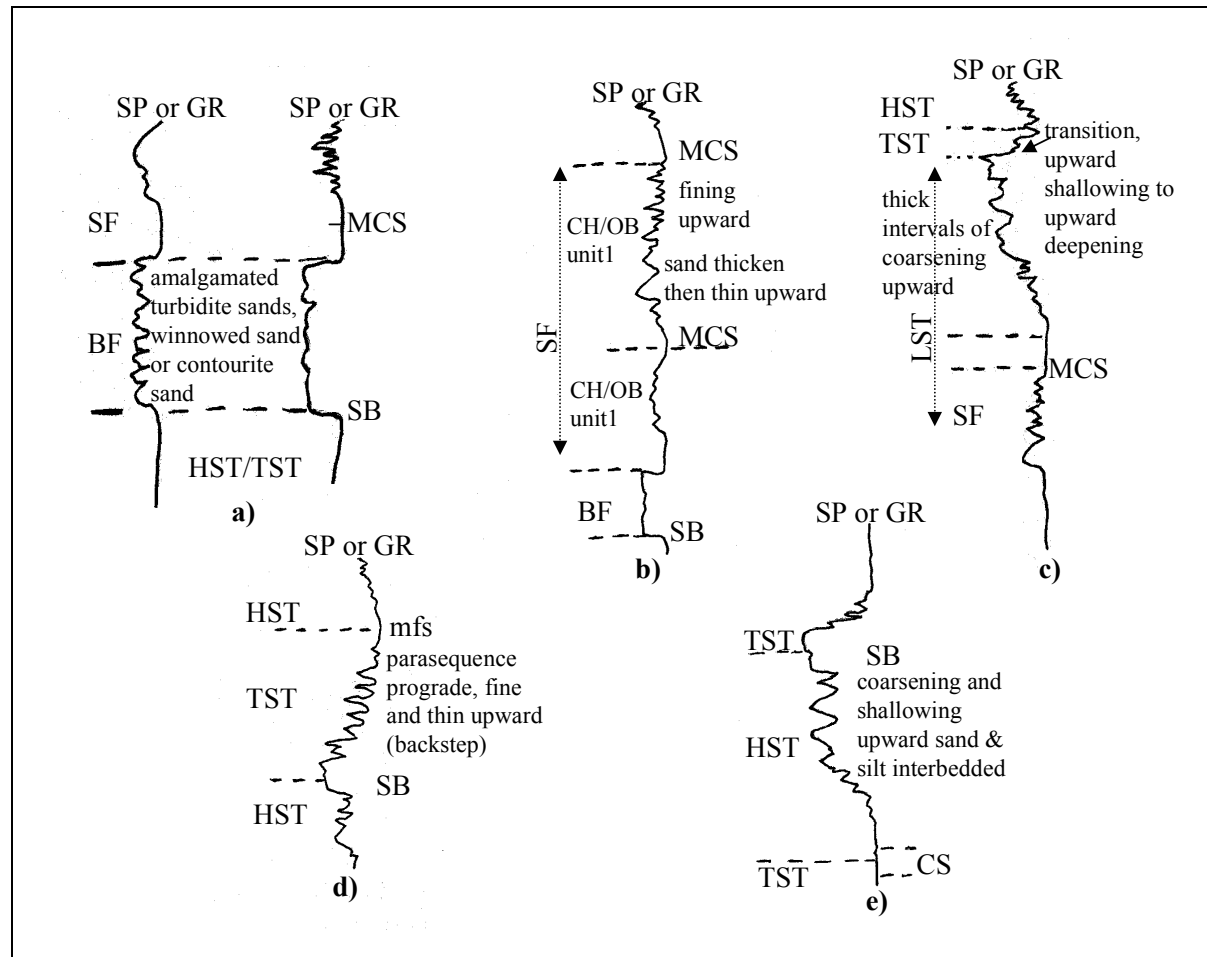
Figure 11. Systems tracts characterization from gamma ray (GR) or spontaneous-potential (SP) log response. Modified from Vail et al. (1991). BF=basin floor fan; CH/OB=channel/overbank; CS=condensed section; HST=highstand systems tract; LST=lowstand systems tract; MCS=Marine condensed section; mfs=maximum flooding surface; SB=sequence boundary; SF=slope fan; TST=transgressive systems tract.

The highstand systems tract is recognized as a prograding basin margin unit and characterized by a log signature that coarsens and shallows upward. It consists of interbedded sand and silt, bounded below by the downlap surface or maximum flooding surface and above by a sequence boundary (Figure 11e).

Salt-Sediment Interaction

Generally, three key controls on sediment dispersal within the late Tertiary and Quaternary in the Gulf of Mexico are (1) mobile salt, (2) sediment supply, and (3) eustatic variations in sea level (Pulham, 1993). Furthermore, Rowan and Weimer (1998) discussed the complex interaction between various structural and sedimentological factors that affect not only sediment dispersal but also lithofacies development in a minibasin into three factor categories: local factor, regional factor and external factor (Figure 12).

1. The local factors are specific in each minibasin. These factors include the mobile salt systems and local sedimentation rate, which create a local bathymetric gradient as a direct agent to lithofacies development.

2. The regional factors are those that influence geometry and content of surrounding sediment pathways and depocenters such as regional sedimentation rate, distribution of shelf deposystems and the geometry of surrounding salt structures.

3. The external factors are the factors that are largely determined by nature of the clastic input into the shelf or slope system, such as eustasy, size of drainage area and climate.
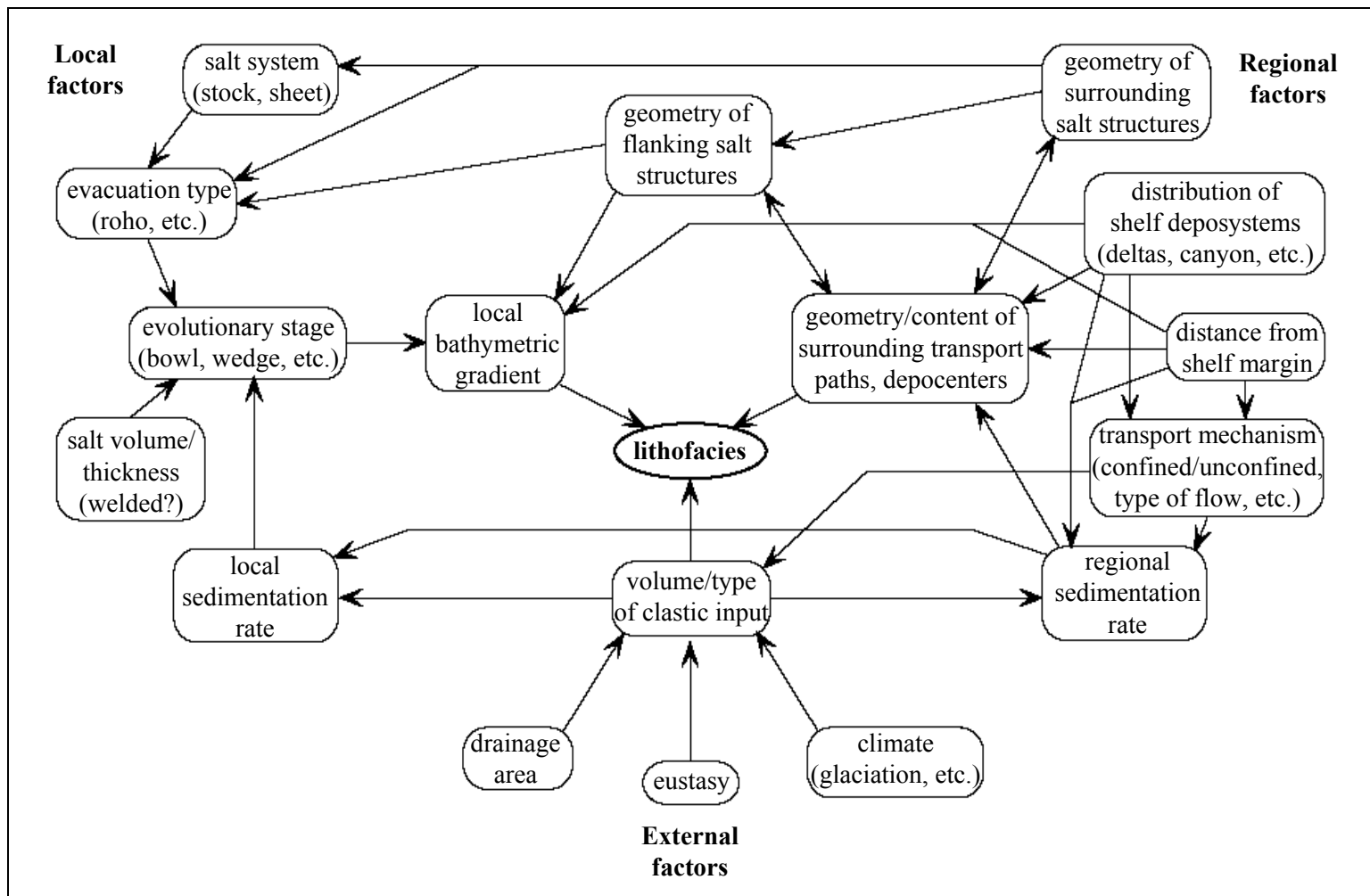
Figure 12. Complex interaction among structural and sedimentological factors that influence lithofacies development, Rowan and Weimer (1998).

CHAPTER III

RESULTS

Salt Structures and Distribution

Salt layers have higher velocities than surrounding sediments. Therefore, they have strong amplitudes on the top because of the high impedance contrast. In the study area, sonic log data indicate that the velocity of the salt varies from 14,500 ft/sec to 15,000 ft/sec and the density varies from 2.0 g/cc to 2.2 g/cc. Salt-body identification on the seismic section is relatively easy because usually the internal character of the salt body is reflection-free because of its homogenous material (Figure 13).

Well-log data show that the salt layer has a very low gamma ray response, very low neutron porosity (Figure 13), and high resistivity (about 10 to 20 times greater than surrounding sediment; Hoversten et al., 1998). The top and bottom of the salt over the study area has been identified and mapped (Figure 14,15,16).

The present-day salt covers almost all of the study area except a small area in the southeast corner (Figure 14). The depth varies from 4,800 ft to 11,500 ft with thickness varying from 500 ft to 4,300 ft with the average around 1,500-2,000 ft (Figure 15).

Locally, a small, bulb-shaped, salt-stock structure in the northwest and a sheet structure in southern have been identified (Figure 16). This structure is part of the Mahogany salt body which is a large allochthonous salt body, which has a trapezoidal shape in plan view (Rowan et al., 2001) and has boundaries that trend north-northwest

south-southeast and northeast-southwest. The entire the salt body in the study area is a
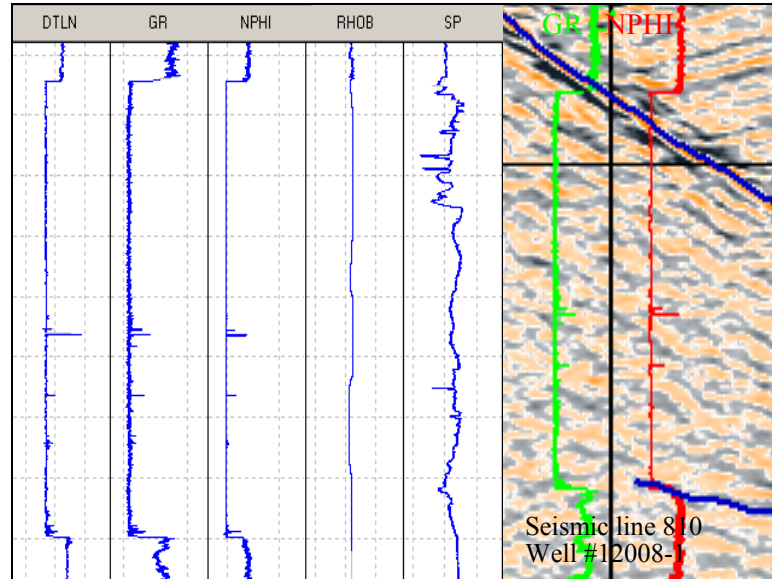
pennant-shaped structure.

Figure 13. Salt identification from well logs (#12008-1) and seismic (line 810).

The Supralobal Basin and Its Evolution

A small supralobal basin has been identified in the middle of the area between

SS349 and SS350 (Figure 17). It has a maximum dimension of 2 miles (3.2 km) in the

north-south direction and 2.9 miles (4.6 km) in the east-west direction. It was bounded

by counter regional fault trending northeast southwest.

The study area has significant deformation or evolution of the small supralobal

basin (or protobasin refers to Rowan et al., 2001) marked by its shifted depocenter
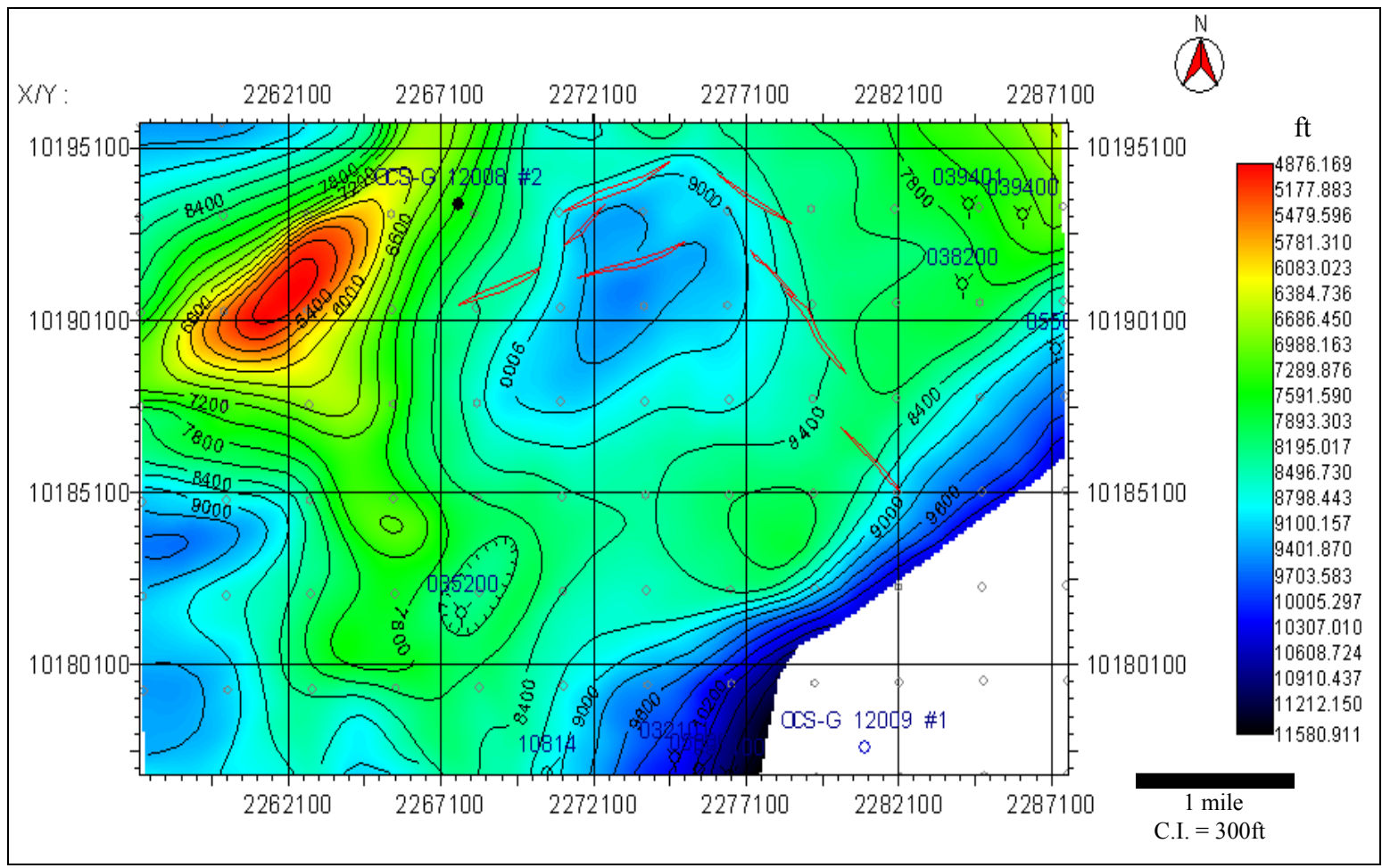
through time (Figure 18).

Figure 14. Present-day top of salt-structure map. The salt covers almost all of the study area.
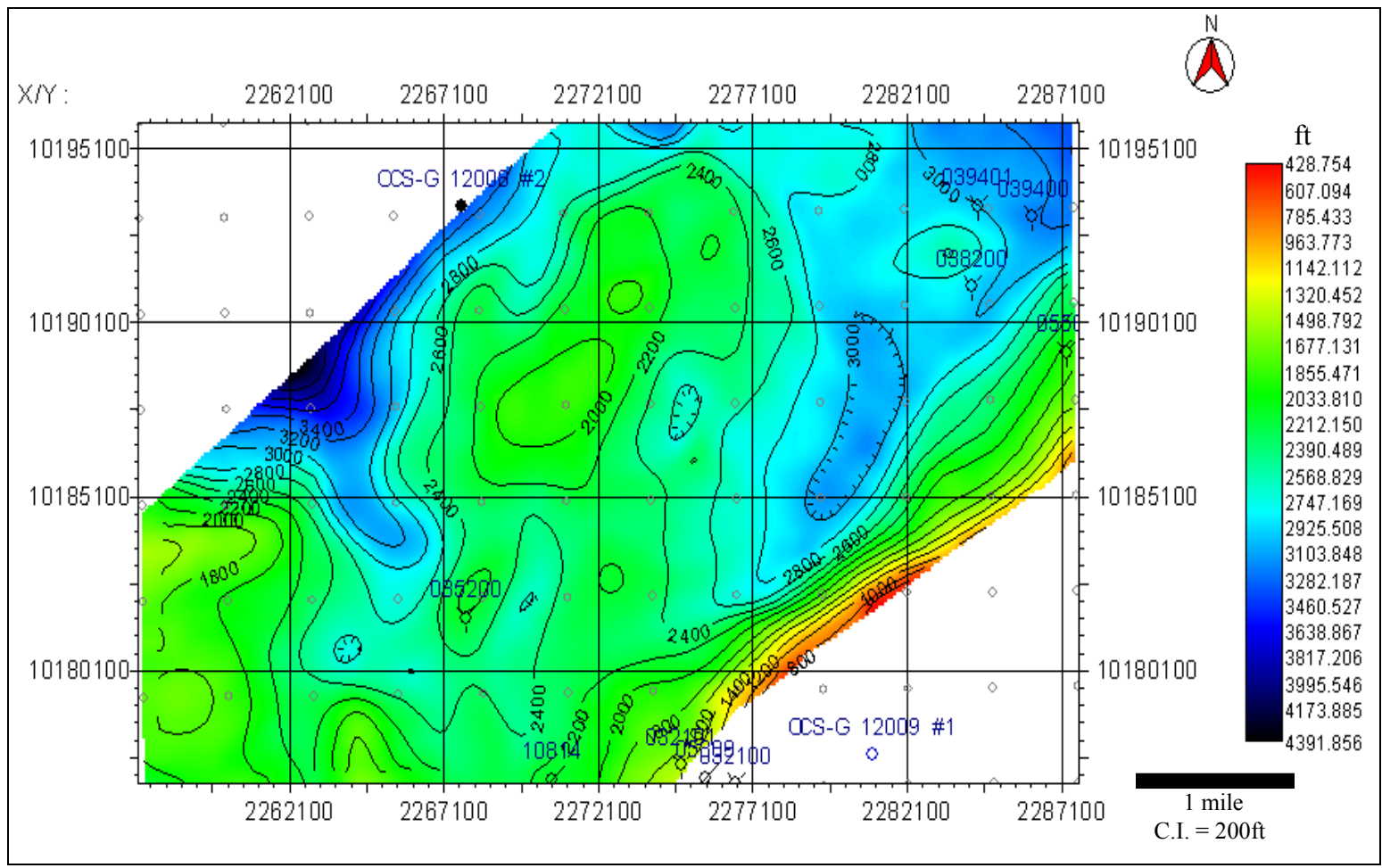
Figure 15. Isopach map of salt. Thickness varies from 500 ft to 4,300 ft.

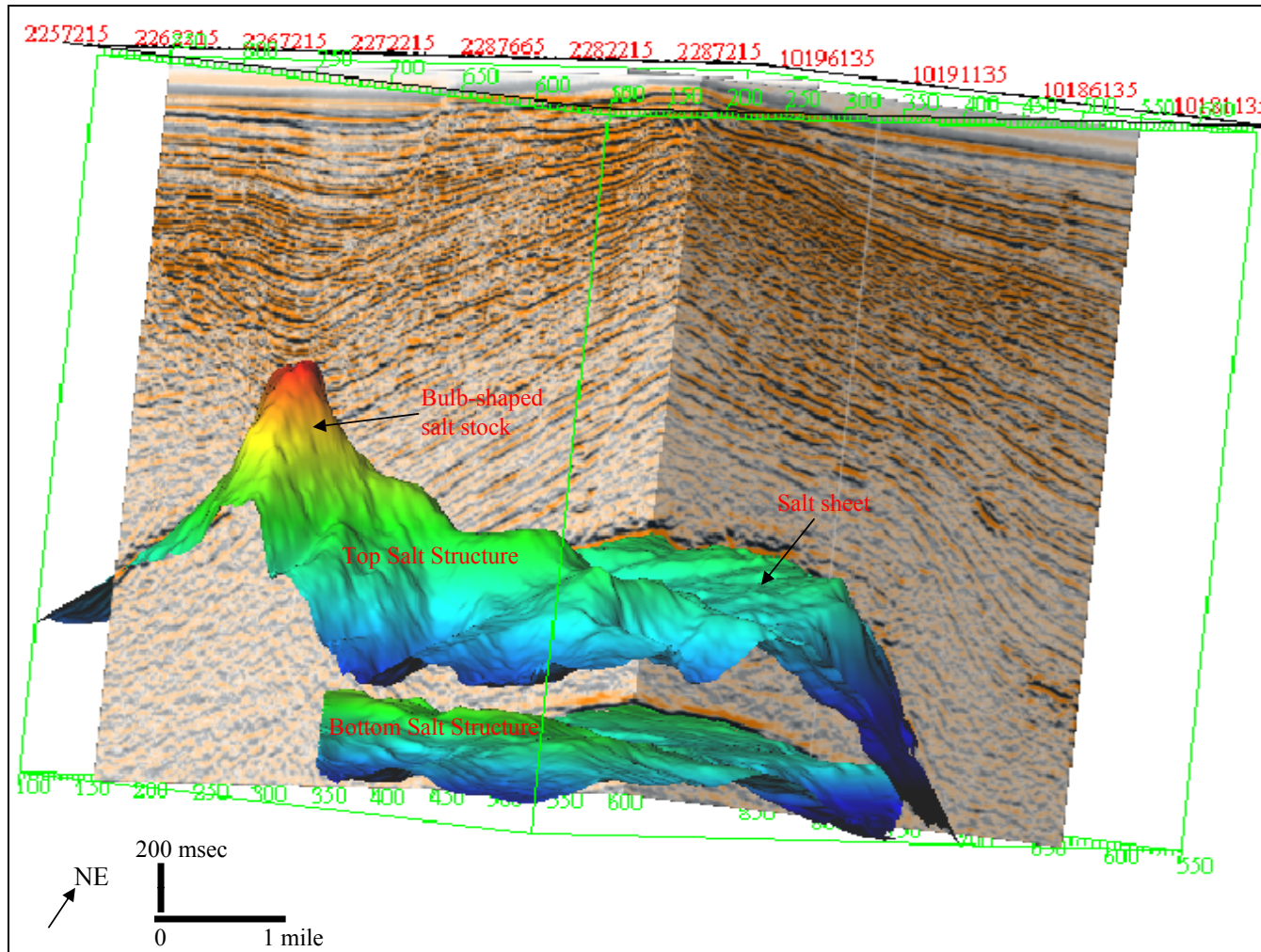**Figure 16**. 3D view of salt body toward NE direction with seismic section as background showing salt-structure distribution. A small, bulb-shaped salt stock is located in the northwest and salt sheet in the southern part. The whole area is similar to a pennant-shape structure.
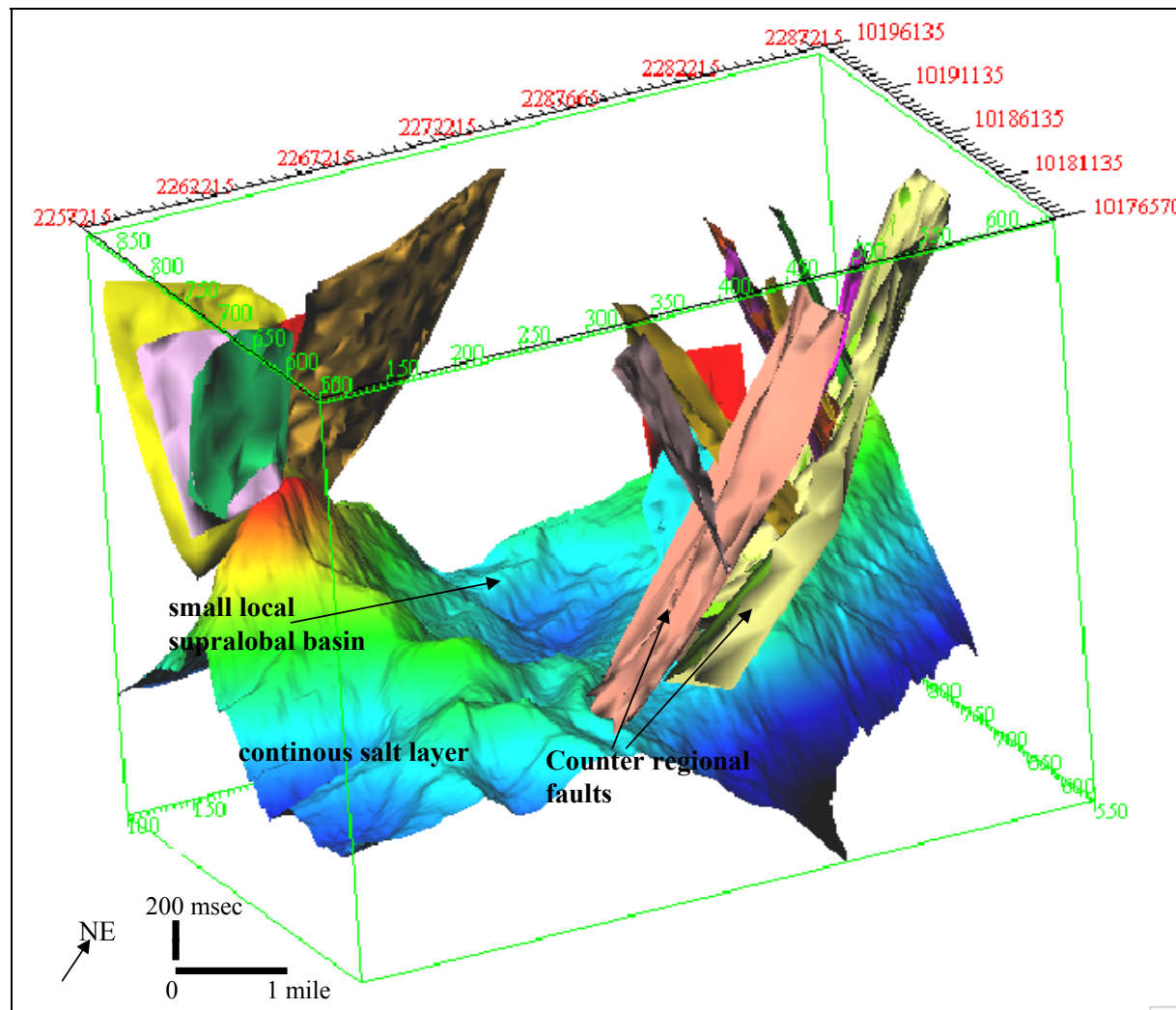
Figure 17. A small basin in the center of the study area classified as a supralobal basin bounded by counterregional faults.

A progressive flattening method was used for the paleotop surface (top salt) reconstruction. This method is basically an isochron method, which assumes that the isochron from a datum to the top of a horizon is the same as time to a horizon when a horizon (datum) was flattened. The reconstructions are based on certain data, which are flattened time by time (using 3.65 Ma, 1.95 Ma, 1.35 Ma, 0.80 Ma, and 0.27 Ma horizons as datum). Although this method is precise enough for evaluating the top of the salt locally in a small area such as the study area, it is not suggested for use in larger areas.

Two cross sections from line-810 and line-750 in Figure 19 show the result of paleosurface reconstruction in 2D. The oldest reconstruction was performed from 3.65 Ma. Because data are limited to a 3-sec vertical section length, no horizon older than 3.65 Ma has been interpreted. Therefore, no balance section has been created for this reconstruction.

The evolution of the local minibasin in the study area, based on 3D seismic interpretation results, is presented as follows (Figure 18).

A. 3.65 Ma stage

No basin or depocenter had been created at this stage. 3D paleo-reconstruction results in the area show that the salt was at a shallow depth and acted like a salt high. It is shown in red to yellow color in Figure 18a.

B. 1.95 Ma stage

A depocenter candidate of a small, supralobal basin bounded with a fault trending northeast-southwest and northwest-southeast marks this stage. The salt high moved to the northwest area and was deeper at this time (Figure 18b).

C. 1.35 Ma stage

The salt high became narrow, trending north-south in the west side of the area. The supralobal basin can be clearly seen in the northeast and expanding to the west. The depocenter had a bigger dimension at this time, approximately the same size as today's depocenter (Figure 18c). Counterregional fault trending northeast in the east was developed during this time.

D. 0.80 Ma stage

There was no significant deformation at this time except that the salt high became narrower to the north-northwest. The depocenter was greater and deeper at this time (Figure 18d). There was another small basin in the west side behind salt high.

E. 0.27 Ma stage

A significant change occurred during this period where the depocenter evolved to the southwest and became deeper. The salt high was evacuated to the northwest, forming a small, bulb-shaped structure (Figure 18e). Both small basins on the east and west sides become larger because of this evacuation. The faults trend northeast-southwest near the salt high in the west side of the area.
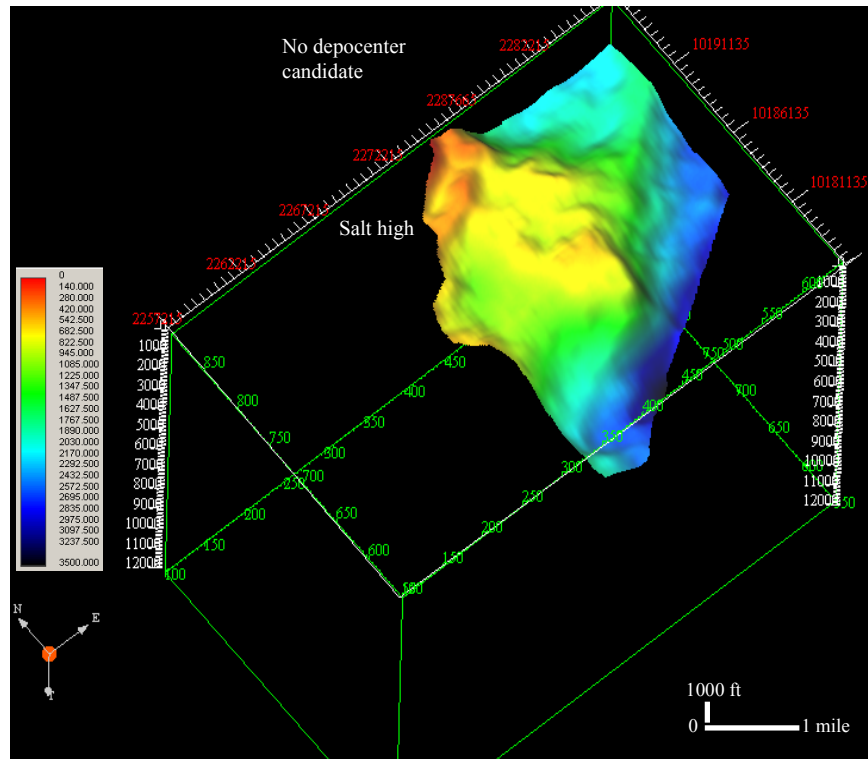
A. Top salt at 3.65 Ma.
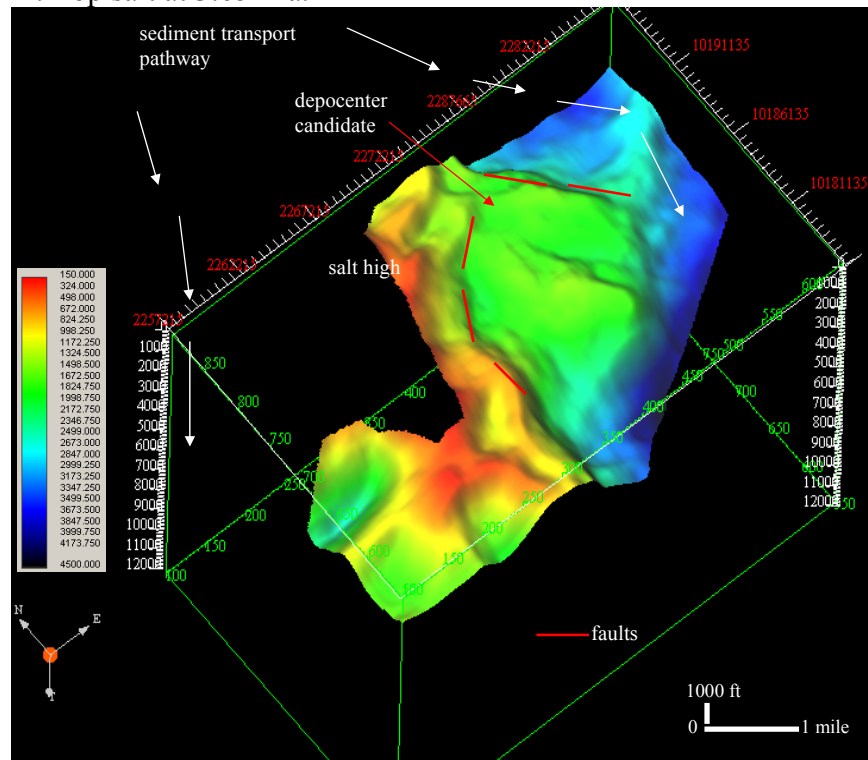
B. Top salt at 1.95 Ma.

Figure 18. 3D paleosurface reconstruction from 3.65 Ma to present   (continued).

C. Top salt at 1.35 Ma.
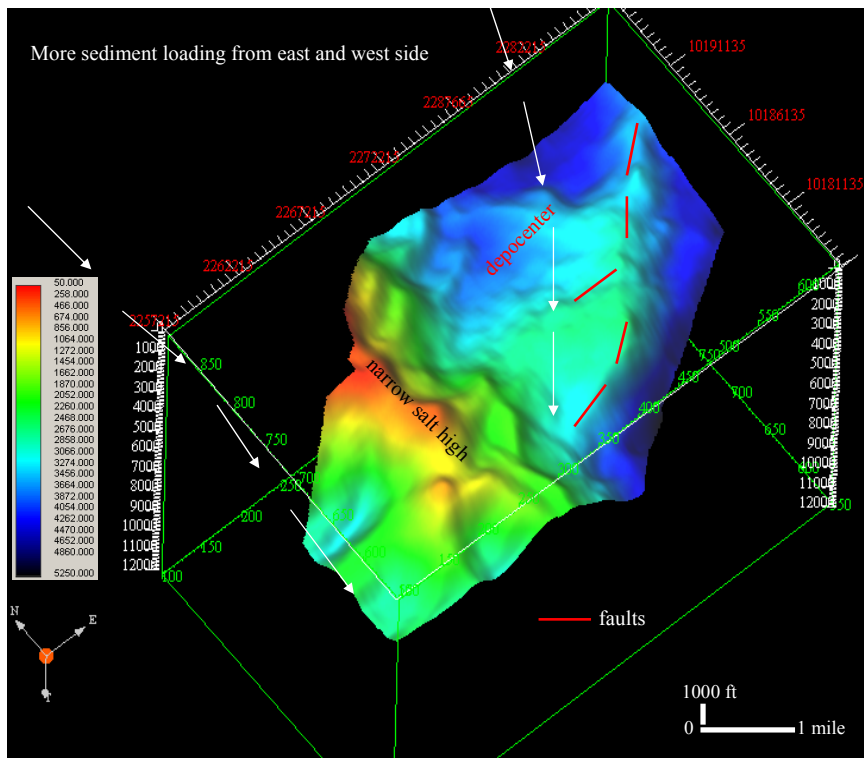

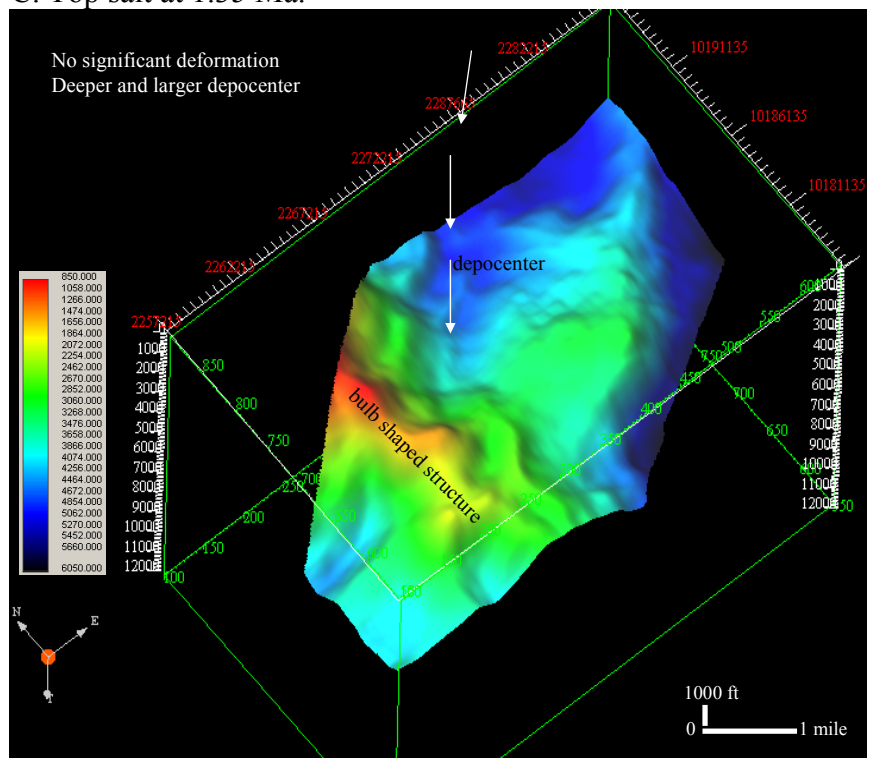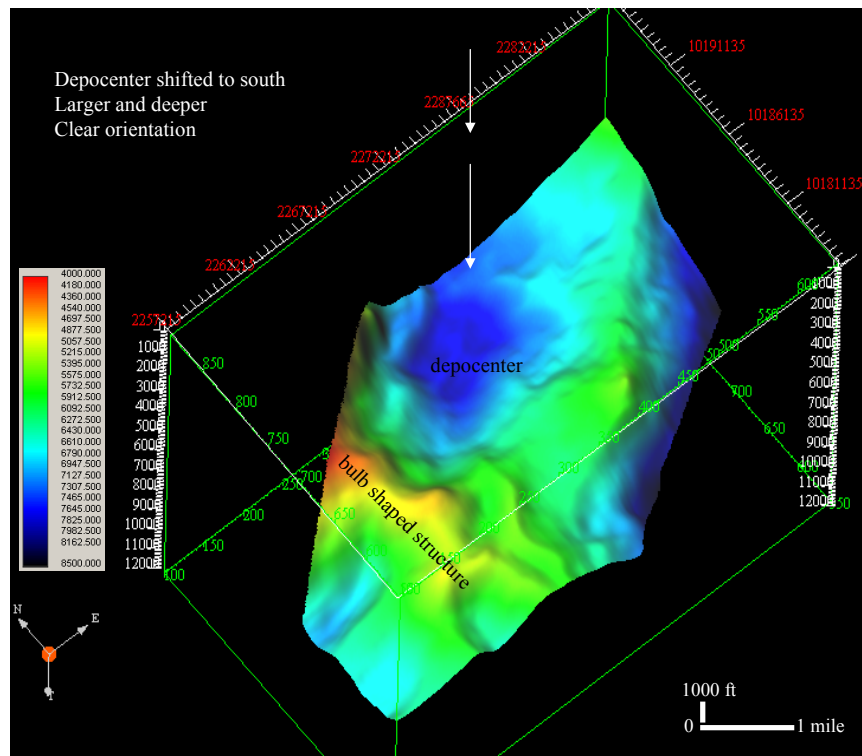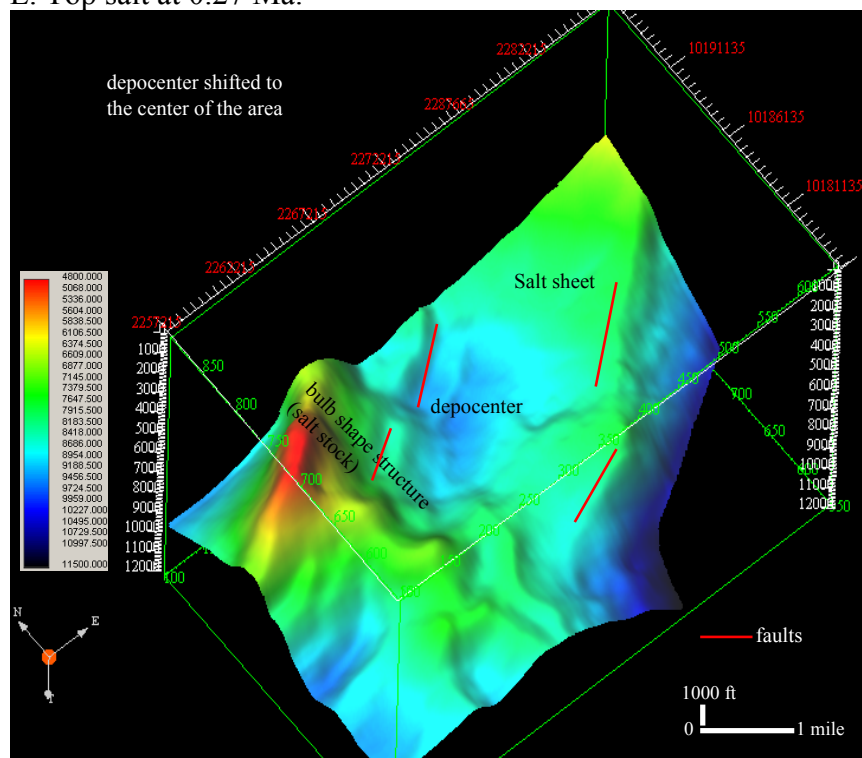D. Top salt at 0.80 Ma.

Figure 18. 3D paleosurface reconstruction from 3.65 Ma to present   (continued).

E. Top salt at 0.27 Ma.

F. Top salt at recent time.
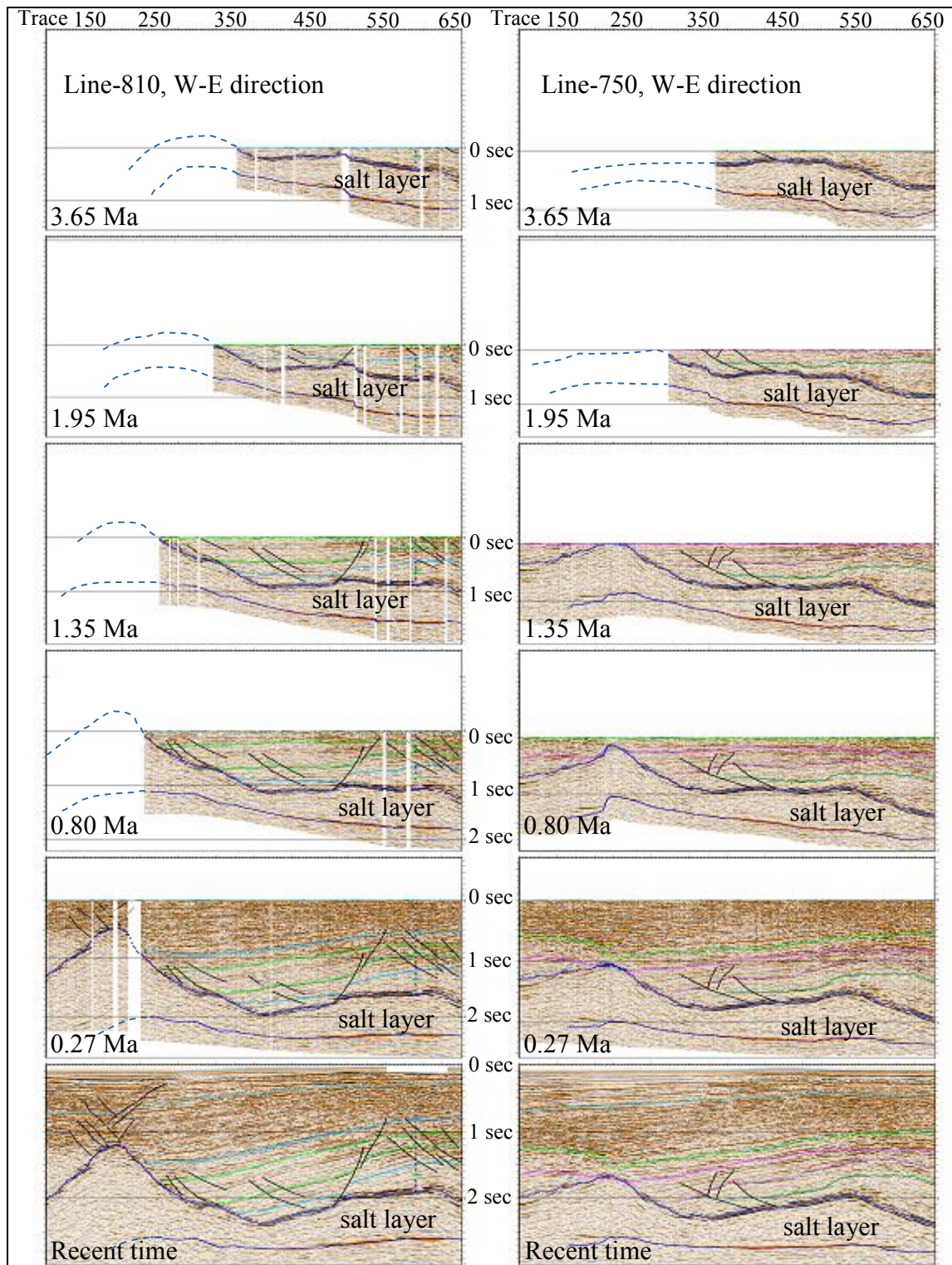**Figure 18**. 3D paleosurface reconstruction from 3.65 Ma to present.

Figure 19. 2D section from line 810 and line 750 showing the evolution through time since 3.65 Ma. Blue dashed line indicate hypothetical extent.

F. Recent time

After the depocenter shifted slighty to the southwest, it was now located in the middle of the study area. The small, bulb-shaped structure in the northwest and the salt sheet in the southeast have been perfectly formed (Figure 18f). There is no significant deformation in recent time. This small basin (the supralobal minibasin) is bounded by a counterregional fault trending northeast-southwest on both sides. Although there is no significant deformation, both the salt and the fault are still active.

Biostratigraphic Correlation

All the paleontologic data were obtained from United States Department of the Interior Mineral Management Service, Gulf of Mexico Region public report November 2000. It consists of four types of paleontologic data:

1. Calcareous Nannoplankton data (*Pseudoemiliania lacunosa* C, *Helicosphaera Sellii*, *Calcadiscus macintyrei*, *Discoaster brouweri*, *Discoaster surculus*, and *Sphenolithus abies*).

2. Planktonic Foraminifera data (*Globorotalia miocenica*, *Globoquadrina altispira*, *Sphaeroidinellopsis seminulina*, *Globorotalia margaritae*, and *Globigerina nepenthes*).

3. Benthic Foraminifera data (*Trimosina* A, *Trimosina* B, *Leticulina* 1, *Valvulineria* H, and *Buliminella* 1).

4. Paleotops data (Pleistocene and Pliocene).

Not all of those data types were available on every well location. The paleontologic data were combined with a biostratigraphic chart (Figure 20) and then tied to the seismic section.

Five horizons with sequence stratigraphic significance were chosen. These represent a maximum flooding surface (mfs) or condensed section or near maximum flooding surface and condensed section. Figure 21 refers to the biostratigraphic chart in Figure 20 (~0.27 mfs, ~0.80 mfs, ~1.35 mfs, ~1.95 mfs, ~3.65 mfs). The "~" sign is used because the paleontologic data were not complete enough to determine all those horizons perfectly. Therefore, the horizons are more interpretatively related to seismic character.
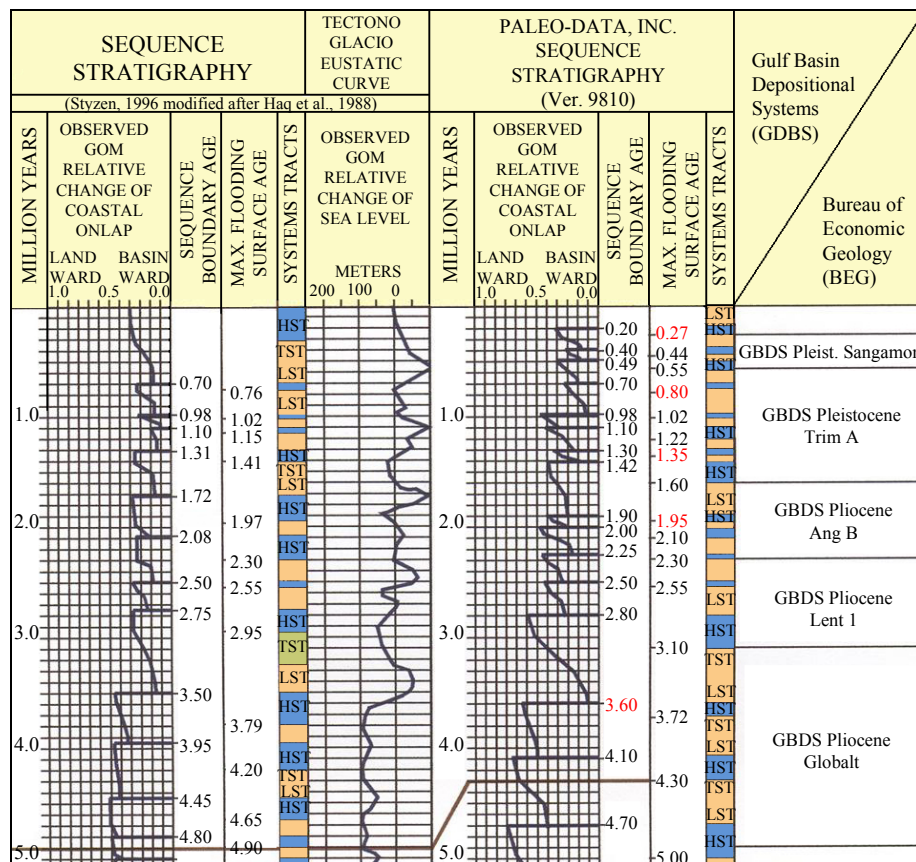
Figure 20. Biostratigraphic chart used in the study. Red color is the age associated with interpreted horizons. Modified from Paleo-Data Inc. version 9810 of PGS Inc., D'Agostino (1999).
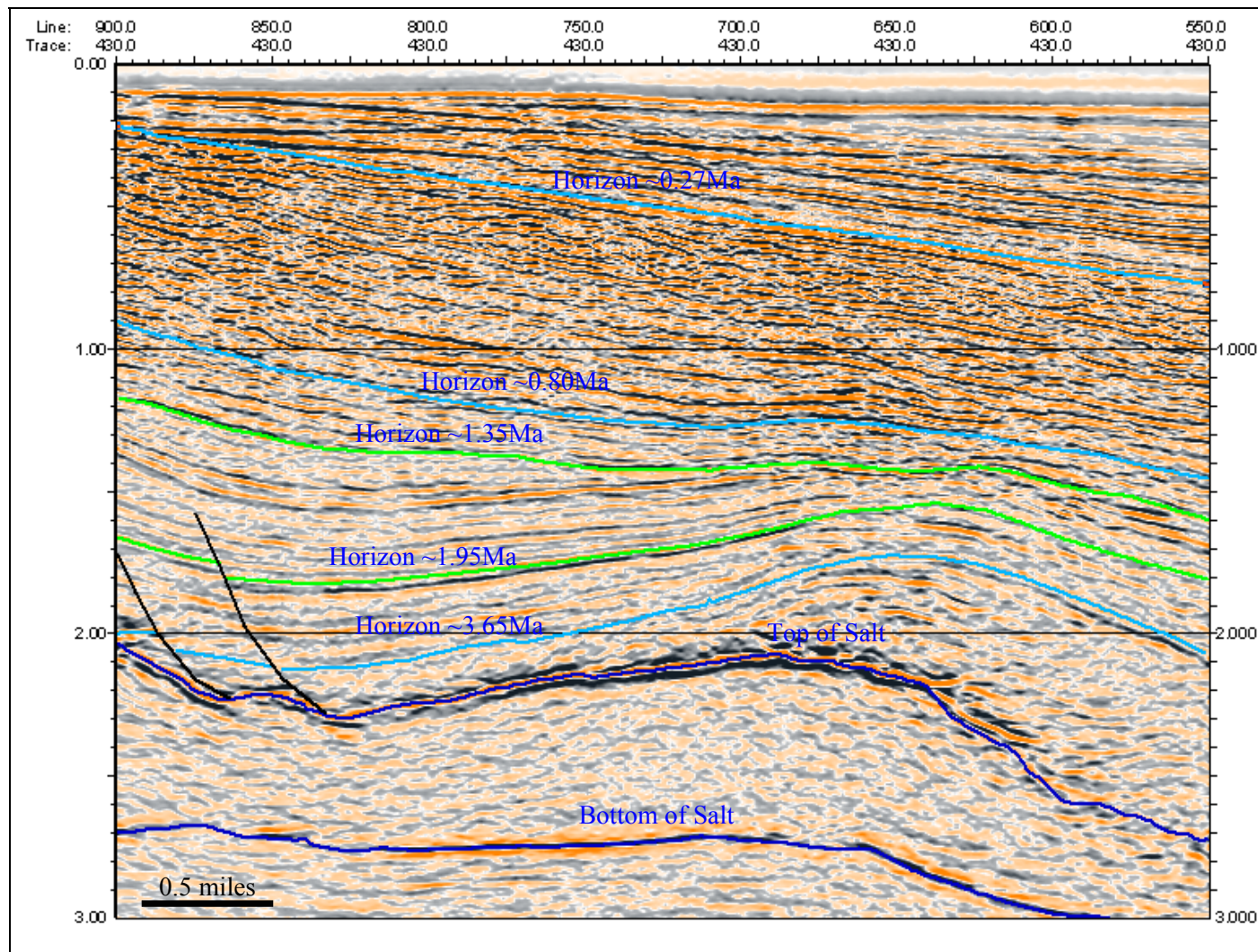
Figure 21. Seven horizons interpreted in this study. Sequence stratigraphic interpretation and seismic attribute analysis are discussed only between 1.35 Ma and 1.95 Ma (the green horizons) interval.
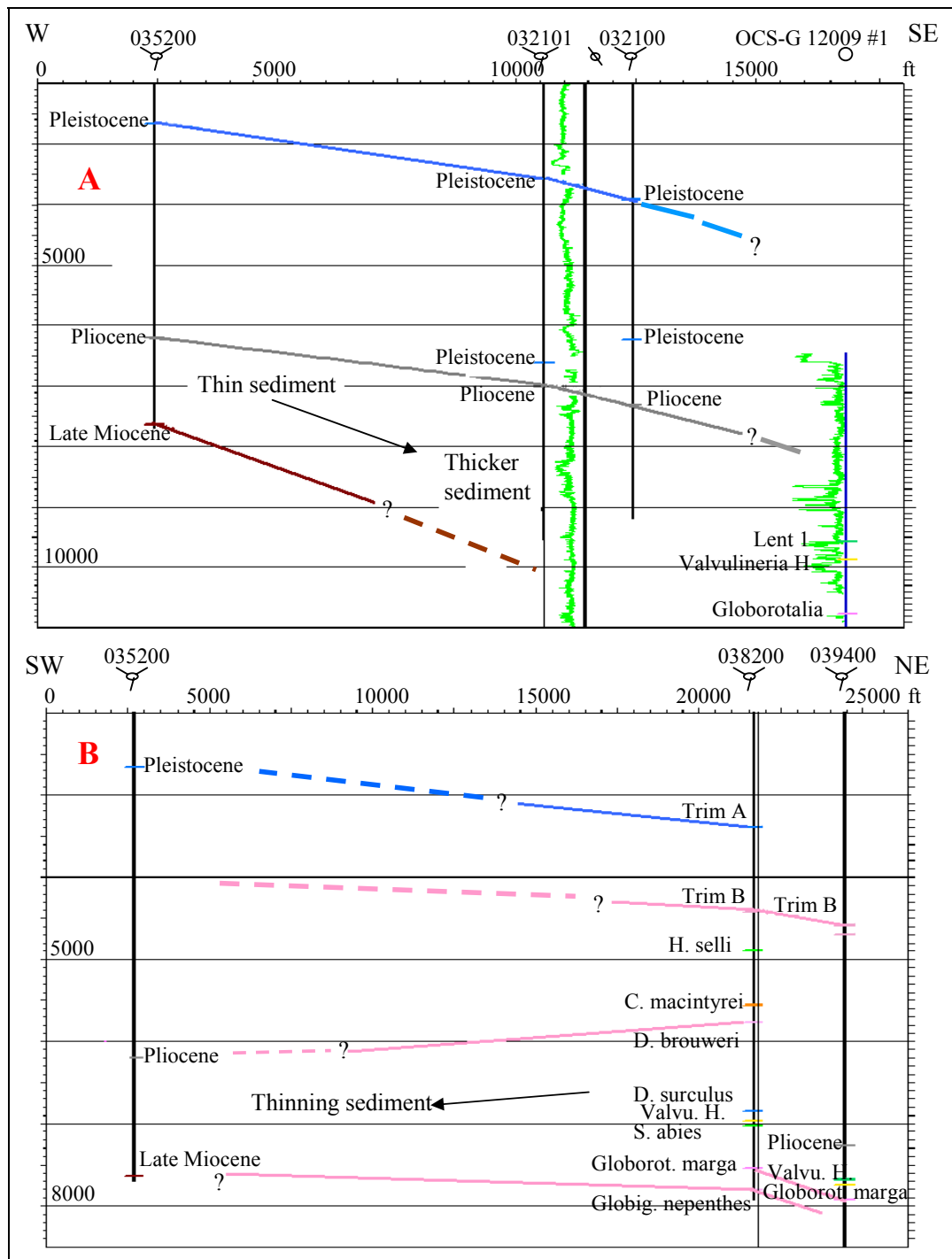
Figure 22. Paleontologic correlation suggests thinning sedimentation to the west and thickening to the south. The well symbol and its name are the same as shown in Figure 1. See Figure 40 for location.
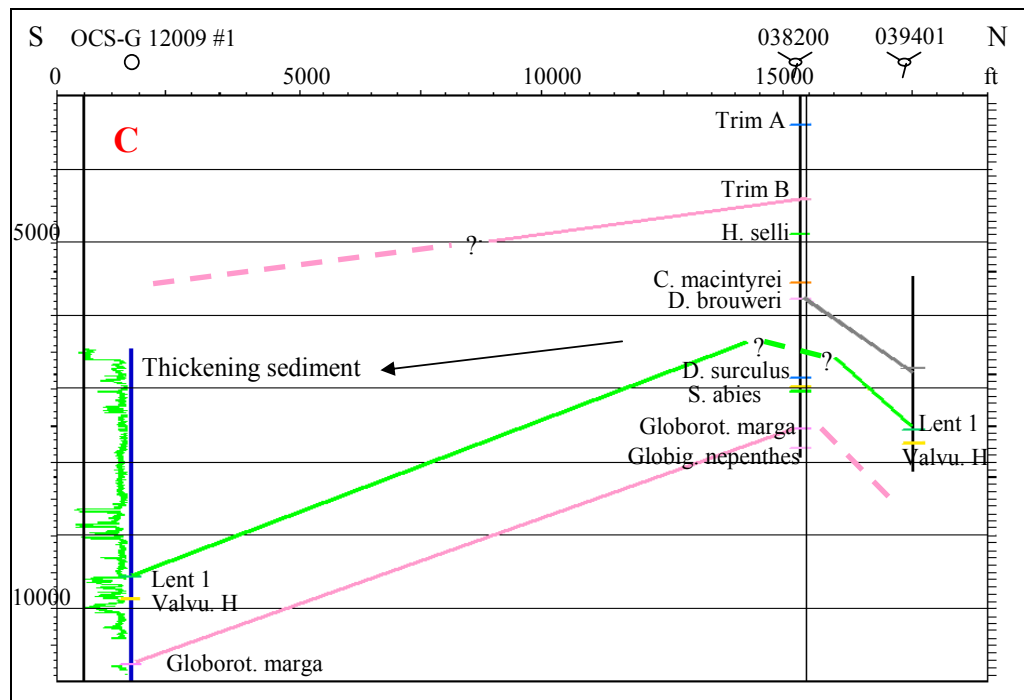
Figure 22. Continued.

These horizons were used in paleosurface reconstruction for the top of the salt in the previous section.

Paleontologic correlation was difficult because of the limited data. Therefore, paleontologic correlation is quite speculative. Paleontologic correlation shows that the thickness of the sediment between late Miocene and Pliocene thins towards the southwest (Figure 22a, 22b). Onlapping sediments to the salt edge on the seismic section in Figure 23 (line-810) supports this indication of thinning.

Although thinning also occurred in the northeast during the Pliocene (Figure 22b), no onlap has been identified on seismic sections. The sediment thinning in the northeast happened because of the salt extrusion to the south, forming a contractional fold in the northeast southwest direction (Figure 24). Thickening also occurred to the southeast (Figure 22a, 22c) because salt extrusion did not reach this area.
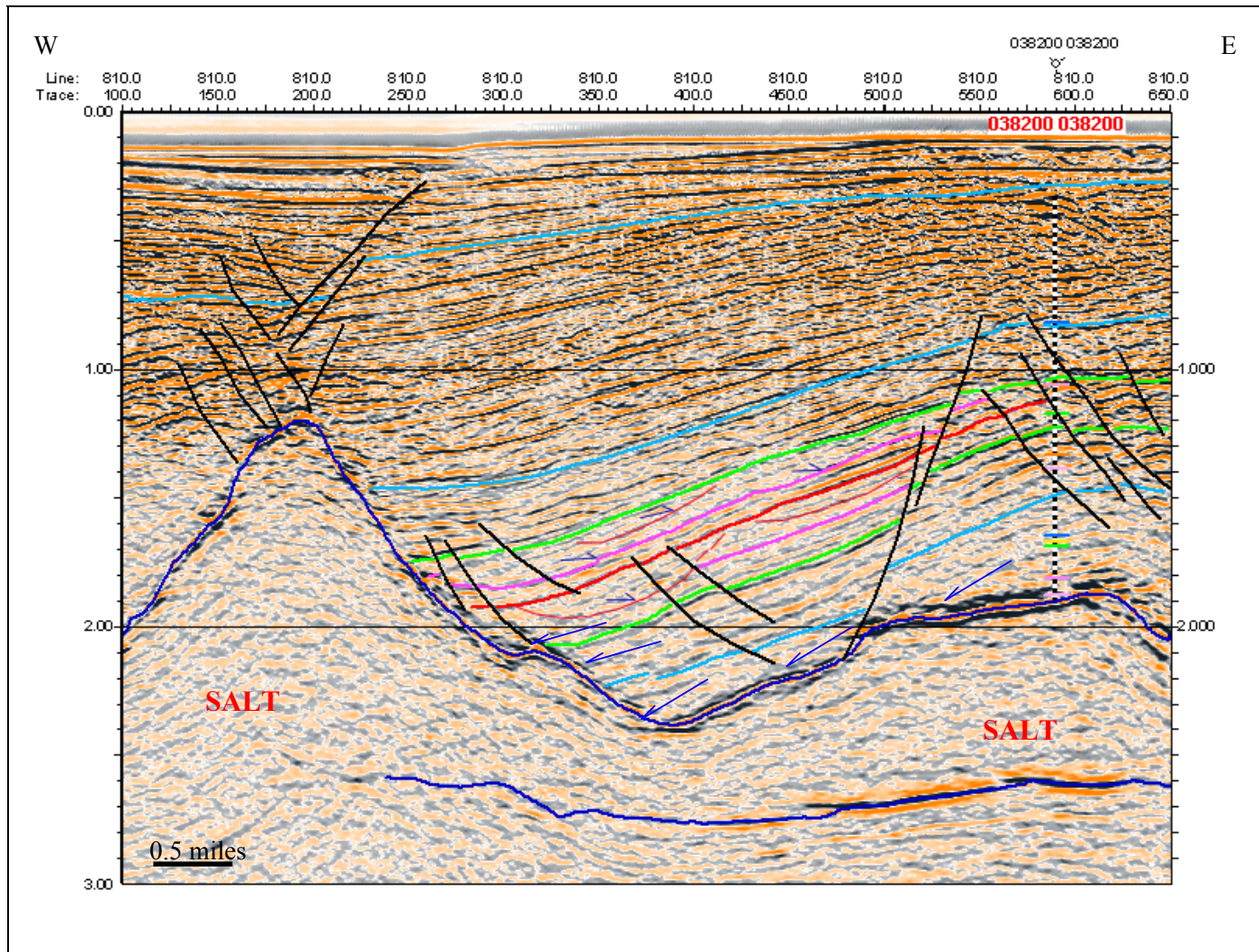
Figure 23. Onlapping sediment to the edge of top salt (blue arrows). Horizon names are the same as shown in Figure 21. See Figure 42 for location.
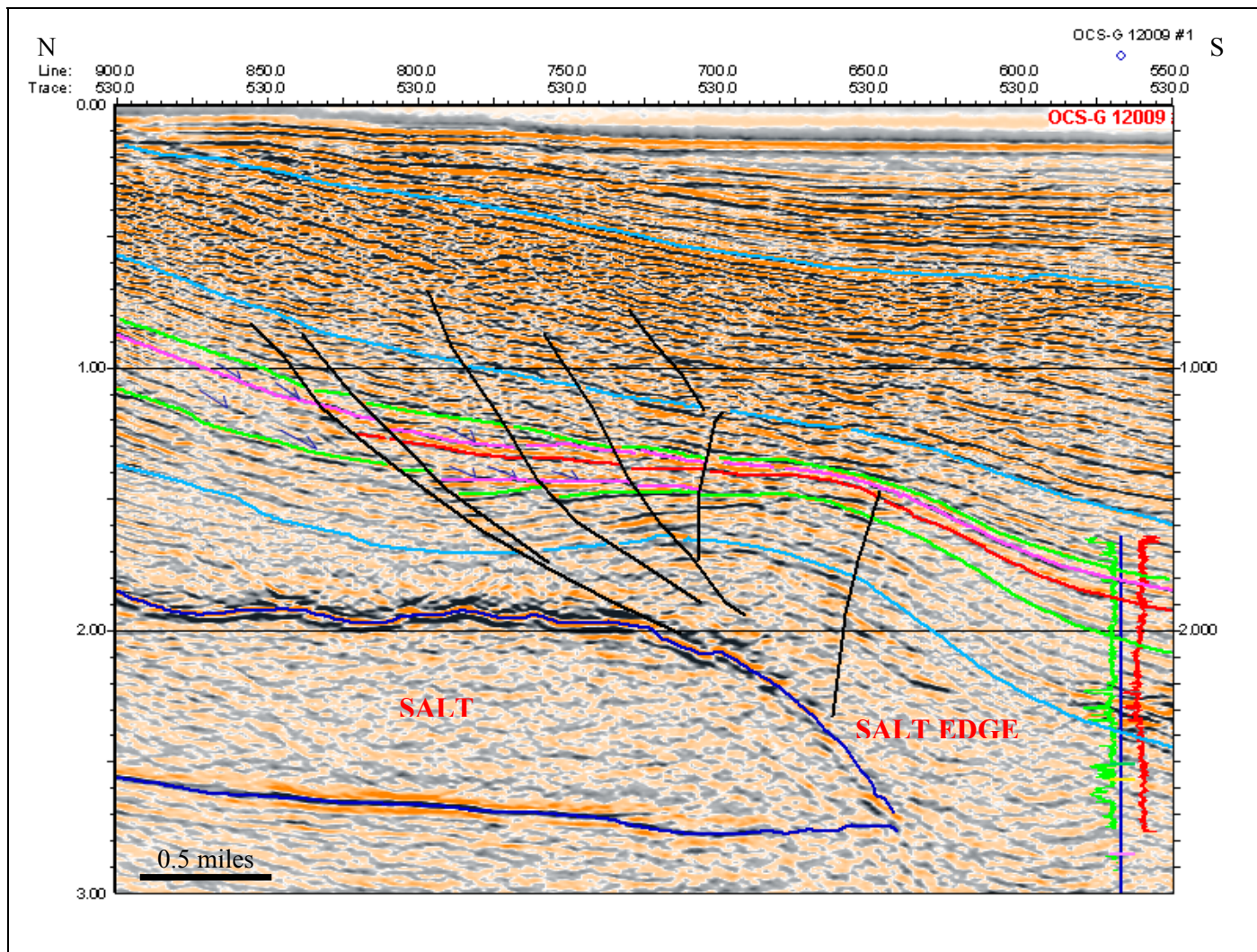
Figure 24. No onlap in the southeast area where the salt extrusion has ended. Salt extrusion forming contractional fold along the salt edge. Horizons are the same as shown in Figure 21. See Figure 42 for location.

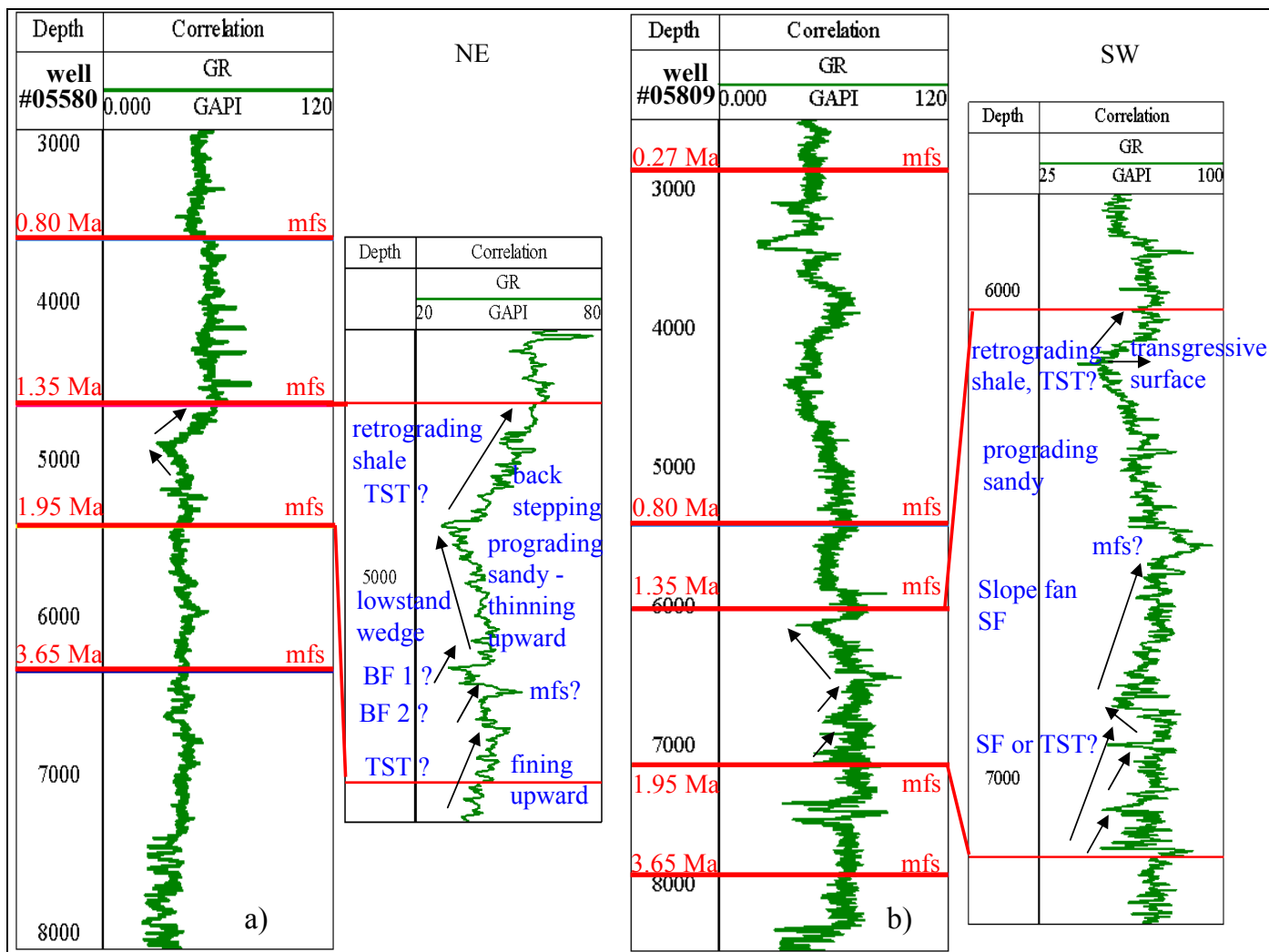**Figure 25**. Type log and its interpretation. a) Well #5580, b) Well #05809. Well location is outside seismic data coverage; see Figure 1 for location.
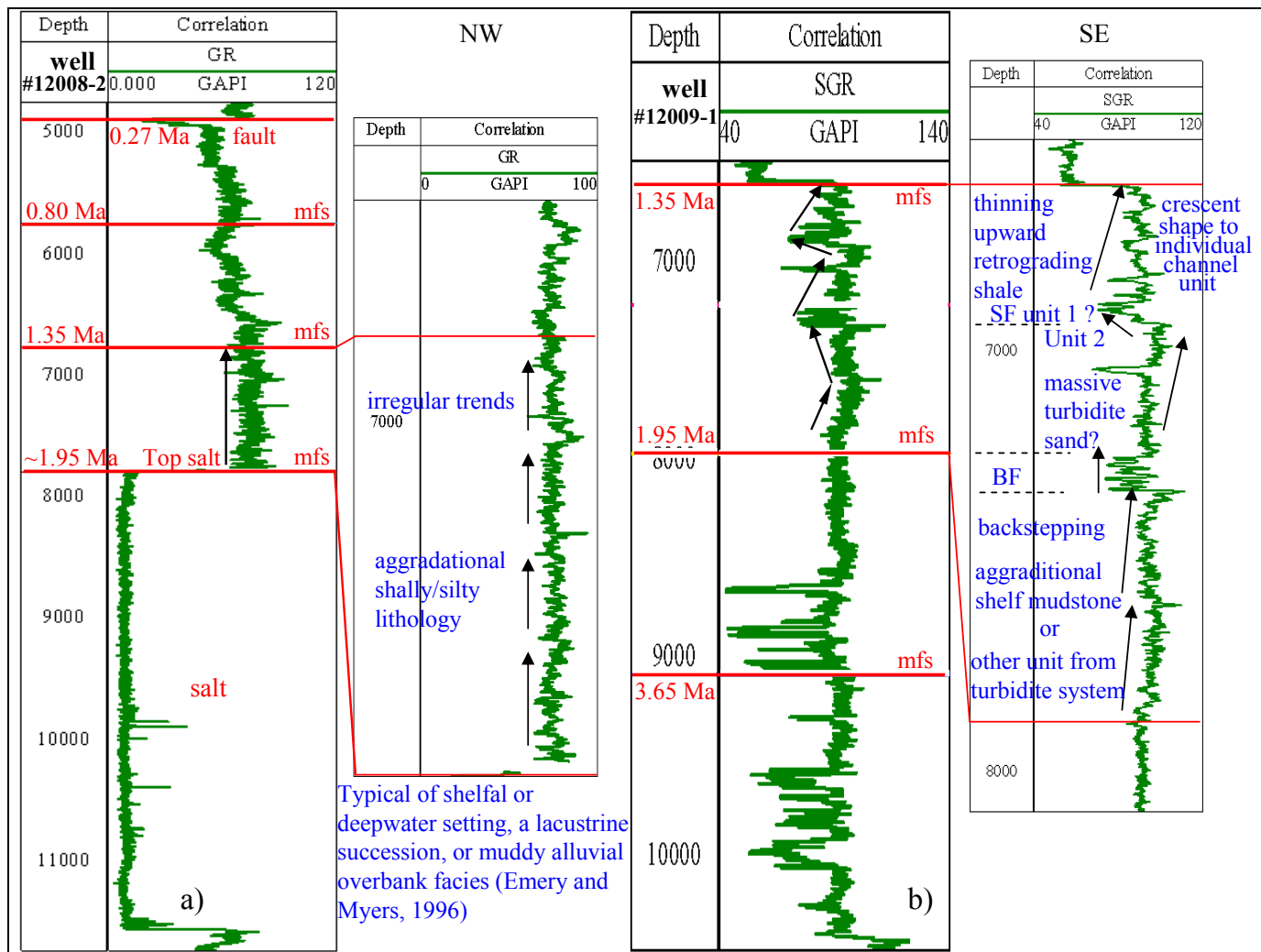
Figure 26. Type log and its interpretation. a) Well #12008-2, b) Well #12009-1. Well location is inside seismic data coverage; see Figure 1 for location.

Well Log Description

All well-log descriptions in this section come from gamma ray log responses as shown in Figure 25 and Figure 26 and will be explained from bottom to top between 1.35 Ma and 1.95 Ma.

The log response for well #05580 (Figure 25a) shows a fining-upward signature, indicating retrograding shale, followed by two blocky shapes with thickness around 100 ft. In the middle part, an approximately 200 ft thick thinning-upward cycle is observed, indicating a prograding sand. This is followed by a back-stepping pattern, indicating a retrograding shale cycle with the same thickness as the previous cycle.

The log response for well #05809 (Figure 25b) shows two 200 to 250-ft thick back-stepping patterns of sediment; these indicate retrograding shale cycles in the bottom part followed by an approximately 350-ft thick coarsening-upward sediment, indicating prograding sand. The top part is a back-stepping pattern that indicates a retrograding shale cycle with a thickness of 50-to100 ft.

The log response of well #12008-2 (Figure 26a) shows an approximately 1,000-ft thick aggradational pattern sediment with irregular trends, indicating a shaly/silty lithology.

The log response of well #12009-1 (Figure 26b) shows an approximately 600-ft thick aggradational pattern sediment followed by about a 100-ft thick blocky, irregular-shape cycle. The upper part consists of two back-stepping cycles with a thickness of approximately 250 ft each. The top one shows clear thinning-upward signature.

Well-log correlation was also established generally in the northwest-southeast and southwest-northeast direction (Figure 27, 28). Figure 27 is a structural cross-section, while Figure 28 is a stratigraphic cross-section. All cross-sections were interpreted along with seismic sections over the study area.
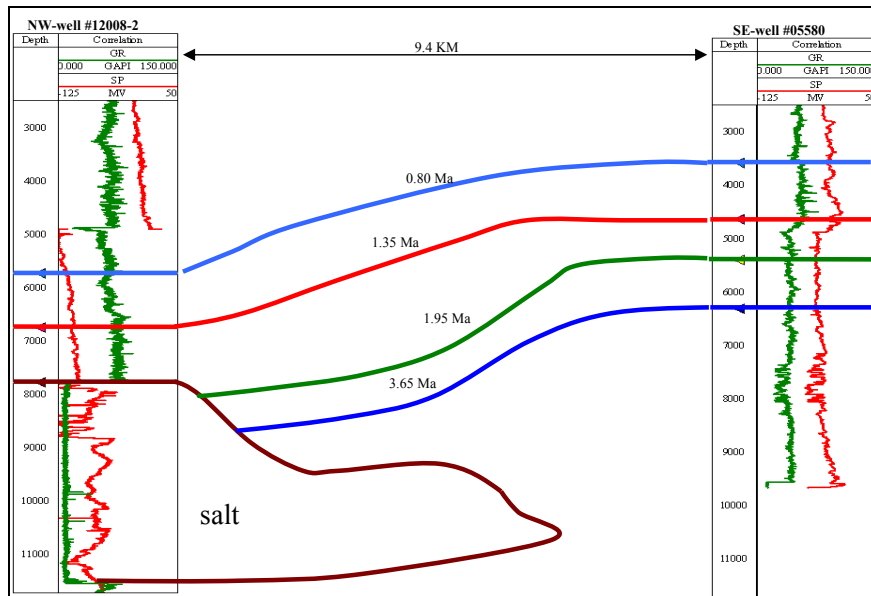
A. Correlation from wells #12008-2 and #05580 in NW-SE direction.
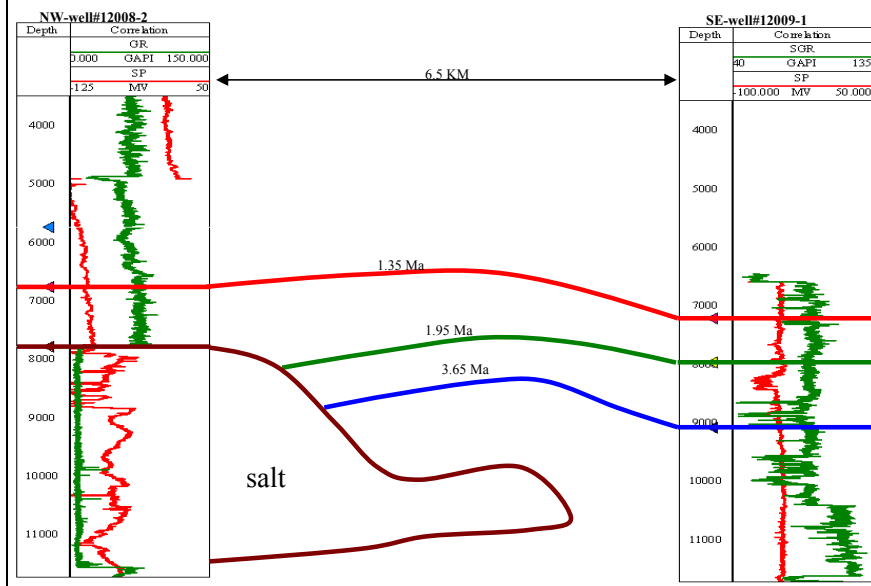
B. Correlation from wells #12008-2 and #12009-1 in NW-SE direction.

Figure 27. Structural cross-sections from the available well logs. See Figure 41 for location.
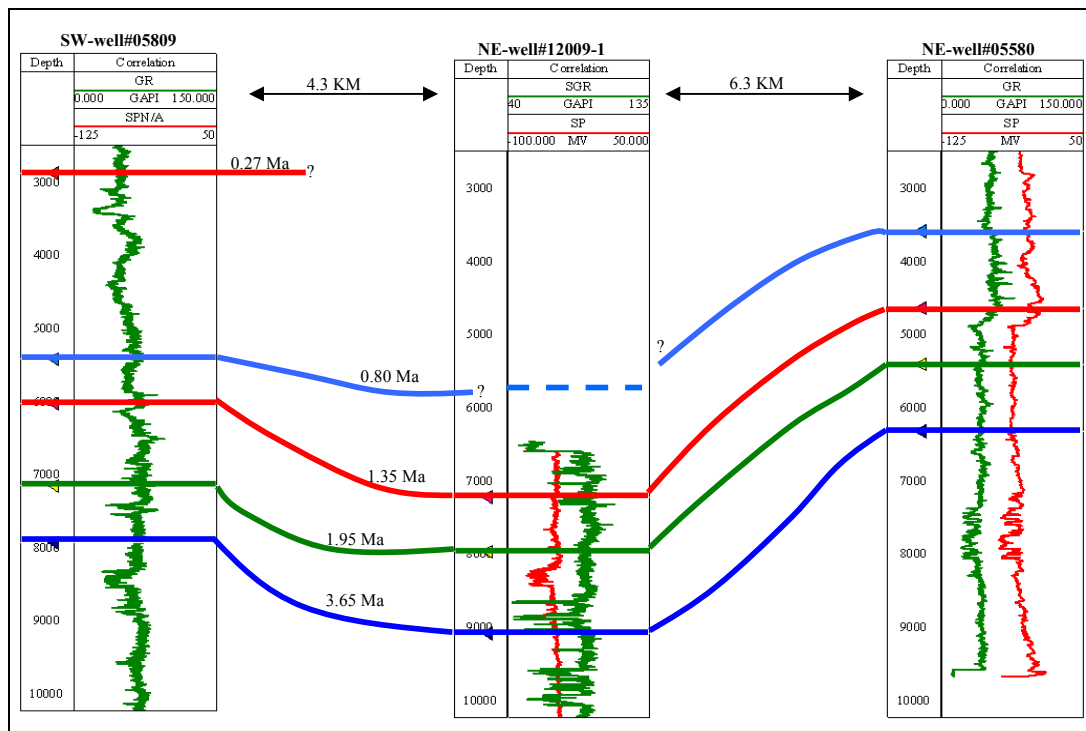
C. Correlation from wells #05809, #12009-1 and #05580 in SW-NE direction.
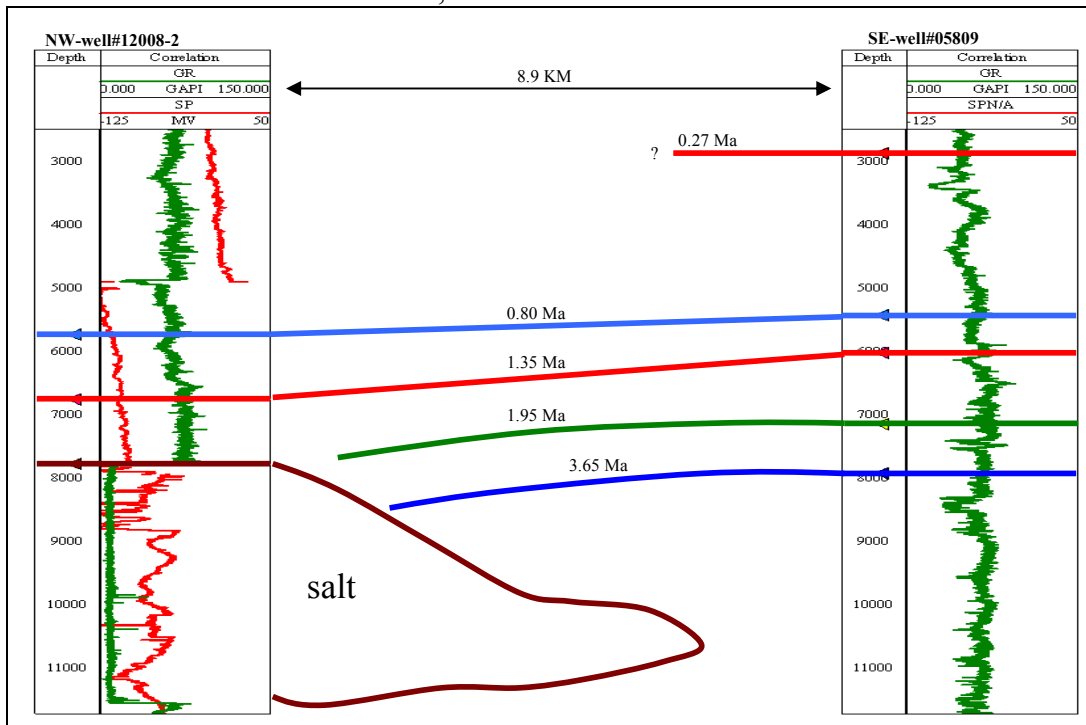
D. Correlation from wells #12008-2 and #05809 in NW-SE direction.

Figure 27. Continued.
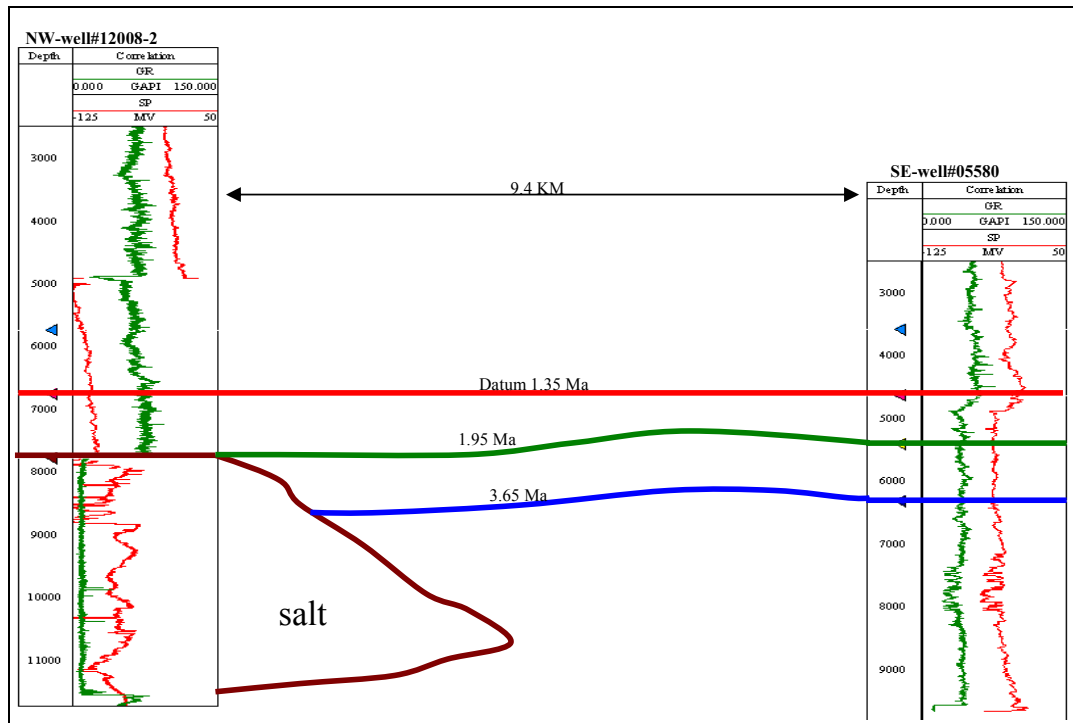
A. Correlation from wells #12008-2 and #05580 in NW-SE direction.
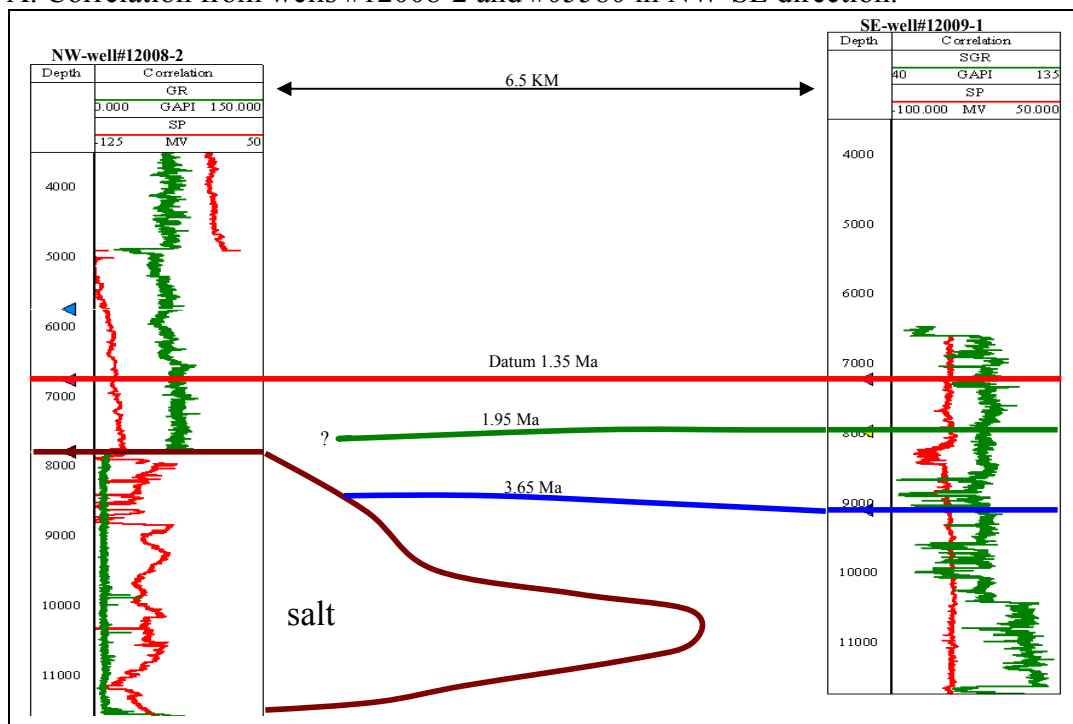
B. Correlation from wells #12008-2 and #12009-1 in NW-SE direction.

Figure 28. Stratigraphic cross-sections from the available well logs. See Figure 41 for location.
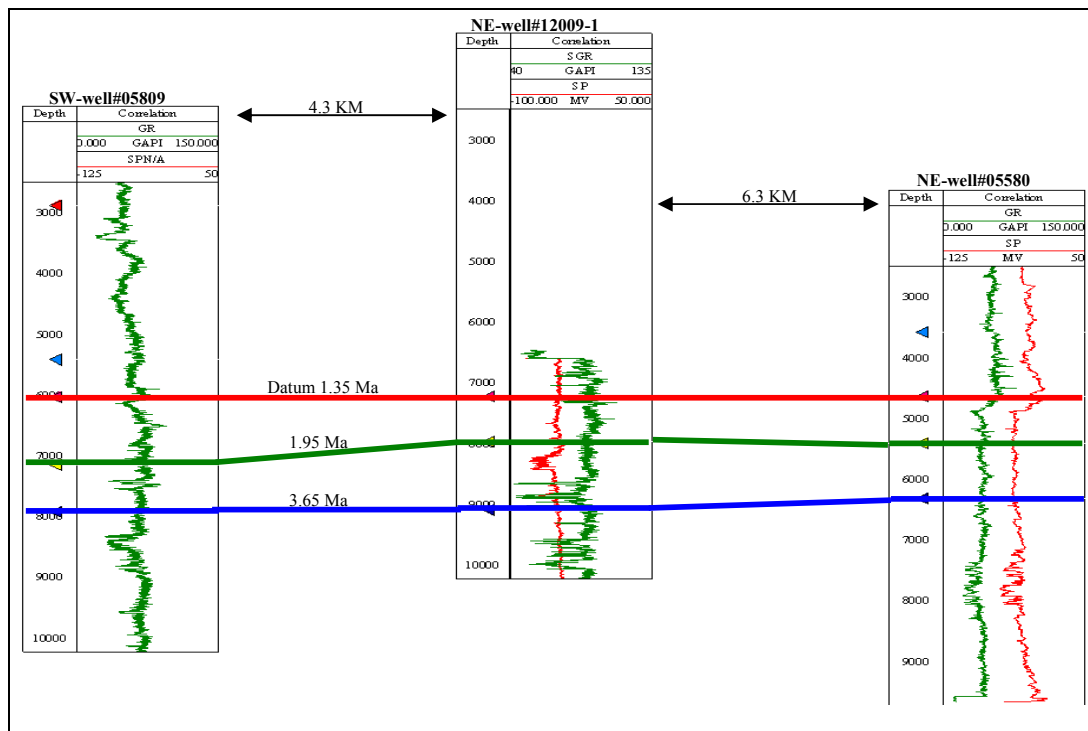
C. Correlation from wells #05809, #12009-1 and #05580 in SW-NE direction.
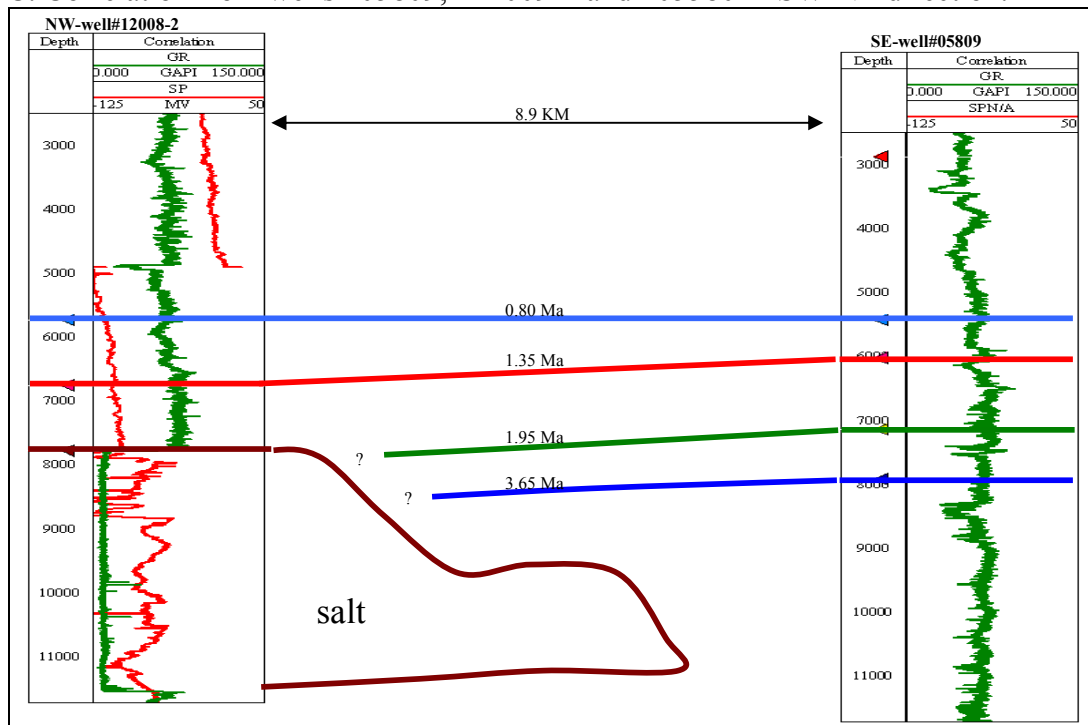
D. Correlation from wells #12008-2 and #05809 in NW-SE direction.

Figure 28. Continued.

Systems Tracts Description

Identification of the systems tracts in the study area between 1.95 Ma and 1.35 Ma was based on boundary and internal configuration characteristics in the seismic section (Figure 29).

The 1.35 to 1.95 Ma has been chosen because the salt at that time was reactivated and the study area, which was at the edge of the rafted overburden area, was transformed to a contractional fold area along the strike-slip fault (Figure 4e). Therefore, this expected structural setting will have great effects in sequence stratigraphic development.

The three blue horizons and two green horizons on Figure 29 represent condensed sections and/or maximum flooding surfaces. The two dark blue horizons are top salt and bottom salt respectively. The interpretation for 1.95 Ma and 1.35 Ma is between two green horizons. The pink horizon is interpreted as a Type 1 sequence boundary as the erosion and truncation occurs at the top of the horizon. This sequence boundary is not extensively clear throughout the area because of salt movement. The particular sediment is thinning near the edge of the salt in the southeast.

The curve of relative sea-level changes in Figure 30 shows that the sea level began to fall in approximately 1.95 Ma. Seismic section crossline 290 (Figure 29a) does not show clear progradation, onlap or downlap. This first package is bounded below by a maximum flooding surface (green horizon) and above by a Type 1 sequence boundary (pink horizon). The first package is interpreted to be a highstand systems tract based on its boundary; it was deposited during the early stage before relative sea level continued to fall.
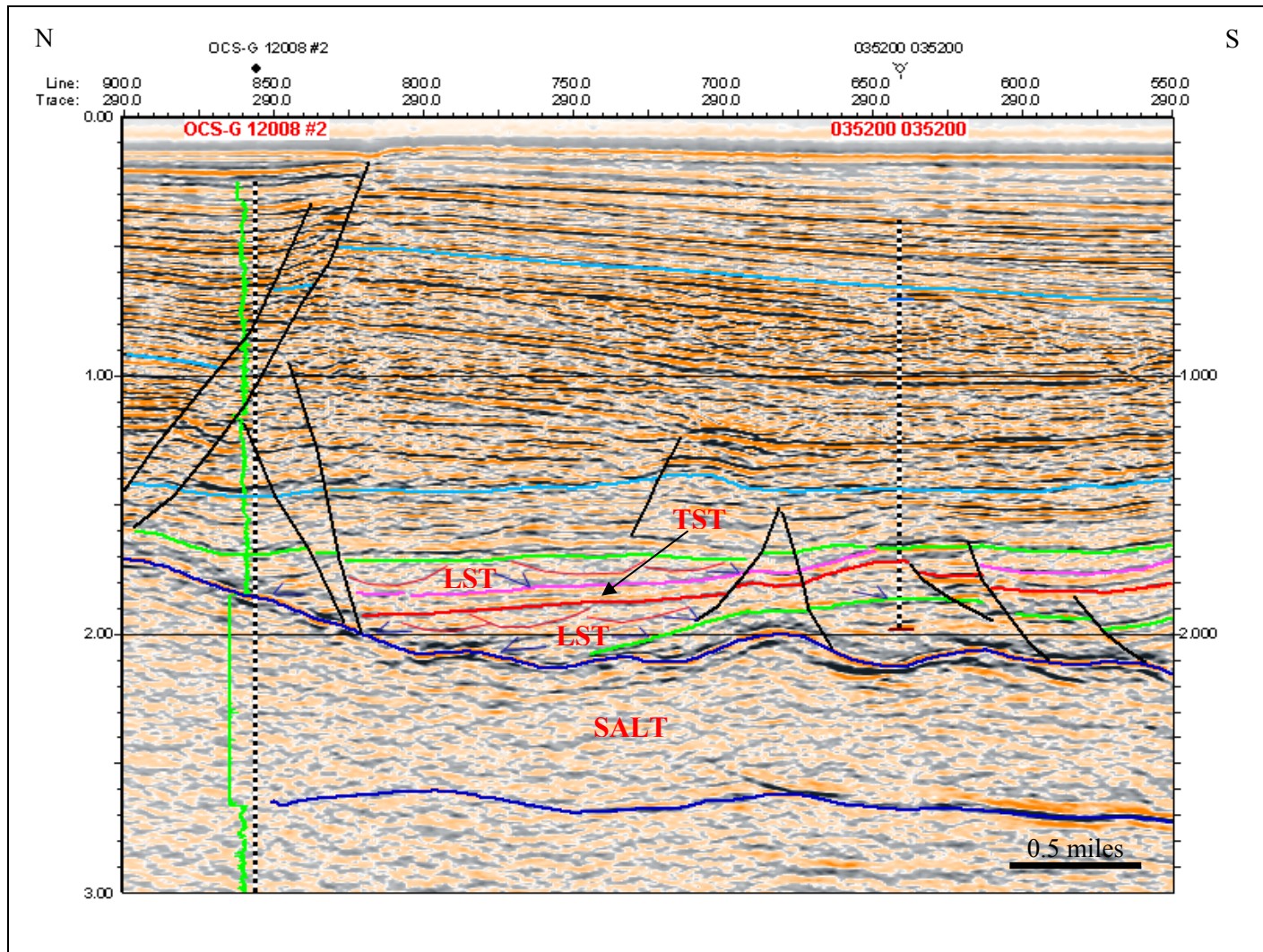
Figure 29a. Seismic section crossline 290. This section showing onlap, downlap (blue arrows), and channels in LST (red curves). Horizon names are the same as in Figure 21. See Figure 42 for location and text for discussion.
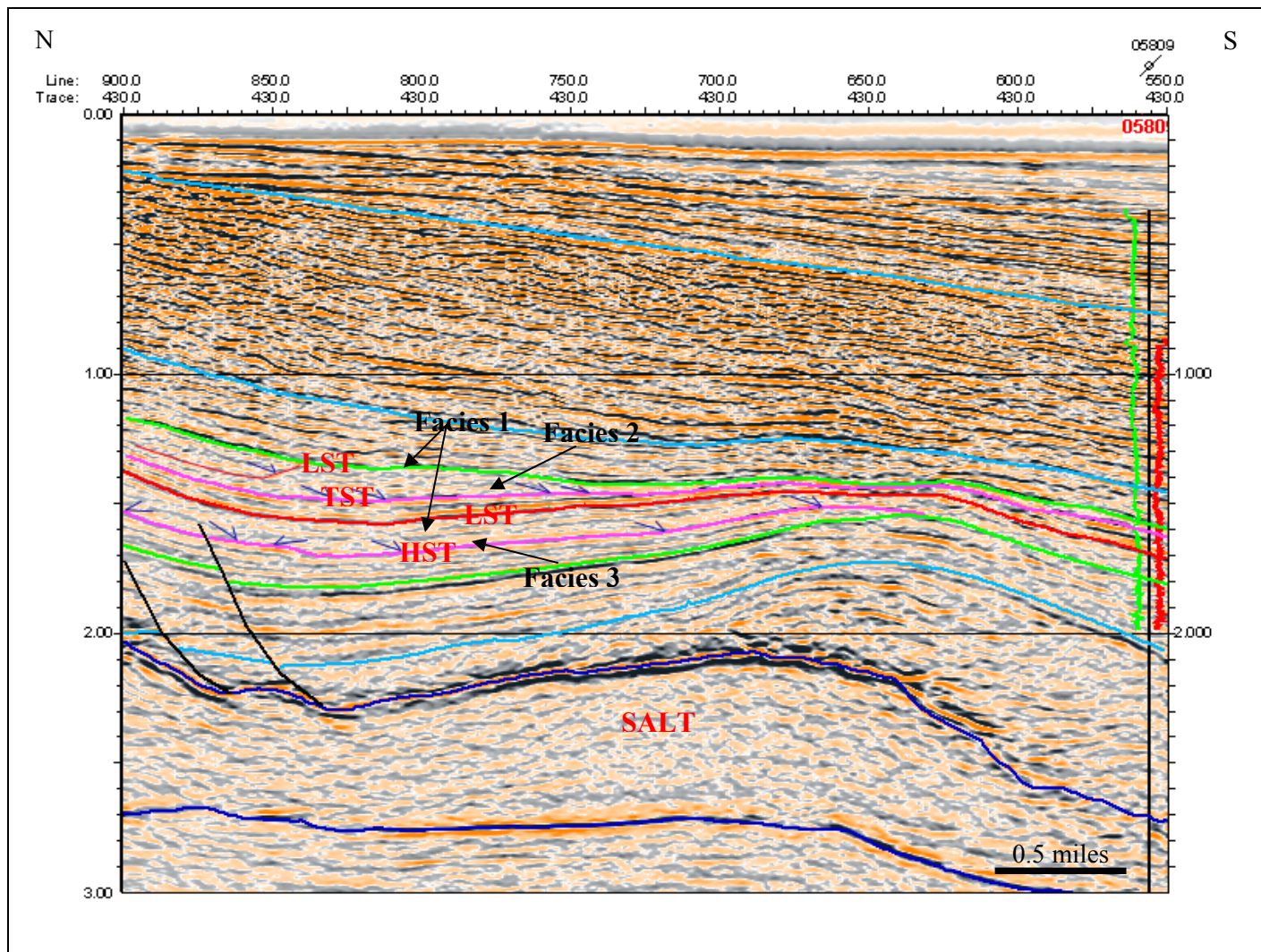
Figure 29b. Seismic section crossline 430. This section showing onlap, downlap (blue arrows), and channel (red curves) in LST.
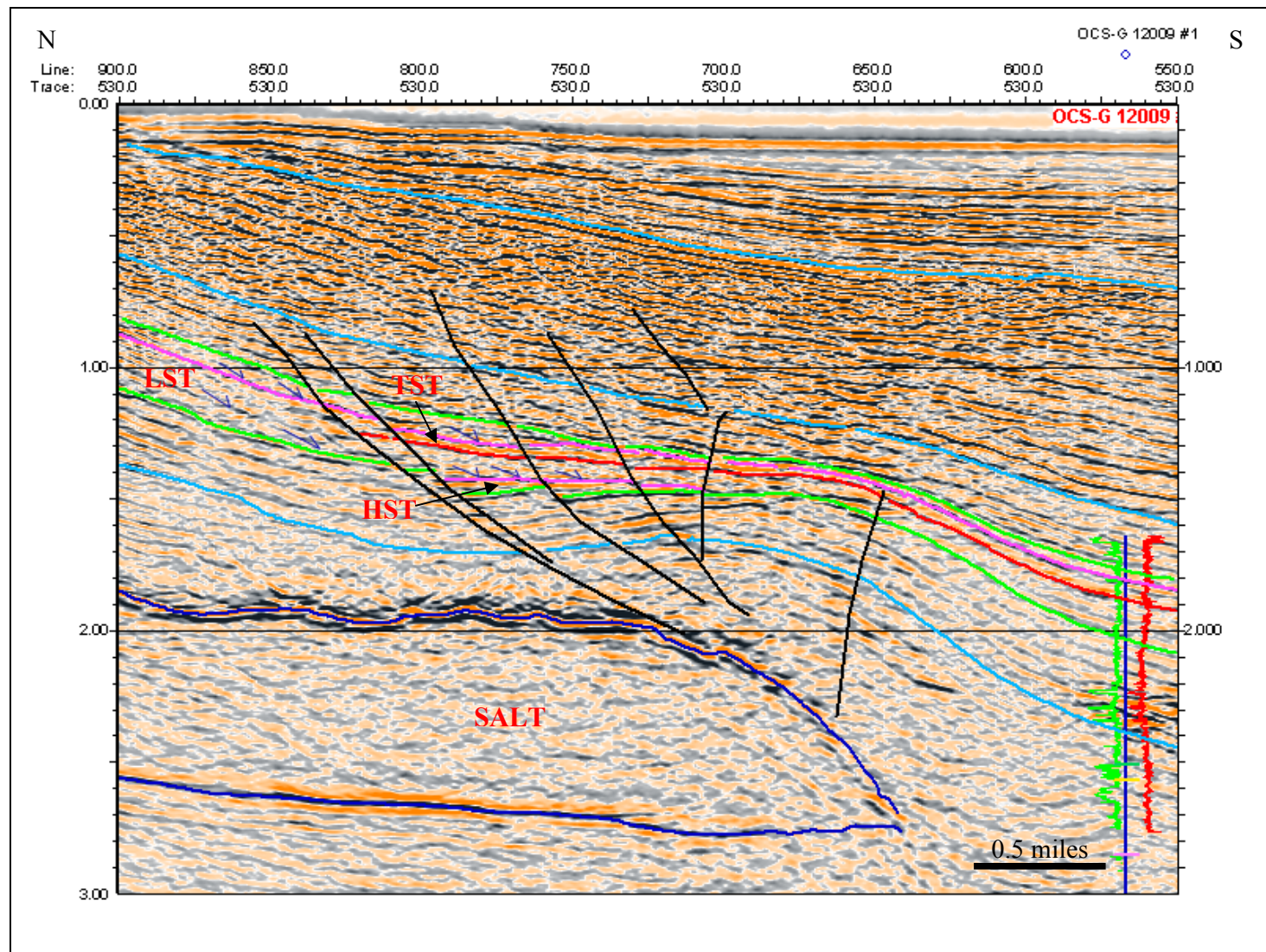
Figure 29c. Seismic section crossline 530. HST (between pink and green in the lower part) is limited to depocenter area.
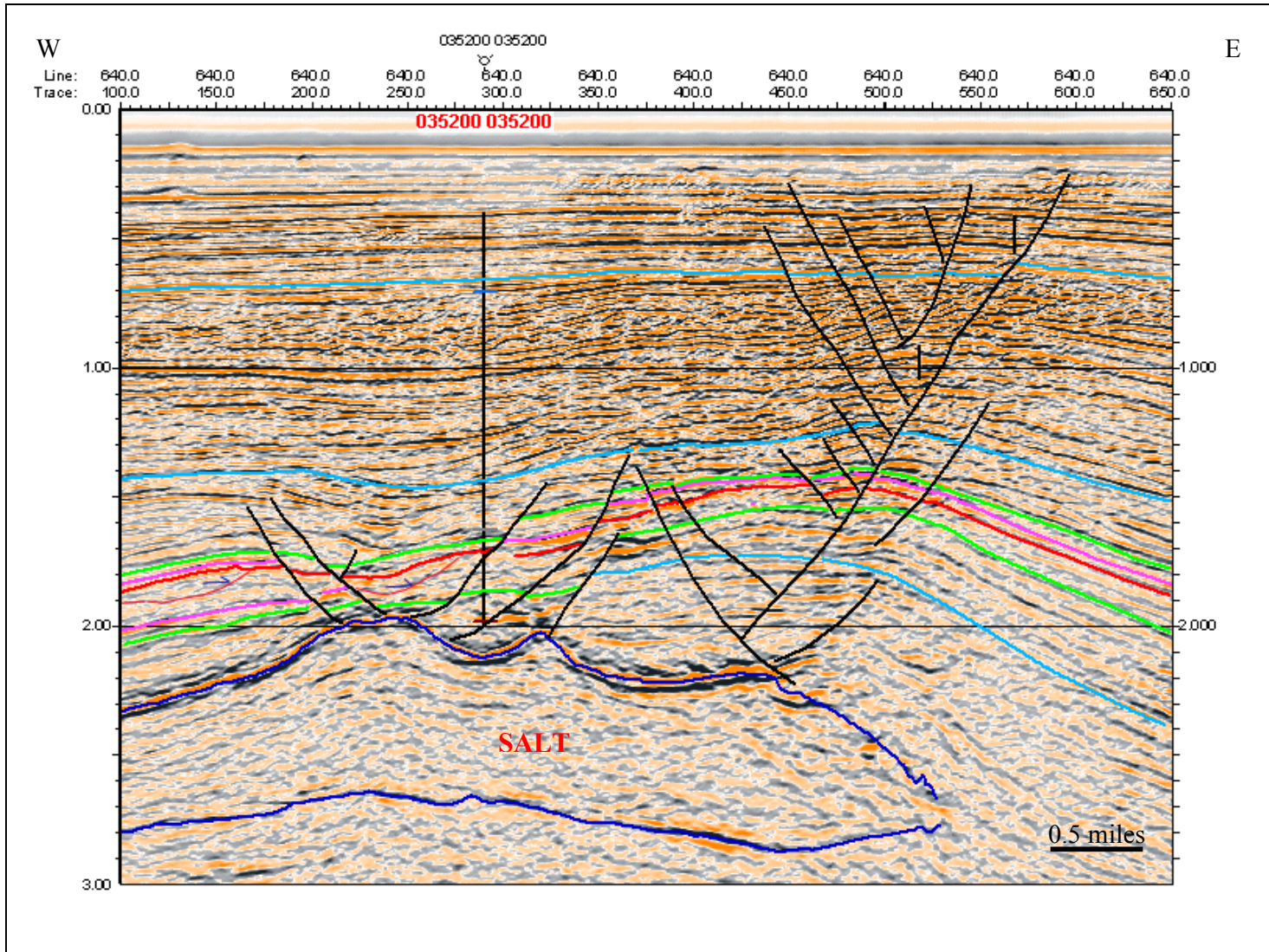
Figure 29d. Seismic section line 640. Faulted area on top of salt.
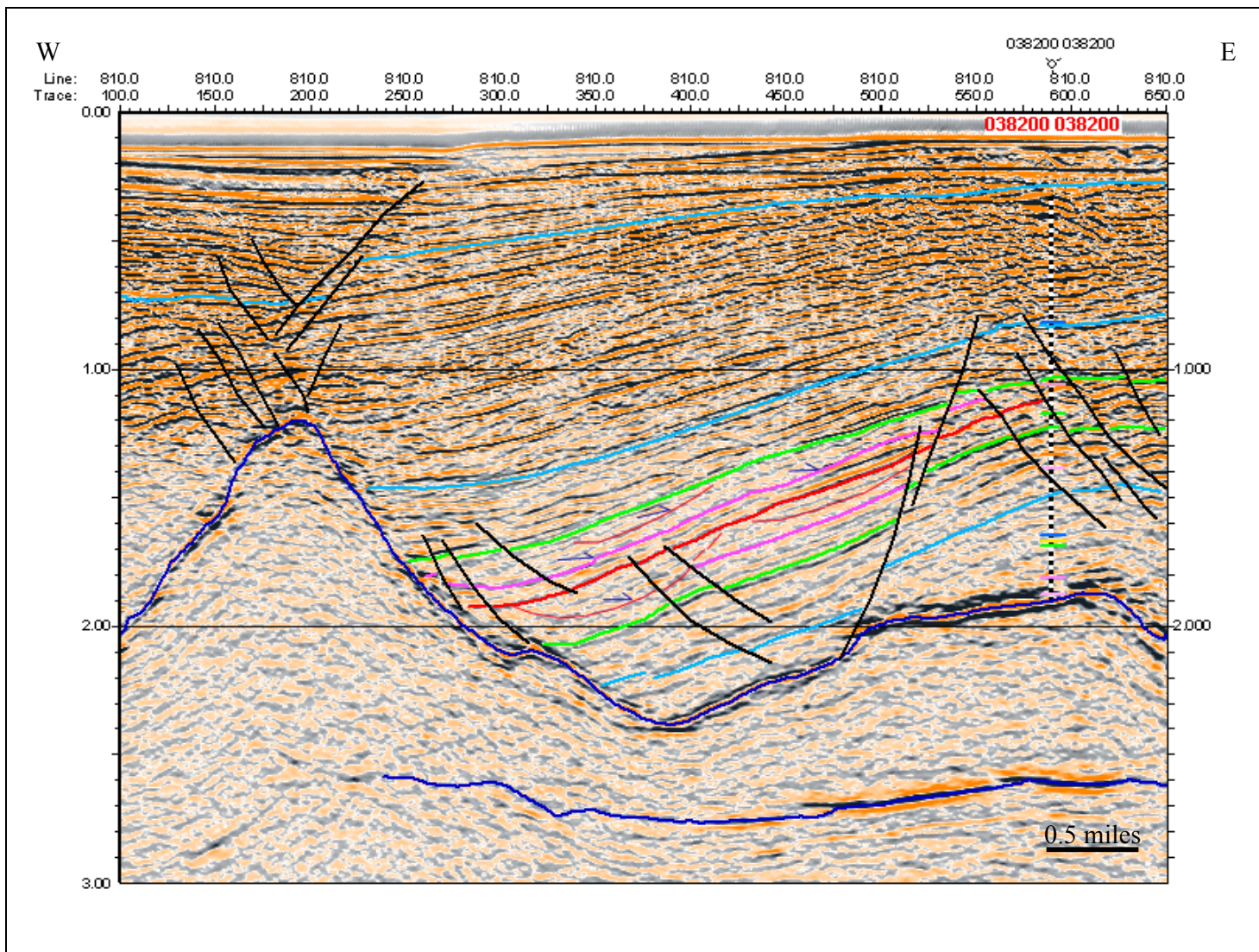
Figure 29e. Seismic section line 810. Downlap (blue arrows) and channels (red curves) in LST.

The second package is bounded below by the pink horizon, which is interpreted as a sequence boundary, and also the green horizon in the area outside between trace 350 to 500 and line 900 to 650 (the area occupied by the highstand systems tract). It is bounded above by the red horizon, which is interpreted as a transgressive surface. The downlap is observed to the base of the sequence boundary (Figure 29). Relative sea level fell rapidly at this time (Figure 30). This second package is therefore interpreted as a lowstand systems tract.

Some channel geometries have been observed in the lowstand systems tracts as shown in Figure 29a, b, d, and e.

The third package in the seismic section is characterized by a transgressive surface (red horizon) below and by a sequence boundary above (pink horizon; Figure 29). This occurred when relative sea level began to rise again (Figure 30). No downlap, offlap or progradation has been observed except onlapping to the salt in some areas. This package is interpreted as the transgressive systems tract.

The relative sea level did not continue to rise and form a highstand systems tract, but shortly after the transgressive cycle was deposited it fell again (Figure 30), forming an erosional surface, while sea level continued to fall. Therefore, the fourth package, bounded below by a sequence boundary (pink horizon, which characterized also by downlap on top, Figure 29), and bounded above by a condensed section (which sometimes interfered with a flooding surface, shown as a green horizon). This package is therefore interpreted as the lowstand systems tract.

Seismic Facies Description

Three seismic facies have been observed in the study area (Figure 31): Facies 1, Facies 2, and Facies 3. Facies 1 is described as chaotic, channel-fill facies. The reflection configuration of this facies was chaotic to contorted-hummocky. It has low-to-moderate amplitude with low-to-very low continuity (Figure 31). This facies is generally observed in the lowstand systems tract in the study area (Figure 29).

Facies 2 is characterized by a parallel-to-subparallel internal configuration, moderat-to-high amplitude, and moderate-to high-continuity reflection configuration. This facies is distributed in the transgressive systems tract (Figure 29).

Facies 3 is characterized by a parallel-to-subparallel internal configuration, low-to-moderate amplitude, and moderate-to high-continuity reflection configuration. This facies is distributed in the highstand systems tract (Figure 29).
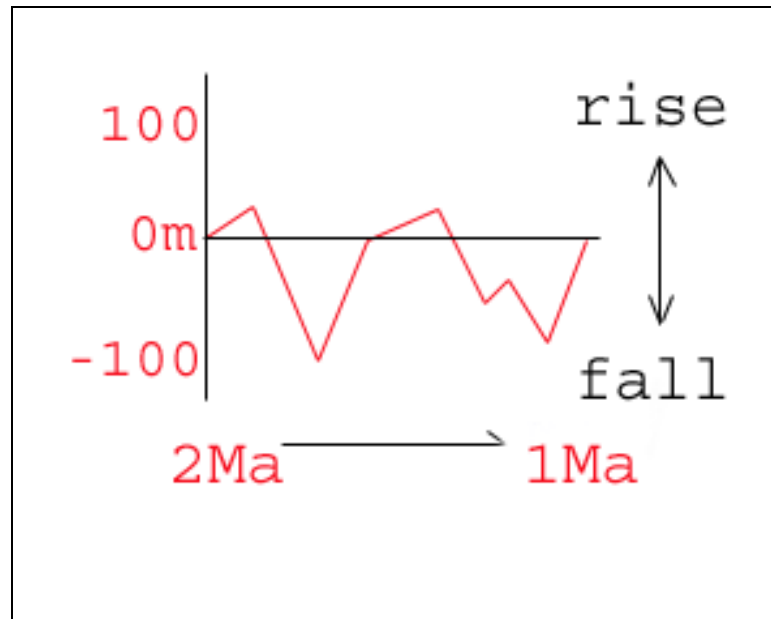
Figure 30. Relative change of sea level between 1 to 2 Ma. Modified from Paleo-Data Inc. version 9810 of PGS Inc., D'Agostino (1999).

Facies 1	Chaotic-hummocky contorted, low-moderate amplitude, low continuity
Facies 2	Parallel-subparallel, moderate-high amplitude, moderate-high continuity
Facies 3	Parallel-subparallel, low-moderate amplitude, mid-high continuity
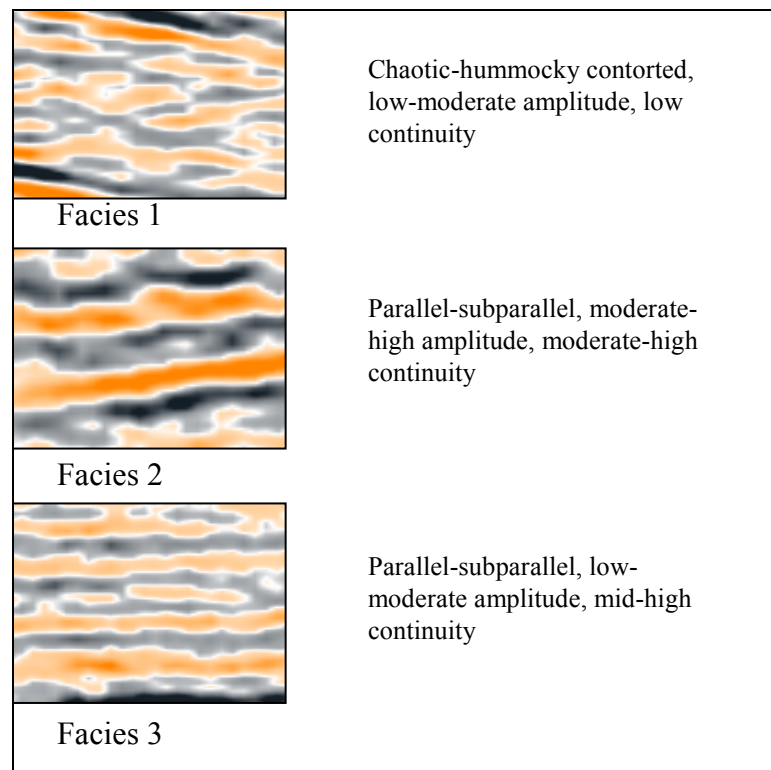
Figure 31. Three seismic facies in the study area. These facies are identified between 1.35 Ma and 1.95 Ma.

Seismic Attributes

Three-interval maps of mean envelope amplitude and maps of sum of zero-crossing attribute between 1.35Ma and 1.95Ma were generated. These attribute maps are approximations and simplifications of the systems tract and seismic-facies distribution identification.

All of the maps were generated using the same scale. The value of the maps of the mean envelope amplitude ranges from 750 to 4,000 and that of the maps of sum of zero-crossing attribute ranges from 1 to 9.

The first attribute volume consists of highstand (HST) and lowstand (LST) systems tracts in the lower part of interval from 1.35 to 1.95-Ma (between the red horizon at top and the green horizon at bottom, see Figure 29). The map of sum of zero-crossing attribute indicates a strong border that differentiates high values and low values of the sum of the zero-crossing value (blue line in Figure 32). The border is interpreted as the HST-LST boundary.

The mean envelope amplitude map from the same interval shows middle-range values (2,000 to 2,500) to a high-value (3,500) channel trending northeast-southwest (Figure 33). This area interpreted as a "deformed zone" is faulted and lies just around the salt edge. Low-amplitude values (< 2.000) are interpreted as seismic facies distibution from HST and LST.

The second attribute volume represents the transgressive systems tract (TST) distibution in the 1.35 to 1.95-Ma interval (between the pink horizon at top and the red horizon at bottom, see Figure 29). The high value in the sum of zero-crossing map is

interpreted as the distibution of seismic facies in the transgressive systems tract (Figure 34).

The mean envelope amplitude of the same interval shows the same response as the first package attribute. Middle-range values to higher values reflect a faulted area ("deformed zone"), and the lower amplitude values represent seismic facies distribution in TST (Figure 35).

The third attribute volume represents LST in the upper part of the 1.35 to 1.95-Ma interval (between the green horizon at top and the pink horizon at bottom, see Figure 29). The sum-of-zero-crossing map shows the same pattern as the sum-of-zero-crossing map from the second interval. The high value is interpreted as the distibution of seismic facies in the LST (Figure 36).

The mean envelope amplitude of the same interval shows a clear amplitude-value (>2,000) distribution trending northeast-southwest. This area again is interpreted as "deformed zone" associated with faulting and the edge of the salt. Low-amplitude values represent seismic facies distribution in LST (Figure 37).
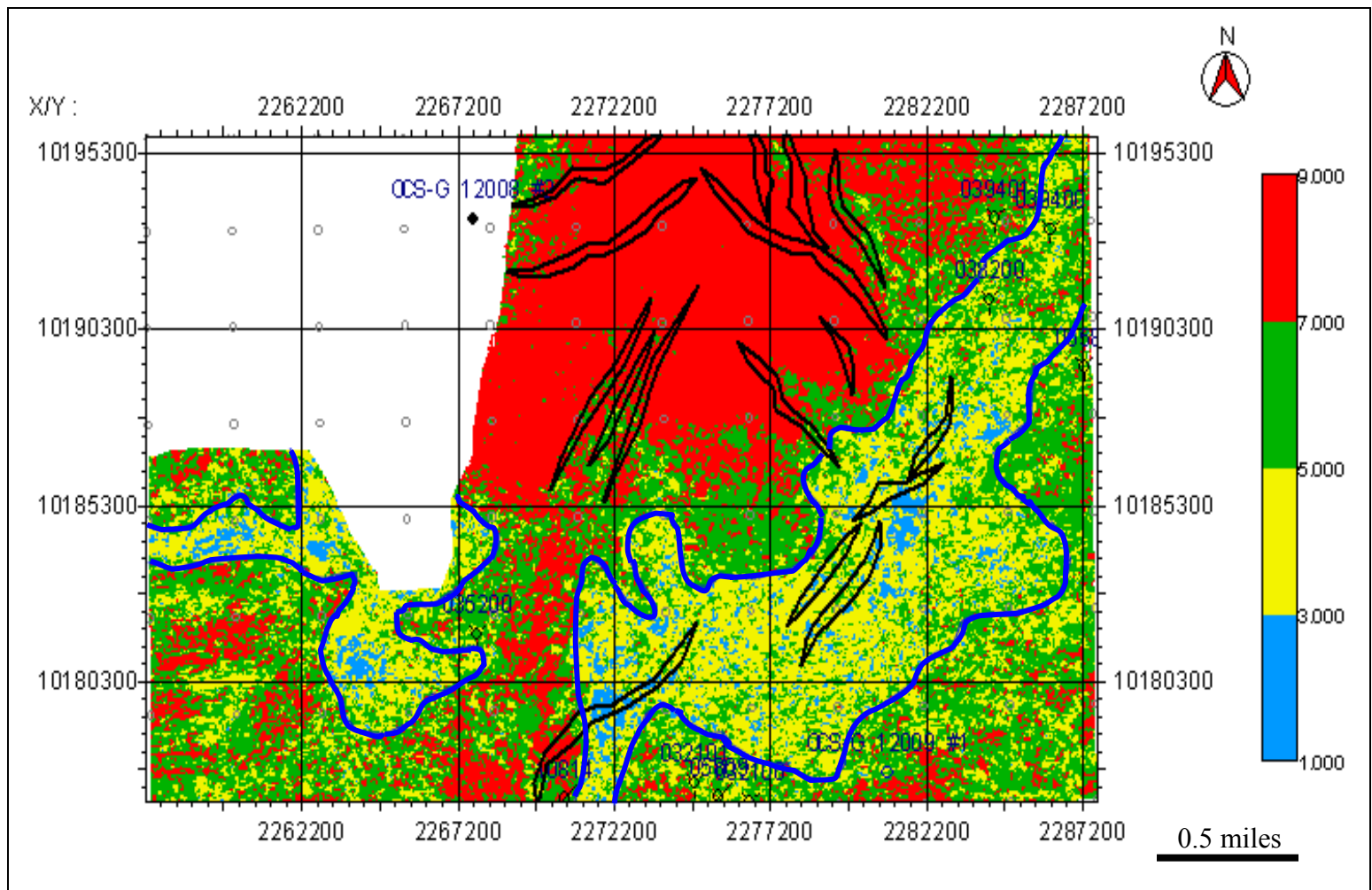
Figure 32. Sum-of-zero-crossing attribute map showing HST-LST boundary (blue line). The interval is generated between red horizon at top and green horizon at bottom, see Figure 29.
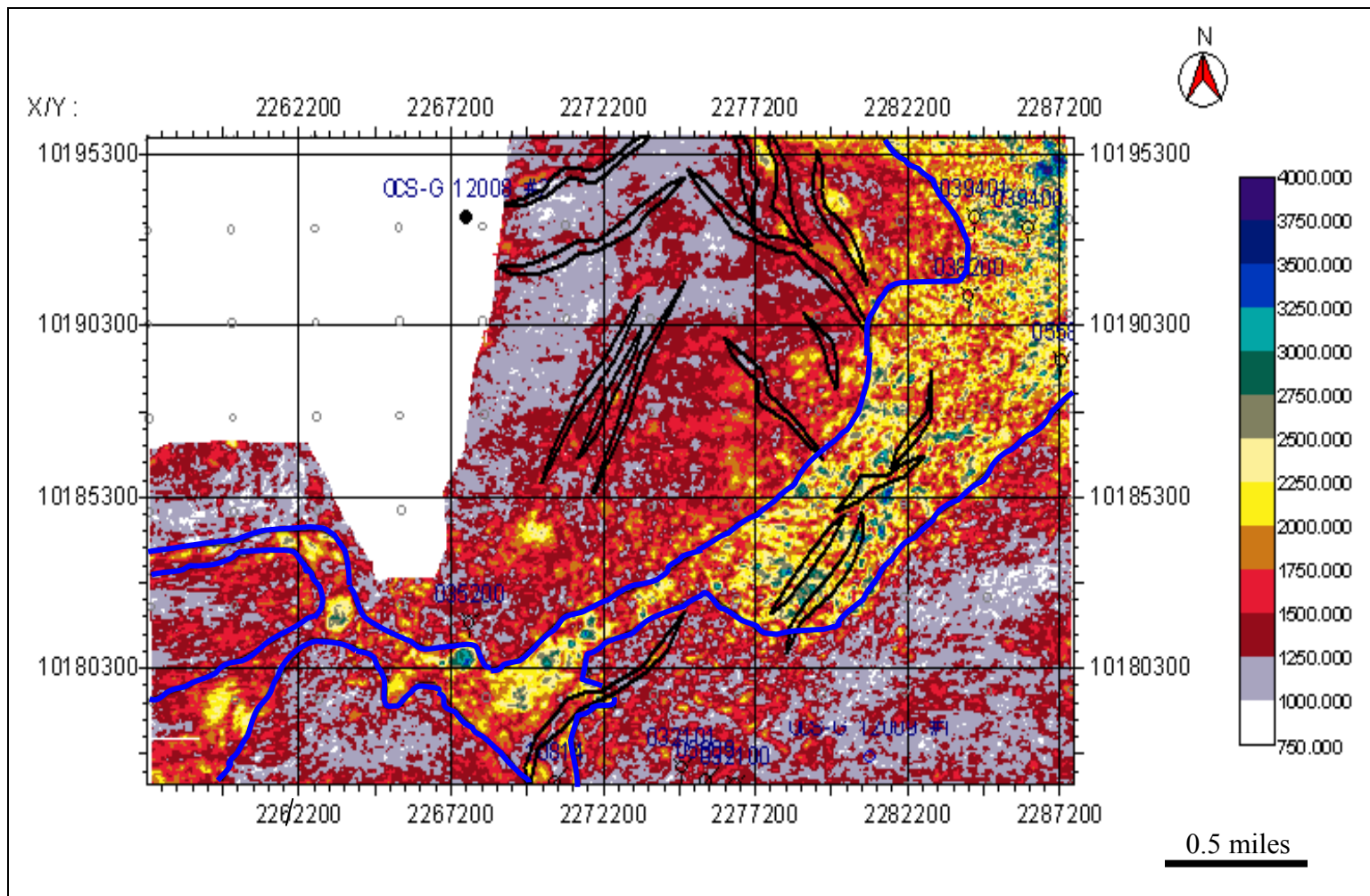
Figure 33. Mean envelope amplitude map in the first interval. It is showing the distribution of seismic facies 1 in very-low-amplitude value (gray color), seismic facies 3 in middle range (reddish color), and "deformed zone" (yellow to blue). The interval is generated between the red horizon at top and the green horizon at bottom, see Figure 29.
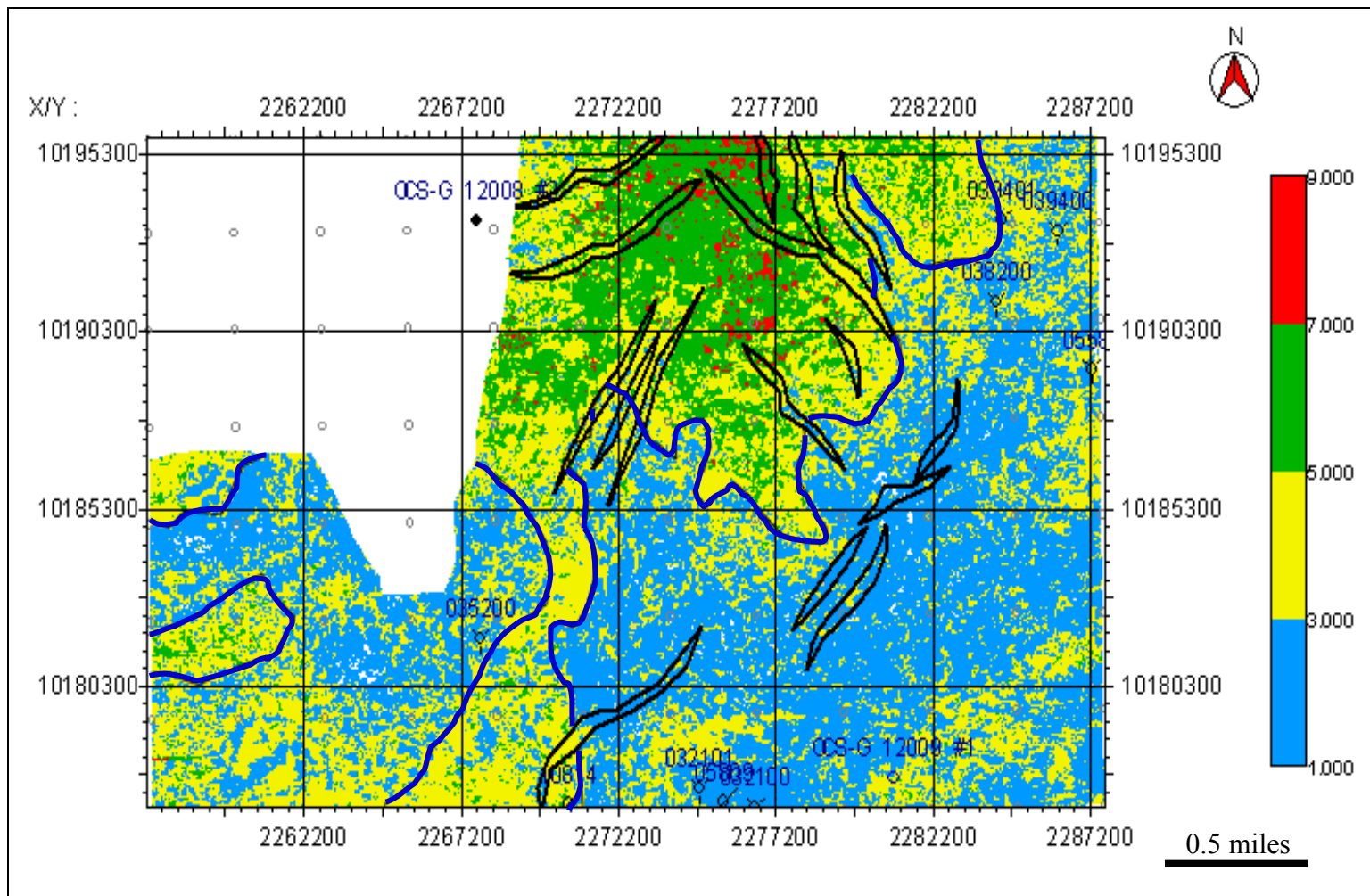
Figure 34. Sum-of-zero-crossing attribute map showing the distribution of seismic facies 2 in TST. The interval is generated between the pink horizon at top and the red horizon at bottom, see Figure 29.
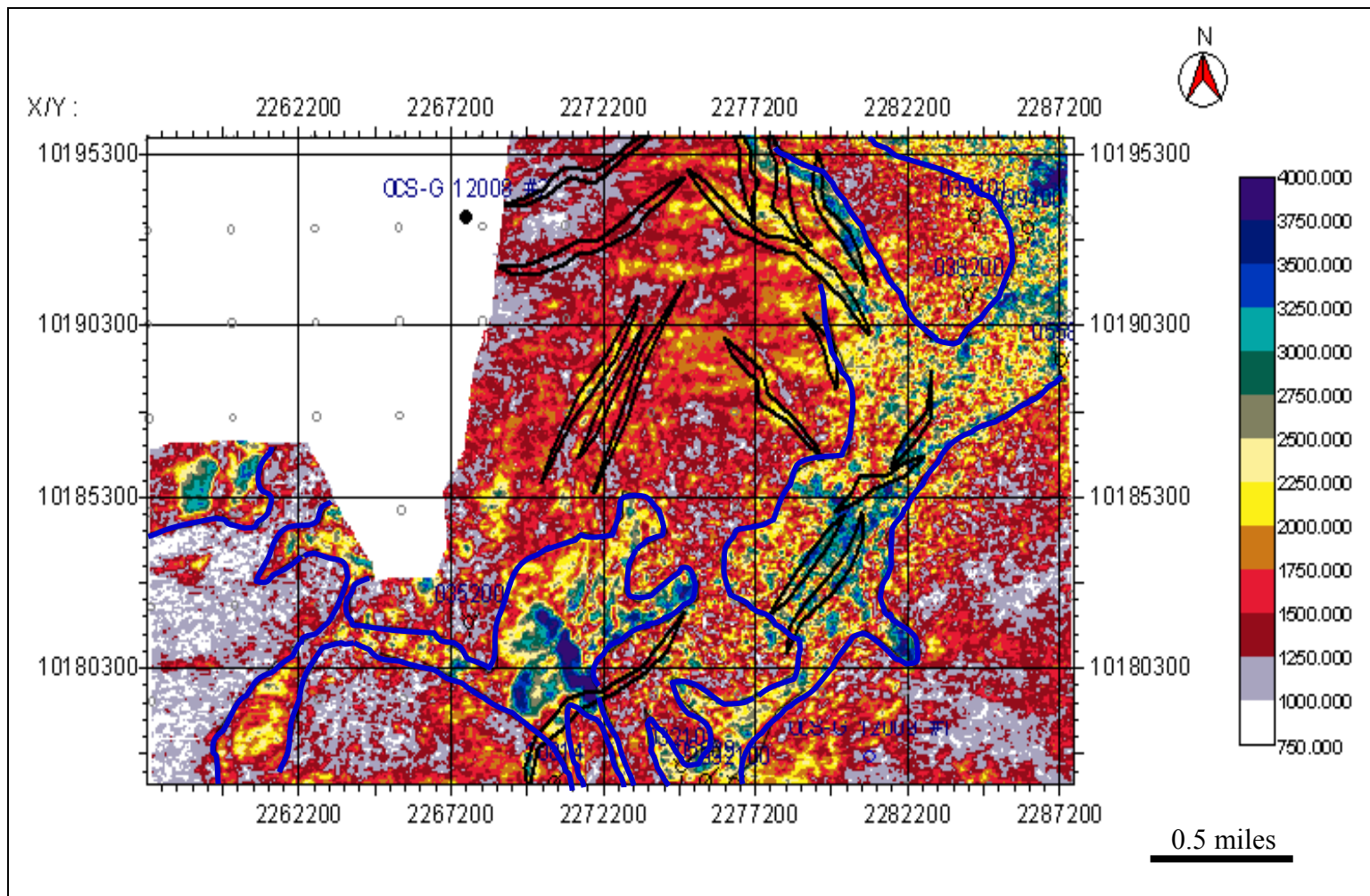
Figure 35. Mean envelope amplitude map that shows more definition on seismic facies 2 in TST and more localized "deformed zone." The interval is generated between the pink horizon at top and the red horizon at bottom, see Figure 29.
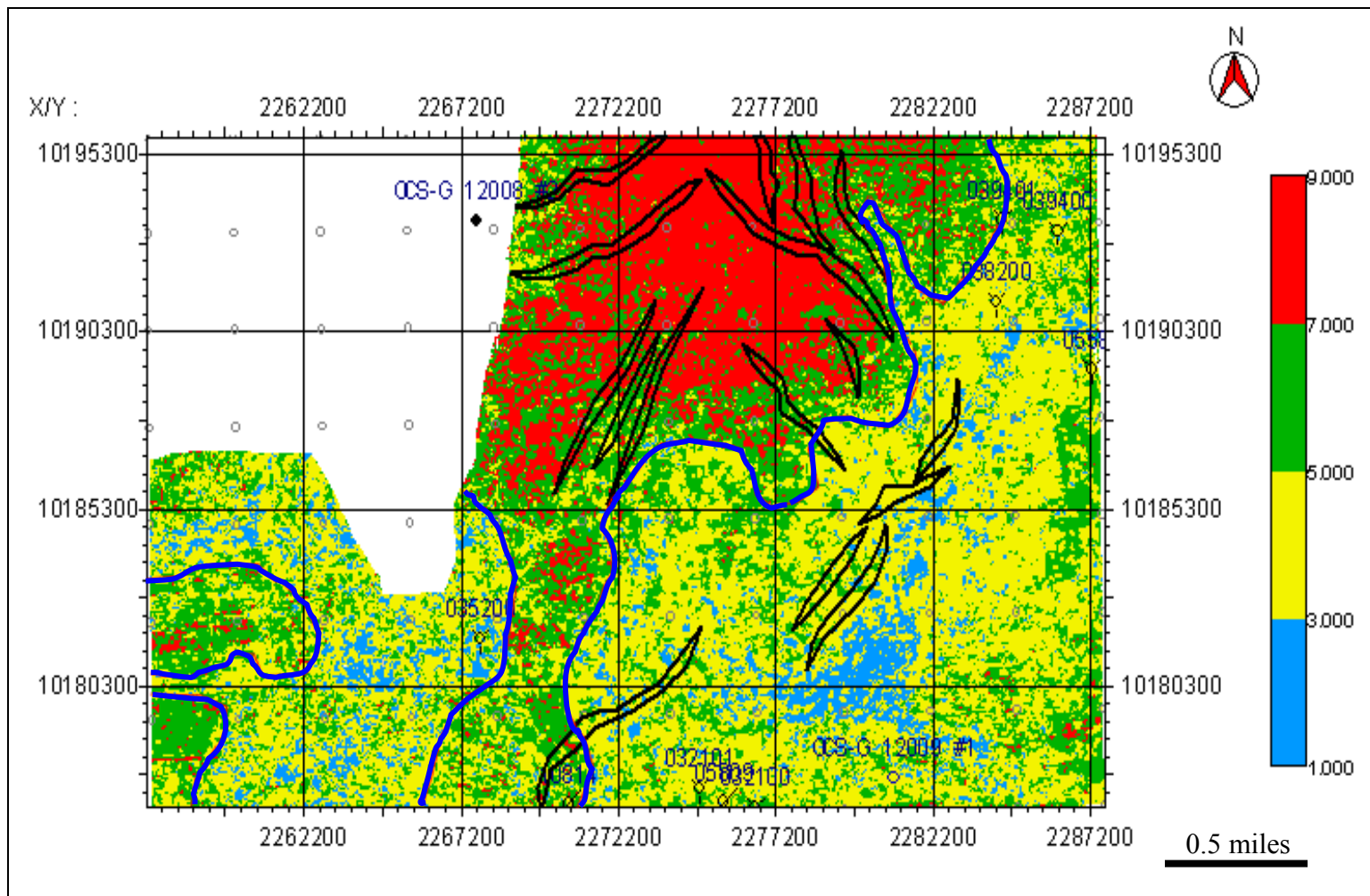
Figure 36. The sum-of-zero-crossing attribute map shows the distibution of seismic facies 1 in LST. The interval is generated between the green horizon at top and the pink horizon at bottom, see Figure 29.
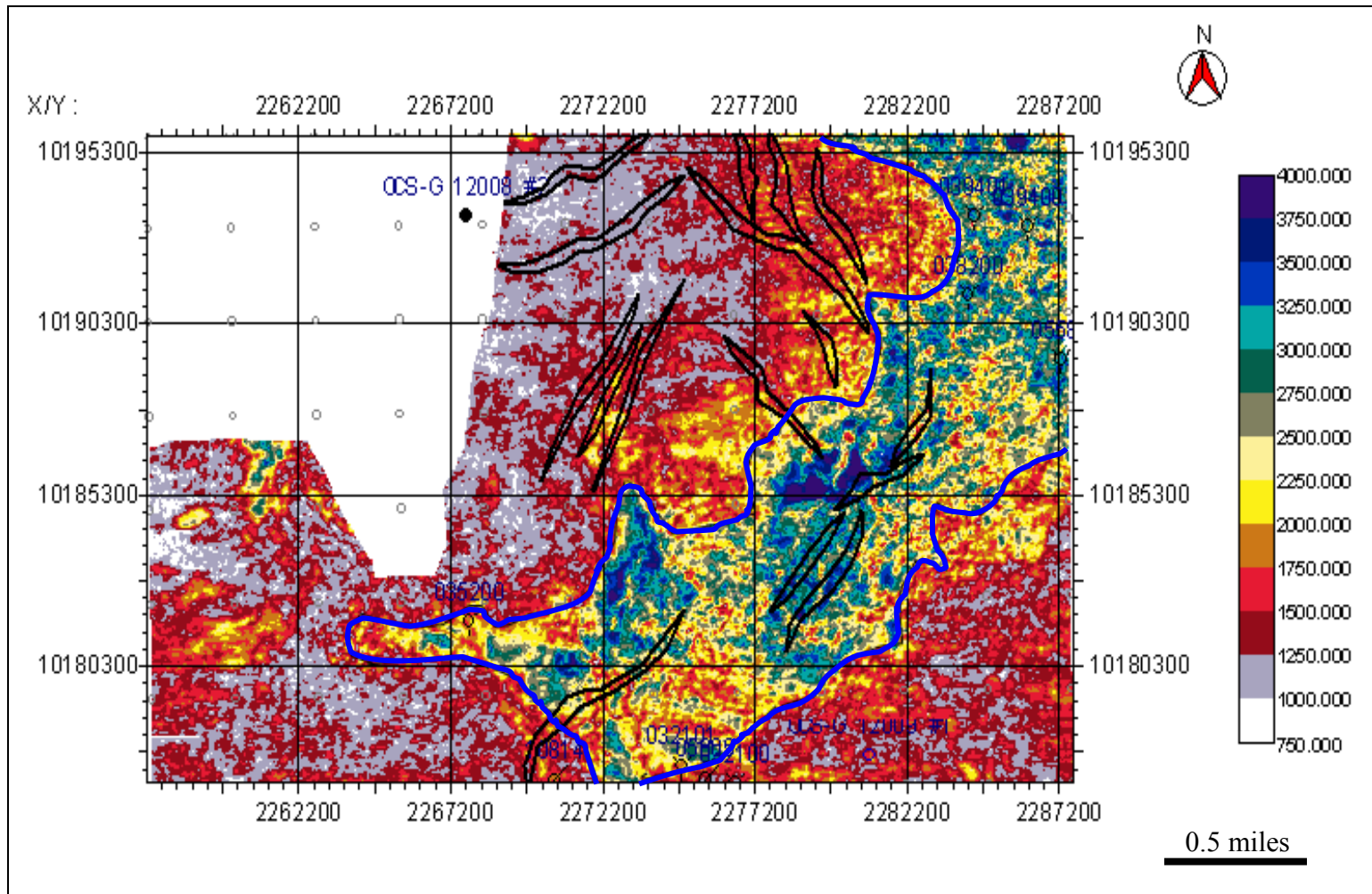
Figure 37. Mean envelope amplitude map shows clear "deformed zone" trending northeast-southwest. The interval is generated between the green horizon at top and the pink horizon at bottom, see Figure 29.

CHAPTER IV

DISCUSSIONS AND INTERPRETATIONS

The Salt Structure and Salt Movement

The salt-structure section in the previous chapter proposed that the salt structure in the area consists of a small, bulb-shaped salt stock in the northwestern part and a salt sheet in the southeastern part (Figure 16). The study area is only 55 km^2; therefore, calling the salt structures a separate bulb-shaped salt stock and a salt sheet is probably too exaggerated. On the other hand, calling the salt body a pennant-shaped body trending northwest-southeast is also quite speculative because we only see a counter-regional fault system without a deep-rooted closed weld in the northwest of the study area. The seismic data are limited in both the vertical and lateral sections. Regardless, the terms small, *bulb-shaped salt stock*, *salt sheet*, and *pennant-shaped* in this study are used to represent the view of what we see as a simplification.

The salt is active through time because of its capability to move and to emplace with sediment loading. The small, supralobal basin was formed by the emplacement of the salt in the middle of the study area. The first stage in the local evolution (Figure 18a) shows that the salt was in a shallower depth, while Rowan's evolution (Figure 4) suggested in lower-to-upper middle bathyal. This is probably because of the different reconstruction techniques because the constraint in this study comes from time only.

The salt high in the earlier stage of evolution blocked sediment transport. The sediment transport pathways possibly trend south-southwest and south-southeast, divided by the salt high. The supralobal basin was shifted from northeast to the west indicating that sediment supply from the northeast toward the south/southwest was greater than from the northwest (Figure 18d-18e). The sediment transport pathways are relatively unchanged through time.

Salt movements also created instability, which triggered faults. When sediment emplaced salt, faults were activated in both the northwest and southeast margin sides, trending northeast-southwest. This situation affects the stratigraphic framework. The middle area where the depocenter of the small supralobal basin is developed seems to be a normal area for sedimentation and startigraphic record except for the area with an active fault near the salt top. The systems tracts and the seismic facies in this should develop normally and be easily identified. The faulted area or the area along the small, supralobal basin margin did not have a good stratigraphic record because of the continuous deformation. Therefore, the systems tracts or seismic facies is difficult to develop normally or to identify.

Well Log Sequence Stratigraphy

LSTs and TSTs have been identified from well-log interpretation.

The blocky and amalgamated-shape gamma ray log response of Wells #05580 and #12009-1 in Figure 25a and 26b respectively are interpreted as basin-floor fan deposits. The fining-upward packages of sediment with sharp bases on the gamma ray

log responses are interpreted as channel/overbank deposits. This deposit is a characteristic of the slope fan facies.

The coarsening-upward signature indicating a prograding sand and the thinning-upward gamma ray log response of Wells #00580 and #05809 (Figure 25) are interpreted as lowstand wedge deposits.

The basin-floor fan, slope fan and lowstand-wedge deposits comprise the lowstand systems tract.

Irregular gamma ray log trends from wells #12008-2 and #12009-1 (Figure 26) respectively show aggradational parasequences. This is probably a unit of turbitide systems or similar to shelfal or deepwater setting, a lacustrine succession or muddy alluvial overbank facies, as described by Emery and Myers (1996). However, there is no clear evidence to include this unit to LSTs.

The thinning-upward, backstepping (retrograding) package is bounded by a transgressive surface from Wells #05580 and #05809 (Figure 25) is interpreted as a transgressive systems tract.

Although the highstand sea-level cycle occurs in the biostratigraphic chart within the 1.35 to 1.95-Ma-period, the HST from the available well logs in the area has not been observed.

Systems Tracts and Seismic Facies Analysis

This section will discuss systems tracts and seismic facies analysis because these are important aspects to help detail interpretation of depositional systems including lithofacies, which are key to interpretation of reservoir rock, seal and stratigraphic traps.

In the study area, each systems tract is uniquely related to a certain seismic facies. This fact made the interpretation easier.

Seismic facies 1 (Figure 31) is related to the LST. It is a chaotic, channel-fill facies interpreted as a slope fan or basin-floor fan channel package resulting from gravity mass transport. This facies is the part of the leeved-channel and overbank-facies environment, which was very well-developed in the Ship Shoal area during the Pliocene-Pelistocene (see channel interpretation on seismic section figure 29).

At the time when TST sediment deposited between 1.35 and 1.95 Ma, the basin moved from the mid-upper slope to the shelf-upper slope. Therefore, seismic facies 2 (Figure 31) in the TST is interpreted typically as being shallow marine-clastic deposits on the shelf environment. The character of this facies is similar to the seismic facies character in marine clastics on shelf environments (Sangree and Widmier, 1977). Seismic facies 2 in the TST is well-developed over the study area, especially in the basin depocenter.

The HST was dominated by seismic facies 3. This facies is interpreted to be a shelf-marine clastic facies deposited by a low-energy-turbidity current. This facies is not well-developed in the study area, because the early 1.95 Ma was the time of fault initiation resulting from continuous salt movement. The distribution of the seismic facies

is limited between trace 350 to 500 and from line 900 to 650. The thickest part is around trace 400 and generally thinning to both east and west sides and wedging out to the south/basinward.

The previous section showed that the area along the small, supralobal basin margin on the northwest and southeast sides did not have good stratigraphic records because of the continuous deformation. This faulted area ("deformed zone") therefore has a very specific reflection configuration. It is chaotic, low-continuity and moderate to high in amplitude. Even though it has a specific reflection configuration, it does not necessarily have a specific facies environment. Therefore, the "deformed zone" could not be considered one single facies.

Seismic Attribute Analysis

The seismic attribute was generated after identification of the systems tract and seismic facies; therefore, the interpretation is more qualitative. No exact quantification with a specific geostatistic method was performed for both seismic attribute analyses to be interpreted as certain facies or systems tracts, although the interpretation is related to a range or interval of attribute values.

The sum-of-zero-crossing attribute should give good contrast for stratum heterogeneity. That is why the TST package (Figure 34) has a lower value than the other packages (Figure 32 and 36), and the package in the lower part of the 1.35- to 1.95-Ma interval (Figure 32) has a higher value than the LST package in the upper part (Figure 36) because it contains both LST and HST.

The seismic facies also give the heterogeneity level of the attributes of the sum of zero-crossing such that the distribution of the seismic facies is also determined by this attribute. Therefore, the chaotic configuration should have a higher value than the parallel/subparallel configuration.

The mean envelope amplitude maps (Figure 33, 35, and 37) generally give a lower value (<2,000) to normal stratigraphic strata (the identified seismic facies) and give a higher value to the strata that were affected by faults and the salt movement along the supralobal basin margin in the southeast, trending northeast-southwest through the area. This trend is the "deformed zone."

It is interesting that the "deformed zone" comes up with low values in maps of sum of zero-crossing, even though it is chaotic and has a low-continuity reflection configuration. This is because the "deformed zone" is very thin (about one or two wiggles on seismic section). This phenomenon implies that the sum-of-zero-crossing attributes also can be identified for thinning or thickening sediments in the particular interval.

The thinning or thickening sediments from the sum-of-zero-crossing attribute support the previous statement that the sedimentation process dominated transport from northeast to southwest. The loading sediment emplaces salt to both the northwest and southeast sides, where the small, bulb-shaped salt stock and salt sheet were formed. While the sediment is onlapping to the edge of the salt in the area where the bulb-shaped salt stock is formed, the sediment over the salt sheet is folded, forming a small, anticlinal axis trending northeast-southwest, where the sediment was pushed and deformed. These

processes explain why the strata in the depocenter of the small, supralobal basin were developed normally compared to the sediment in the basin margins.

Salt-Sediment Interaction

As discussed previously under salt tectonics, salt movement indirectly created the small protobasin in the study area. The sedimentation pathway from the northeast around the minibasin margin was retained by the continuous movement of the salt. Deformation of the strata and faults also occurred because of salt instability and sediment loading during the deposition.

Sea-level changes controlled the sedimentation in terms of systems tract development and facies distribution. However, sea-level changes cannot be regarded as the main controlling factor of the whole process because evidence of onlap on seismic section between 1.95 Ma and 1.35 Ma is limited, particularly around the salt edge.

Stratigraphy in the central area of the study developed more normally than in the surrounding areas. This is because the area is the depocenter, which has the maximum thickness of sediment deposited, and the probability of salt movement to cause deformation in the depocenter is much less than in the basins margin area. Although sedimentation during the Pliocene-Pleistocene was relatively slow, the load was sufficient to bury salt.

The depositional system interpretation from systems tracts and seismic facies analysis led to the better understanding that the interval from 1.95Ma to 1.35Ma is mainly in the environmental from the mid-upper slope to the shelf-upper slope,

dominated by leveed-channel and overbank facies. The sedimentation processes may result from gravity mass transport and/or turbidity current (mostly low energy) or even slumping from slope instability.

Overall, salt is considered the main factor controlling sedimentation and deformation in the study area (Figure 38). Sediment supply also plays an important role. The effect of sea-level changes is mainly on facies distribution.

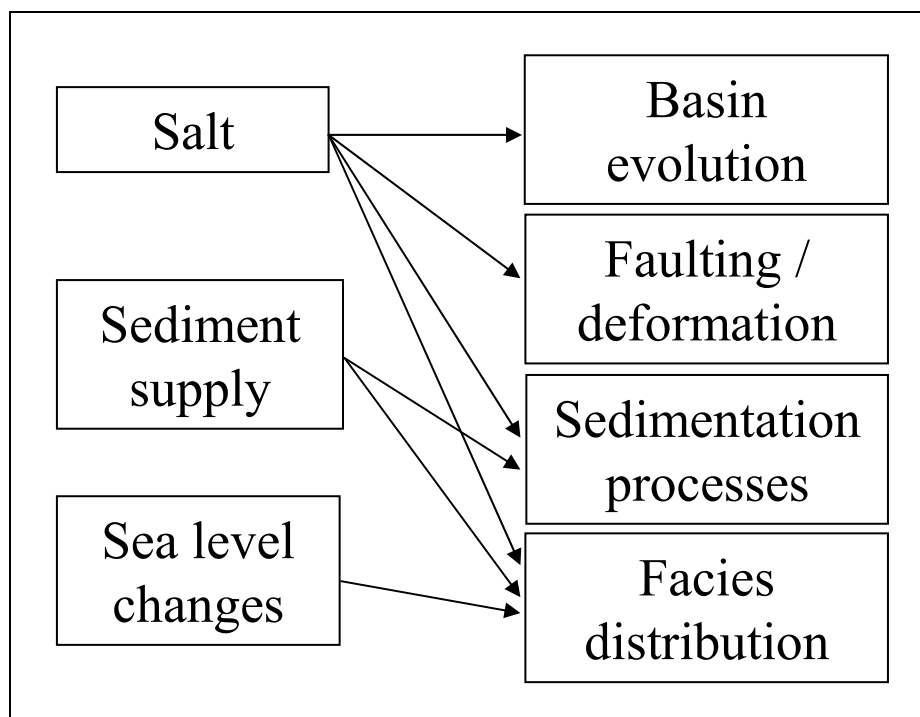**Figure 38**. Diagram of the most common factors controlling the geologic processes in the study area. Salt is considered to dominate sediment supply, sea level changes or (eustasy) as factors that control sedimentary processes in the study area.

CHAPTER V

CONCLUSIONS

An integrated study related to salt tectonics, sequence stratigraphy and seismic attributes has been established in the study area and gives a better understanding of salt-related sedimentary processes. Interpretation of seven horizons leads to the paleosurface reconstruction of the salt body and its implication on local-basin evolution. Five horizons represent maximum flooding surfaces and/or condensed sections and/or a sequence boundary relatively associated with the age of 3.65 Ma, 1.95 Ma, 1.35 Ma, 0.80 Ma, and 0.27 Ma. Two other horizons are the top and bottom of the salt body.

A small, salt-stock bulb-shaped structure in the northwest and a salt sheet in the southern part of the study area have been identified. In the center of the study area, a mini basin that is interpreted as a supralobal basin type also has been identified. It has formed since late Pliocene or early Pleistocene. The minibasin depocenter has shifted through time in response to salt movement from the northeastern part in the early Pleistocene to the center of the study area in recent time.

The salt movements also create slope instability, causing a counter-regional fault along the minibasin margin trending northeast-southwest. Some of faults are attached to the top of the salt and some of them developed near the ocean bottom today.

An HST, a TST, and two LSTs have been identified between 1.35 Ma and 1.95 Ma. All of these systems tracts were normally developed and reached maximum thickness at depocenter in the middle of the study area. The systems tracts were not well developed in the area near the minibasin margin because of salt constraints.

Three seismic facies have been identified. The facies 1 is configuration chaotic-to-contorted reflection, low-to-moderate amplitude, and low continuity, associated with chaotic channel fill in the LST. The facies 2 configuration is a parallel-to-subparallel reflection, moderate-to-high amplitude, and moderate-to-high continuity, associated with marine clastic deposits on shelf environments in the TST. The facies 3 configuration is a parallel-to-subparallel reflection, low-to-moderate amplitude, and moderate-to-high continuity, associated with a shelf-marine clastic facies deposited by low-energy-turbidity current in the HST.

Analyses of mean envelope amplitude and sum-of-zero-crossing attribute were applied to incorporate the systems tracts and seismic-facies distributions, over the study area. A "deformed zone" was recognized from attribute maps as an area that has a different seismic reflection configuration relusting from a highly faulted region along the basin margin in the southeastern part of the study area.

Channel geometry was identified from seismic in the LST and is a potential area for hydrocarbon exploration activity.

Finally, incorporating salt-tectonics processes, sequence-stratigraphy interpretation, and seismic-attribute analysis led to the new conclusion that salt has dominates sediment supply and sea level changes (eustasy) in controlling the sedimentary processes in the study area. This because the salt is able to move, to emplace sediment, to create instability and to block the sediment-transport pathway.

REFERENCES CITED

Acosta, Zurilma, and Paul Weimer, 1994, Sequence stratigraphy of Plio-Pleistocene sedimentary rocks in north-central Green Canyon and western Ewing Bank, northern Gulf of Mexico: Gulf Coast Association of Geological Societies Transactions, v. 44, p. 41-51.

Armentrout, John M., Steve L. Maleecek, Vinod R. Mathur, Gary L. Neuder, and Gerry M. Ragan, 1996, Intraslope basin reservoir deposited by gravity-driven processes: Ship Shoal and Ewing Banks areas, offshore Louisiana, extended abstracts: Gulf Coast Association of Geological Societies Transactions, v. 46, p. 443-448.

Armentrout, John M., 1999, Sedimentary basin analysis, *in* Edward A. Beaumont and Norman H. Foster, eds., Treatise of Petroleum Geology / Handbook of Petroleum Geology: Exploring for oil and gas traps: AAPG Special Publication, p.1-123.

Brown, Jr. L. F., and W. L. Fisher, 1977, Seismic stratigraphic interpretation of depositional systems: examples from Brazilian rift and pull-apart basins, *in* Charles E. Payton, ed., Seismic stratigraphy-application to hydrocarbon exploration: AAPG Memoir 26, p. 213-248.

Budhijanto, Fadjar M., and Paul Weimer, 1995, Sequence stratigraphy and tectonic setting of Plio-Pleistocene sediments, northeastern Green Canyon and eastern Ewing Bank areas, northern Gulf of Mexico: Gulf Coast Association of Geological Societies Transactions, v. 45, p. 104-111.

Buffler, Richard T., and Dale S. Sawyer, 1985, Distribution of crust and early history, Gulf of Mexico basin: Gulf Coast Association of Geological Societies Transactions, v. 35, p. 333-344.

Camp, Wayne K., 2000, Geologic model and reservoir description of the deepwater "P Sand" at subsalt Mahogany field, Gulf of Mexico: AAPG Hedberg Research Conference, Galveston, Texas, "Integration of geologic models for understanding risk in the Gulf of Mexico," 11p.

Crews, Jennifer R., Paul Weimer, Andrew J. Pulham, and Arthur S. Waterman, 2000, Integrated approach to condensed section identification in intraslope basins Pliocene-Pleistocene, northern Gulf of Mexico: AAPG Bulletin, v. 84, p. 1519-1536.

D'Agostino Tony, 1999, Chronostratigraphic Correlation Chart, PGS Reservoir, Inc., <http://www.pgsreservoir.com/ProdFrame/miocene.htm>, Accessed May 22, 2002.

Diegel, F. A., J. F. Karlo, D. C. Schuster, R. C. Shoup, and P. R. Tauvers, 1995, Cenozoic structural evolution and tectono-stratigraphic framework of the northern Gulf coast continental margin, *in* M. P. A. Jackson, D. G. Roberts, and S. Snelson, eds., Salt tectonics: a global perspective: AAPG Memoir 65, p. 109-151.

Edgell, H. S., 1996, Salt tectonism in the Persian Gulf basin, *in* G. I. Alsop, D. J. Blundell, and I. Davison, eds., Salt tectonics: Geological Society Special Publication No. 100, p. 126-151.

Edwards, Marc B., 2000, Origin and significance of retrograde failed shelf margins; tertiary northern Gulf coast basin: Gulf Coast Association of Geological Societies Transactions, v. 50, p. 81-94.

Emery, Dominic, and Keith Myers, eds., 1996, Sequence stratigraphy: Cambridge, Blackwell Science, 297p.

Hoversten, G. Michael, Steve Constable, H. Frank Morrison, 1998, Marine magnetotellurics for base salt mapping: Gulf of Mexico field-test at the Gemini structure, <www.appliedgeophysics.berkeley.edu:7057/geoengineering/ appliedgeophysics/papers/hcm98.pdf >, Accessed August 22, 2002.

Jamieson, George, John F. Karlo, and Robert C. Shoup, 2000, Tectonic provinces of the northern Gulf of Mexico: AAPG Hedberg Research Conference, Galveston, Texas, "Integration of geologic models for understanding risk in the Gulf of Mexico," 8p.

Karlo, J. F., R. C. Shoup, 2000, Classification of syndepositional system and tectonic provinces of the northern Gulf of Mexico: Search and Discovery Article #30004, <http://www.searchanddiscovery.com/documents/karlo/index.htm>, Accessed August 22, 2002.

Lee, Gwang Hoon, 1990, Salt tectonics and seismic stratigraphy of the Keathley Canyon area and vicinity, northwestern Gulf of Mexico: Ph.D. dissertation, Texas A&M University, 182p.

Martinez, Rafael E., and Paul Weimer, 1994, Sequence stratigraphy of Upper Pliocene and Pleistocene sedimentary rocks of northwestern Green Canyon area, northern Gulf of Mexico: Gulf Coast Association of Geological Societies Transactions, v. 44, p. 457-466.

McBride, Barry C., Mark G. Rowan, and Paul Weimer, 1998, The evolution of allochthonous salt systems, northern Green Canyon and Ewing Bank (offshore Louisiana), northern Gulf of Mexico: AAPG Bulletin, v. 82, p. 1013-1036.

McBride, Barry C., Paul Weimer, and Mark G. Rowan, 1998, The effect of allochthonous salt on the petroleum system of northern Green Canyon and Ewing Bank (offshore Louisiana), northern Gulf of Mexico: AAPG Bulletin, v. 82, p. 1083-1112.

Mitchum, Jr. R. M., P. R. Vail, and J. B. Sangree, 1977, Seismic stratigraphy and global changes of sea level, Part 6: Stratigraphic interpretation of seismic reflection pattern in depositional sequences, *in* Charles E. Payton, ed., Seismic stratigraphy-application to hydrocarbon exploration: AAPG Memoir 26, p. 117-133.

Navarro, Alonso F., and Paul Weimer, 1995, Sequence stratigraphy of Pleistocene sediments, northwestern Green Canyon, Gulf of Mexico: Gulf Coast Association of Geological Societies Transactions, v. 45, p. 457-465.

Pacht, Jory A., Bruce E. Bowen, John H. Beard, and Bernard L. Shaffer, 1990, Sequence-stratigraphy of Plio-Pleistocene depositional facies in the offshore Louisiana South Additions: Gulf Coast Association of Geological Societies Transactions, v. 40, p. 643-659.

Posamentier, H. W., and P. R. Vail, Eustatic controls on clastic deposition II-sequence and systems tract models, *in* Cheryl K. Wilgus, Bruce S. Hastings, Christopher G. St. C. Kendall, Henry W. Posamentier, Charles A. Ross, John C. Van Wagoner, eds., Sea level changes: an integrated approach: SEPM Special Publication No. 42, p. 125-154.

Posamentier, H. W., M. T. Jervey, and P. R. Vail, Eustatic controls on clastic deposition I-conceptual framework, *in* Cheryl K. Wilgus, Bruce S. Hastings, Christopher G. St. C. Kendall, Henry W. Posamentier, Charles A. Ross, John C. Van Wagoner, eds., Sea level changes: an integrated approach: SEPM Special Publication No. 42, p. 109-124.

Pulham, Andrew J., 1993, Variation in slope deposition, Pliocene-Pleistocene, offshore Louisiana, northeast Gulf of Mexico, *in* Paul Weimer, and Henry Posamentier, eds., Siliciclastic sequence stratigraphy recent developments and applications: AAPG Memoir 58, p. 199-233.

Rowan, Mark G., and Paul Weimer, 1998, Salt-sediment interaction, northern Green Canyon and Ewing Bank (offshore Louisiana), northern Gulf of Mexico: AAPG Bulletin, v. 82, p. 1055-1082.

Rowan, Mark G., Martin P. A. Jackson, and Bruce D. Trudgill, 1999, Salt-related fault families and fault welds in the northern Gulf of Mexico: AAPG Bulletin, v. 83, p. 1454-1484.

Rowan, Mark G., Robert A. Ratliff, Bruce D. Trudgill, and Jaime Barcelo Duarte, 2001, Emplacement and evolution of the Mahogany salt body, central Louisiana outer shelf, northern Gulf of Mexico: AAPG Bulletin, v. 85, p. 947-969.

Salvador, Amos, 1987, Late Triassic-Jurassic paleogeography and origin of Gulf of Mexico basin: AAPG Bulletin v. 71, p. 419-451.

Sangree, J. B., and J. M. Widmier, 1977, Seismic stratigraphy and global changes of sea level, Part 9: seismic interpretation of clastic depositional facies, *in* Charles E. Payton, ed., Seismic stratigraphy-application to hydrocarbon exploration: AAPG Memoir 26, p. 165-184.

Shoup, Robert C., and John F. Karlo, 2000, Syndepositional structural systems, northern Gulf of Mexico: AAPG Hedberg Research Conference, Galveston, Texas, "Integration of geologic models for understanding risk in the Gulf of Mexico," 6p.

Simmons, Gregory Raymond, 1992, The regional distribution of salt in the northwestern Gulf of Mexico: styles of emplacement and implication for early tectonic history: Ph.D. dissertation, Texas A&M University, 183p.

Stuart, Charles J., and Charles A. Caughey, 1977, Seismic facies and sedimentology of terrigenous Pleistocene deposits in northwest and central Gulf of Mexico, *in* Charles E. Payton, ed., Seismic stratigraphy-application to hydrocarbon exploration: AAPG Memoir 26, p. 249-275.

US Department of the Interior Mineral Management Service Gulf of Mexico Region, 2000, Paleo for Public Release 15 November 2000, pp 12552-12585.

Vail, Peter R., and Walter Wornardt Jr., 1991, An integrated approach to exploration and development in the 90s: well log-seismic sequence stratigraphy analysis: Gulf Coast Association of Geological Societies Transactions, v. 41, p. 630-650.

Van Wagoner, J. C., R. M. Mitchum, K. M. Campion, and V. D. Rahmanian, 1990, Siliciclastic sequence stratigraphy in well logs, cores, and outcrops: concepts for high-resolution correlation of time and facies: AAPG Methods in Exploration Series, No. 7, 55p.

Weimer, Paul, Mark G. Rowan, Barry C. McBride, and Roy Kligfield, 1998, Evaluating the petroleum systems of the northern deep Gulf of Mexico trough integrated basin analysis: an overview: AAPG Bulletin, v. 82, p. 865-877.

Weimer, Paul, Peter Varnai, Fadjar M. Budhijanto, Zurilma M. Acosta, Rafael E. Martinez, Alonso F. Navarro, Mark G. Rowan, Barry C. McBride, Tomas Villamil, Claudia Arango, Jennifer R. Crews, and Andrew J. Pulham, 1998, Sequence stratigraphy of Pliocene and Pleistocene turbidite systems, northern Green Canyon and Ewing Bank (offshore Louisiana), northern Gulf of Mexico: AAPG Bulletin, v. 82, p. 918-960.

Zhang, Jie, Joel S. Watkins, and Jih-Ping Shyu, 1993, Plio-Pleistocene sequence stratigraphy, outer shelf and upper slope, central offshore Louisiana, Gulf of Mexico: TAMU-UTIG Gulf of Mexico structural and stratigraphic synthesis project report, 43p.

Zhang, Jie, 1994, Salt tectonics and sequence stratigraphy of central offshore Louisiana, Gulf of Mexico: Ph.D. dissertation, Texas A&M University, 160p.

Zhang, Jie, and Joel S. Watkins, 1994, Plio-Pleistocene structural characteristic of central offshore Louisiana with emphasis on growth-fault interplay with salt tectonics, Gulf of Mexico: Gulf Coast Association of Geological Societies Transactions, v. 44, p. 745-754.
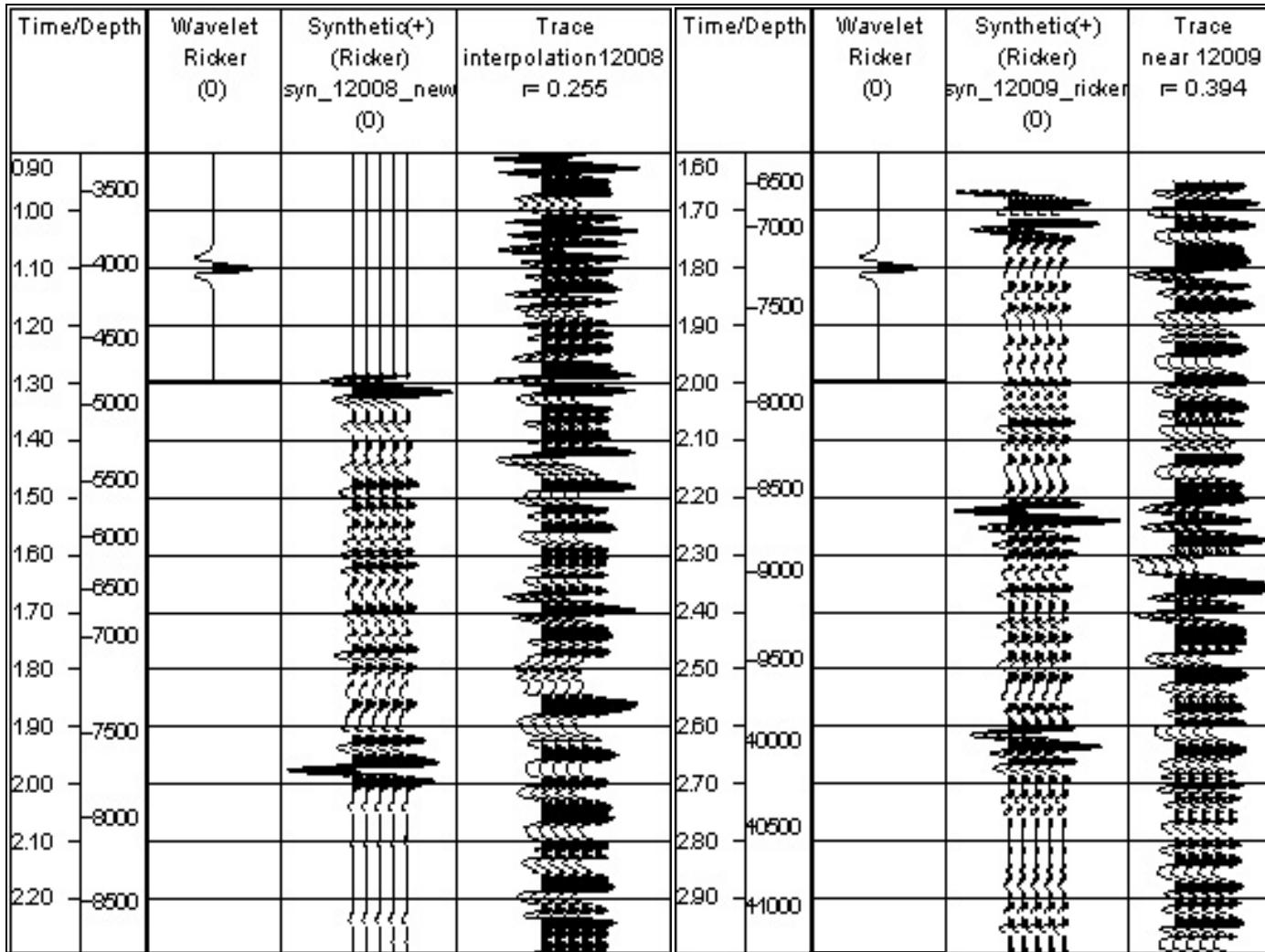
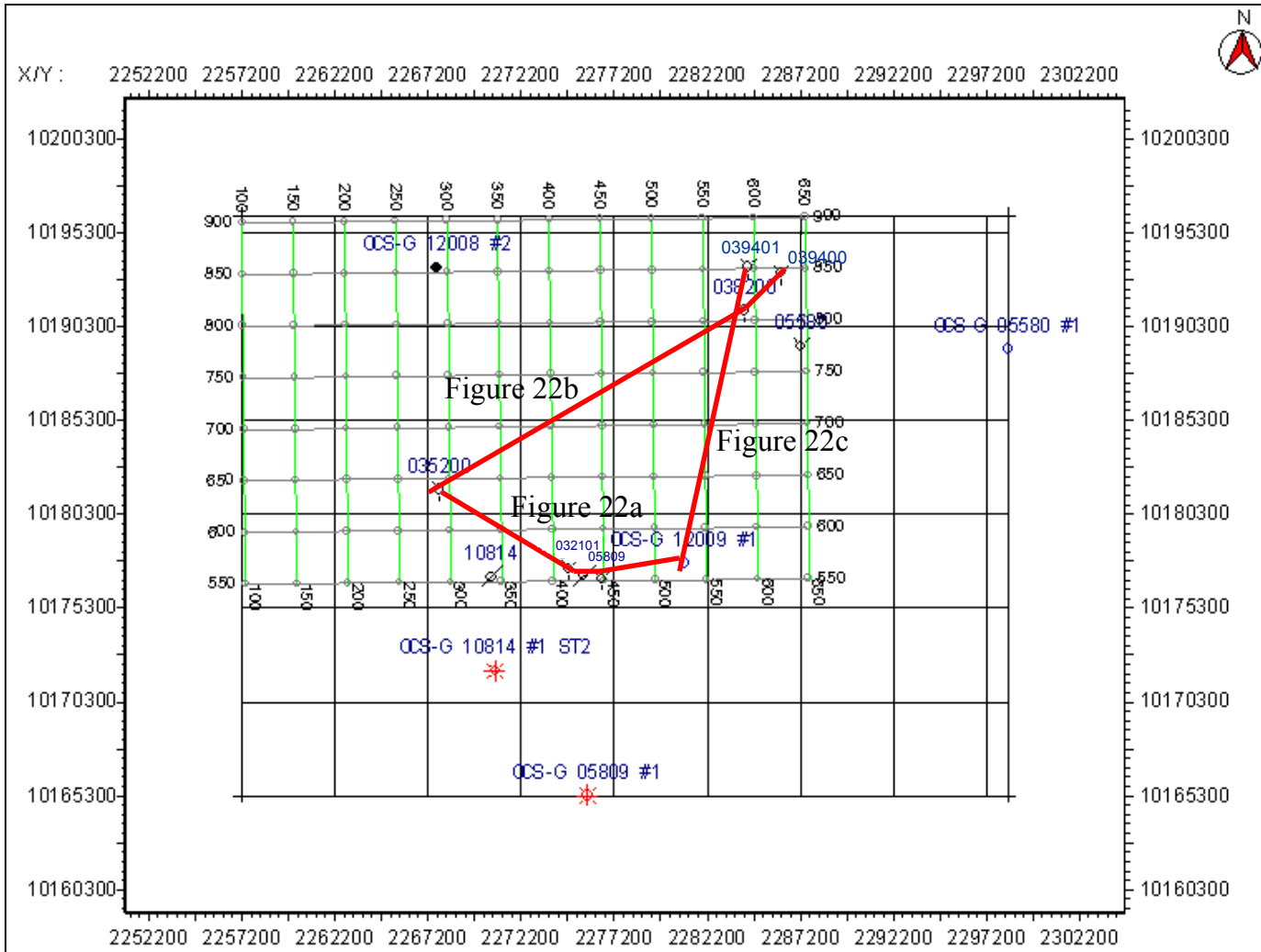**Figure 39**. Seismic synthetic from Wells #12008-2 and #12009-1.
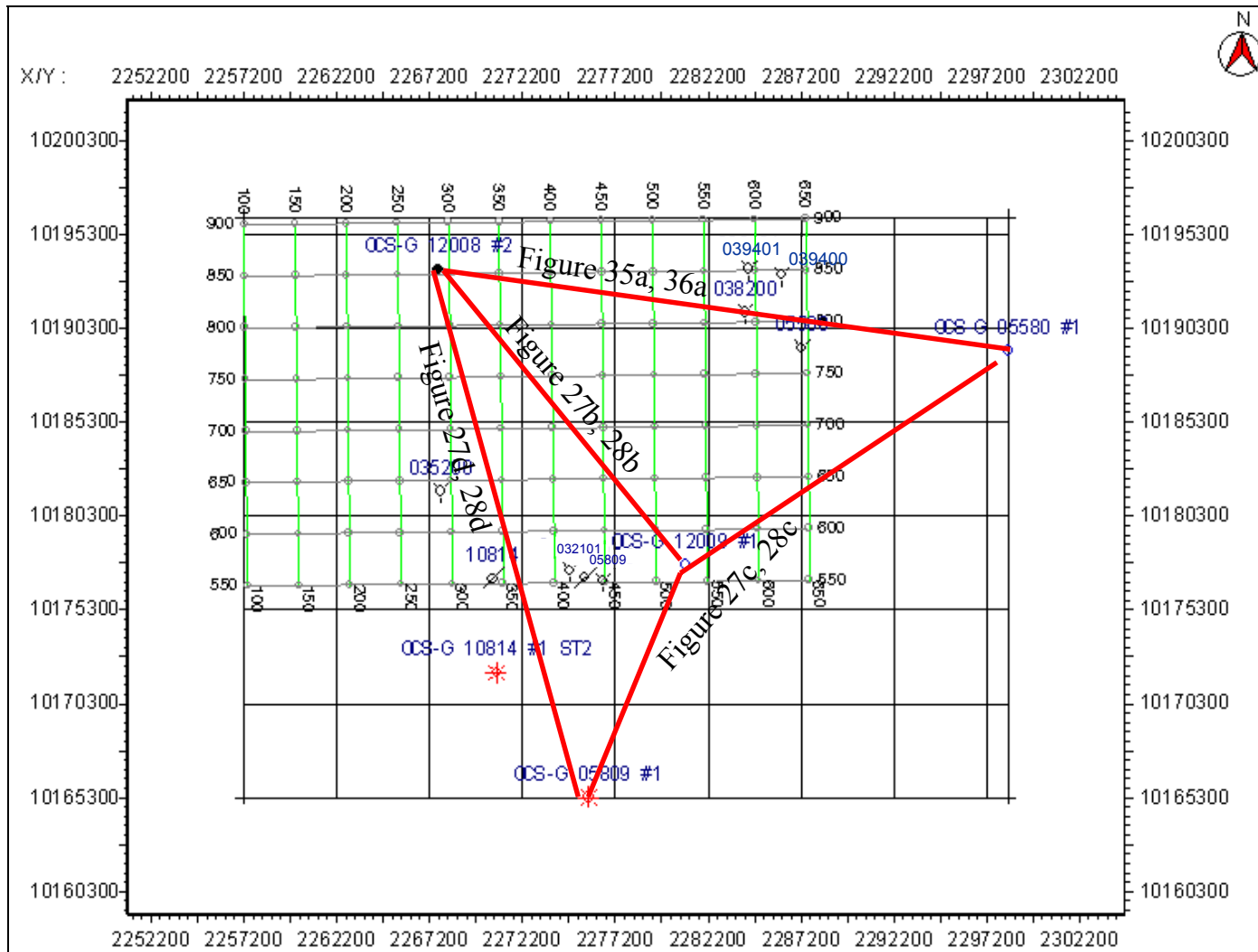
Figure 40. Location map for Figure 22.

Figure 41. Location map for Figure 27 and 28.

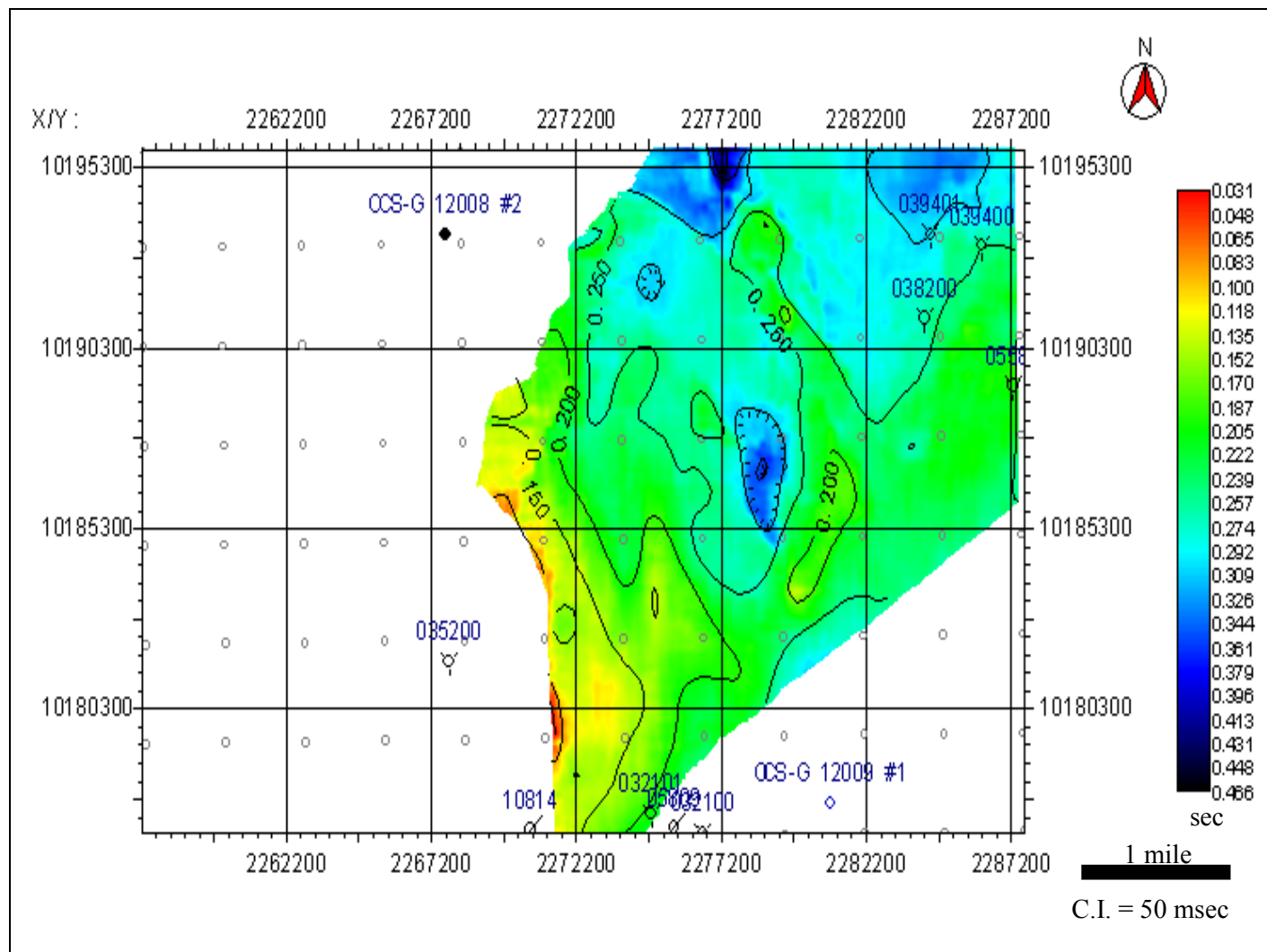**Figure 42**. Location map for Figure 23, 24 and 29.

Figure 43. Isochron map of interval between 3.65 Ma and 1.95 Ma. The thickest sediment is in the northeast of the study area.
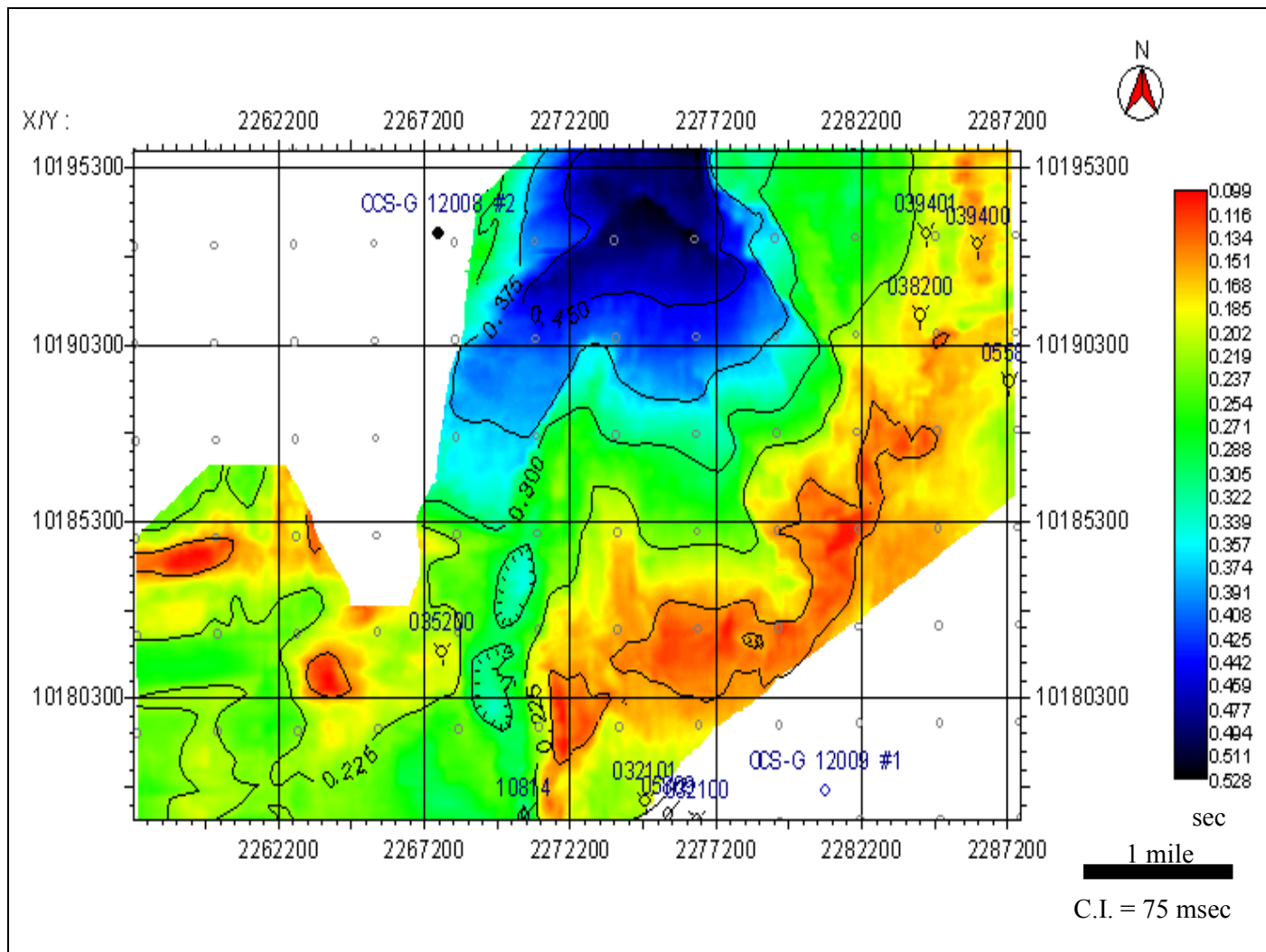
Figure 44. Isochron map of interval between 1.95 Ma and 1.35 Ma. The depocenter shifted to the center of the study area in the north.
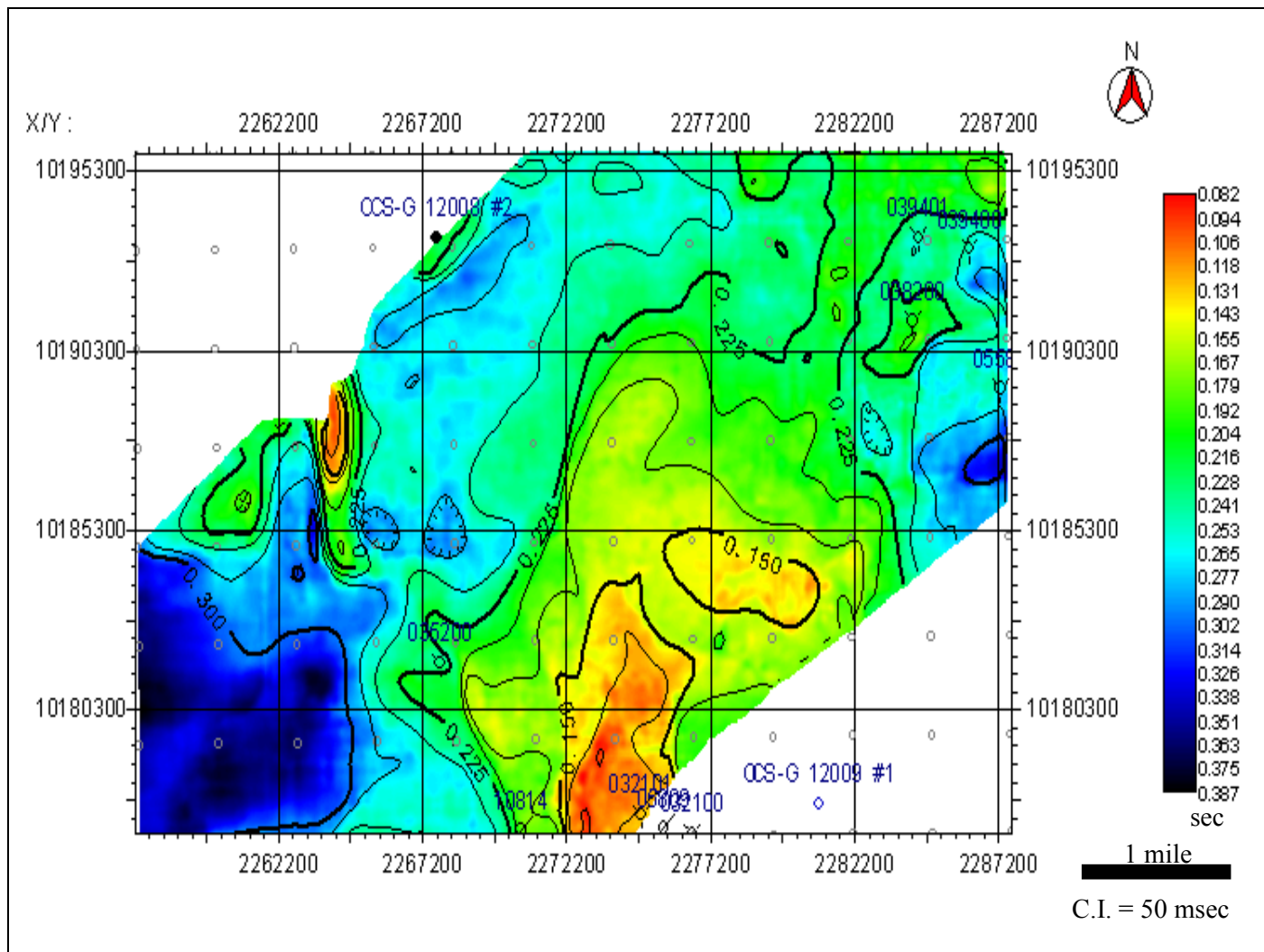
Figure 45. Isochron map of interval between 1.35 Ma and 0.80 Ma. Sediment transport pathways interpreted from northeast and northwest.
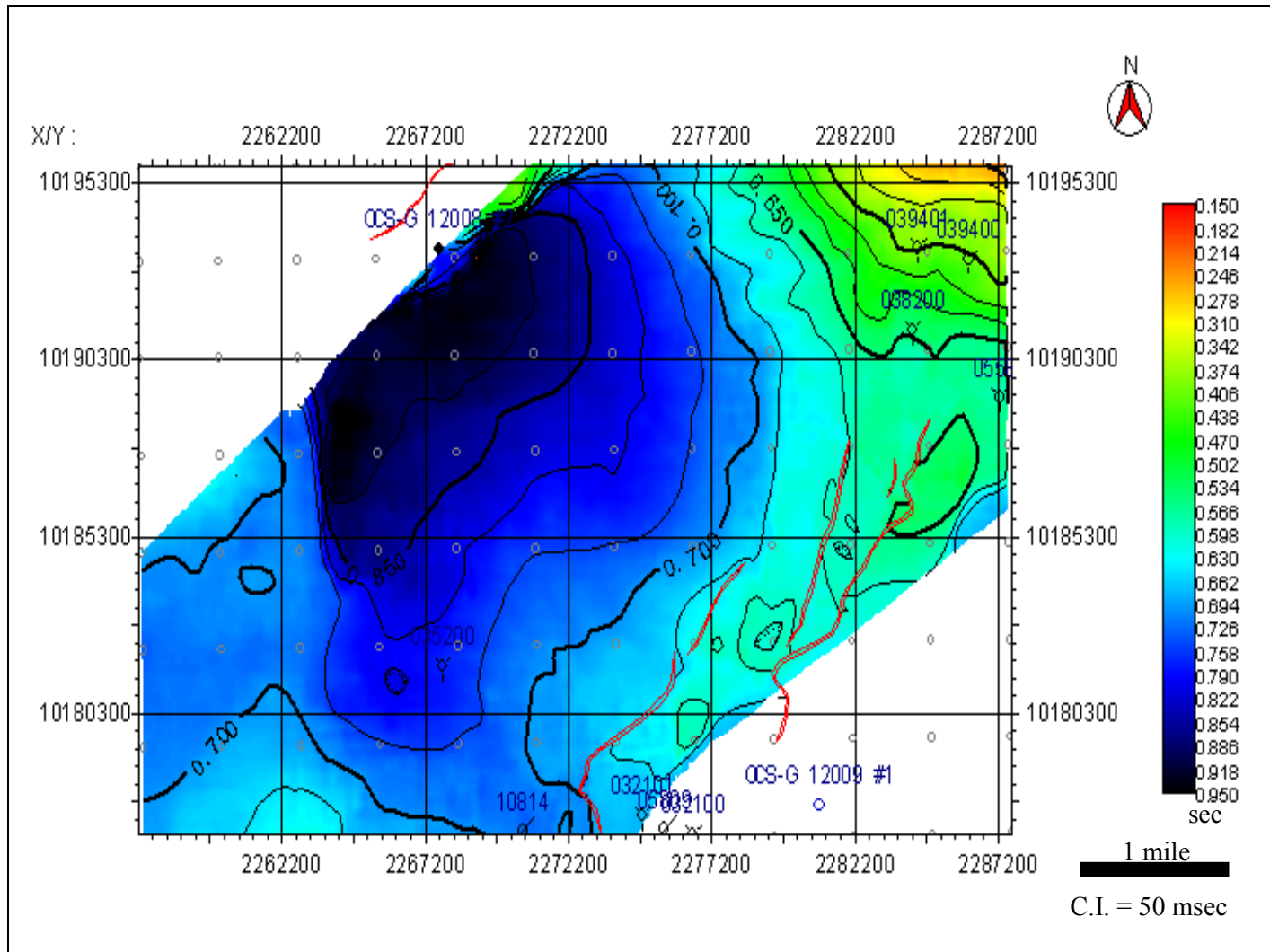
Figure 46. Isochron map of interval between 0.80 Ma and 0.27 Ma. The sediment from northeast was greater than from northwest. Faults are in red lines.
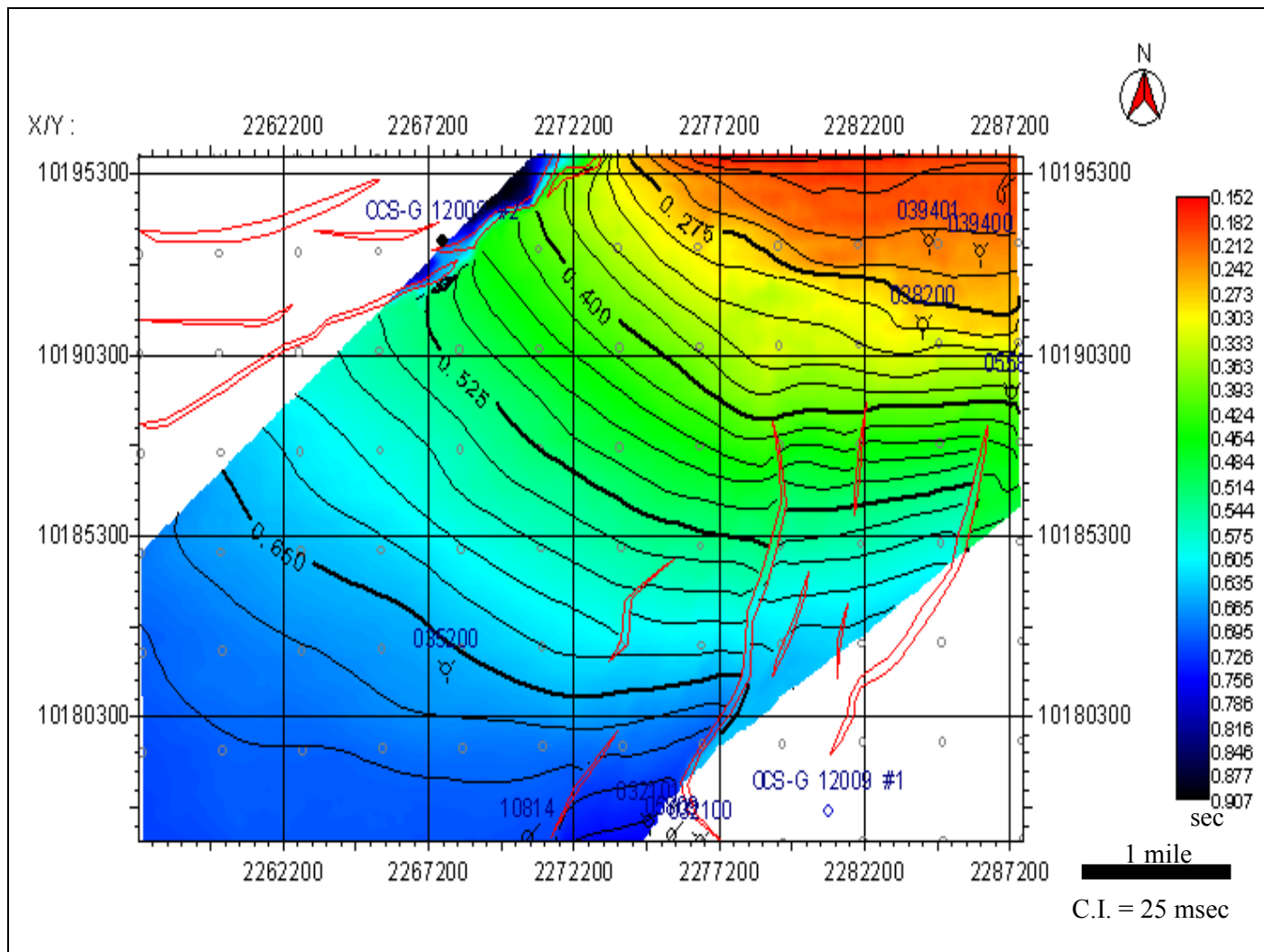
Figure 47. Isochron map between 0.27 Ma and today's sea bottom. The sediment transport continues from northwest to the southeast of the study area. Faults are in red lines.

VITA

Munji Syarif

Date of Birth	May 21, 1977
Mailing Address	Jl. Cijerah No 4 Bandung 40213 West Java, Indonesia.
Education	B.S., Bandung Institute of Technology (Geophysics)
	M.S., Texas A&M University (Geophysics)
	expected December 2002
Experience	May 2001 to August 2001- Intern student, Apexus (Repsol-YPF), Denver, Colorado.
	March 2000 to August 2000- Junior Geophysicist, Repsol-YPF, Jakarta, Indonesia.
	May 1999 to September 1999- Co-op student, YPF-Maxus SES, Jakarta, Indonesia.